Intelligent Shoes as Platform to Study Human Motion Abnormality

CHEN, Meng

A Thesis Submitted in Partial Fulfillment

of the Requirements for the Degree of

Doctor of Philosophy

in

Automation and Computer-Aided Engineering

The Chinese University of Hong Kong

December 2009

Thesis/Assessment Committee

Professor Du Ruxu (Chair)

Professor Xu Yangsheng (Thesis Supervisor)

Professor Wang Changling, Charlie (Committee Member)

Professor Zhang Jianwei (External Examiner)

Abstract

Keeping abnormal motion for long time will ultimately lead to pain in the feet, ankles, legs and skeletal disease, and badly influences the skelecton growth especially for children and adolescents. In biomedicine, gait analysis has been proved as an useful approach in revealing helpful insights into the recognition of motion abnormalities. Analysis of gait is commonly used as a routine procedure in identifying movement or posture related abnormalities of humans and aiding the therapeutic processes. Our goal is to monitor and study gaits of humans in order that proper motion adjustments can be advised to improve their posture style and long-term well being.

Most currently utilized measurement systems for motion and gait analysis have the shortcomings of that the monitoring and analysis of motion is constrained in a limited environment and human-related assistance is essential. All of them cannot be acceptable for the purpose of long-term monitoring and studying of motion abnormalities. In this thesis, a new concept of an inexpensive, compact, and lightweight shoe-integrated platform is introduced. The shoe-integrated system is composed of a suite of sensors for wirelessly capturing gait parameters and generating well qualified analysis results. The ideal platform requires no specialized equipment or lab setup, allowing data to be collected not only in the narrow confines of a research lab, but essentially anywhere, both indoors and outdoors.

Assessment of different gait patterns of daily living could provides useful information in studying one individual's stability and mobility during locomotion. As the foundation for better assessment of different gait patterns, the ability to automatically identity different patterns and walking surroundings provide valuable information for further understanding the relations between gait pattern and energy consumption. We apply Discrete Wavelet

Transform (DWT) for feature generation and Fuzzy-logic based approach for designing the multi-class classifier to identify gait patterns among flat walking, descending stairs, and ascending stairs based on continuous kinematic signals.

To be one of the common postural abnormalities, postural kyphosis is studied and modeled. We apply Cascade Neural Networks with Node-Decoupled Extended Kalman Filtering (CNN-NDEKF) to train the model for this binary classification problem. This proposed study is of particular significance to provide feedback in the application of postural kyphosis rectification.

Falls in the aging population has always been one of the most challenging problems in public health care. We propose an automatic falling detection algorithm based on the analysis of plantar force on both feet, because plantar forces are an important parameters directly associated with postures of human locomotion. The proposed two-stage algorithm efficiently overcome the shortcomings of the widely proposed accelerometer or gyroscope based algorithms and could provide efficient assistant for automatic detection of falls once they occur.

Finally, the research of studying gait abnormalities is introduced. We develop the methodology for modeling and classifying abnormal gaits including toe-in, toe-out, over-supination, and heel walking via machine learning algorithms, hidden Markov models (HMM) and support vector machine (SVM) based on a suite of gait parameters. The trained classifiers can classify abnormal gait patterns mentioned above and the proposed methodology will make it possible to provide realtime feedback to assist persons with gait abnormalities in the development of a normal walking pattern in their daily life.

摘要

长时间的不良运动姿态将最终引发足部、脚踝、腿部的疼痛以及骨骼疾病。特别对于儿童和青少年，不良姿态将严重影响骨骼的发育。在生物医学领域，步态分析早已被证明其在识别不良运动姿态方面的功用，是一种行之有效的测量以及辅助治疗方法。我们的研究目标是通过监控和学习步态,实现实时的正确姿态指导，以便人们改进不正确的运动姿态。

目前普遍应用的运动姿态以及步态分析测量系统都存在一些缺点。运动行为的监测以及分析被制约在有限的空间当中，并且专业人士的辅助是不可缺少的。这些传统的系统不能为长时间的运动检测提供良好的平台。在这种情况下，我们提出了一种新的测量理念：智慧鞋测量平台。这个系统具备价格低廉、质轻等优点。其集成了一系列传感器可以进行无线的步态数据采集以及被应用于高质量的步态分析。这个理想的测量平台不需要特殊器械以及实验室的辅助。运动数据的采集不再局限在狭小的实验室，而被扩展到更加广阔的室外空间。

在日常生活中，对不同步态模式的评估可以为人类运动过程中的稳定性以及移动性提供有效的分析信息。作为步态模式的有效评估基础，自动检测、辨识不同的步态以及行走环境为进一步理解步态模式同能量消耗之间的联系提供了有效的信息。我们运用离散小波变换对连续的运动信号进行了特征提取，并且提出了基于模糊逻辑的方法来实现多种步态模式的辨识，其中包括，平地行走、上楼梯、下楼梯的行走步态。

作为一种常见的姿态异常，我们对姿态型驼背进行了分析与建模。我们应用了一种有效的神经网络学习体系来建立模型以解决姿态型驼背与正常姿态之间的辨识问题。此方面的研究在姿态型驼背矫正方面具有特殊的意义。

老年人的摔倒问题一直是公共健康护理的一个难题。考虑到在人类的运动当中，脚底压力是表明姿态特征的一个重要参数，我们提出了基于双足压力分析的自动摔倒检测

方法。所提出的两阶段分析算法有效的克服了目前基于加速度以及角速度传感器的摔倒检测方法的不足，能有效的实现对摔倒瞬间的检测。

最后，我们介绍了在异常步态方面的研究。运用隐马尔可夫模型和支持向量机，我们提出了对几种常见异常步态建模及分类的方法。通过一系列步态参数，训练后的分类器可以有效的分辨出我们所关注的异常步态。此方法为异常步态者在日常生活中改进行走姿态提供了良好的辅助功能。

Acknowledgments

This thesis would not be completed without the support and encouragement of many people to whom I would like to express my sincere gratitude.

At the very first, I am honored to express my deepest gratitude to my supervisor, Professor Yangsheng Xu for his valuable ideas, suggestions, and constant supervision throughout the years. He offered me an opportunity of obtaining academic training and helped me on learning efficient research skills and methodologies. With his instructions, my insight skill, presentation skill, and other related skills have been improved.

I would also like to thank the rest of my thesis committee for their supports. Professor Ruxu Du, Professor Changling Wang, and Professor Jianwei Zhang provided me their invaluable instructions and advices on my research.

I am also grateful to all my colleagues, present and past, from the Advanced Robotics Laboratory at CUHK. Among them are Dr. Ka Keung Lee, Dr. Yongsheng Ou, Dr. Panfeng Huang, Dr. Bufu Huang, Dr. Zhancheng Wang, Dr. Xi Shi, Dr. Weizhong Ye, Mr. Weimin Li, Mr. Jingyu Yan, Mr. Xiaoning Meng. The discussions and working life with you during these years have been the great memorable for me. Thanks are also due to Mr. Hang Tong, Mr. Wai-kit Mok and Mr. Yun-yee Leung from the Department of Mechanical and Automation Engineering for their technical supports.

What is more, I wish to thank the colleagues in the Human Movement Laboratory, including Professor Youlian Hong, Ms. Y. L. Cheng, and Mr. Pui-lam Wong who generously shared data about pressures of the Novel Pedar insole system. I would like to thank all the volunteers for subject testing, who are very important for making this thesis possible.

Finally, with great love and respect, I would like to thank my parents whom I missed

so much these years. Thanks for their eternal love and support that encouraged me to complete this work. I also want to give my special thanks to my boyfriend Dong Wang, thanks for his strong support all the way of my postgraduate study.

Contents

List of Figures

List of Tables

Chapter 1

Introduction

1.1 Motivation

Human motion, the physical movement in the position of a body relative to a reference point, can be generally divided into normal and abnormal ones. Human motion is influenced by many factors, including general health, body build, strength, personal habits, environment and so on. Ideal motion is associated with the continuous posture defined as the balance state of muscles and skeletons which protects the supporting structures of the body against injuries and deformities. Under these conditions, the muscles will function most efficiently and the optimum skeletal positions are afforded for thoracic and abdominal organs. However, prolonged abnormal motion will ultimately lead to pain in the feet, ankles, legs and skeletal disease, and badly influence the skelecton growth especially for children and adolescents. In biomedicine, gait analysis has been proved as an useful approach in revealing helpful insights into the recognition of motion abnormalities. Analysis of gait is commonly used as a routine procedure in identifying movement or posture related abnormalities of humans and aiding the therapeutic processes. Our goal is to monitor and study the gaits of humans in order that proper motion adjustments can be advised to improve their posture style and long-term well being.

Currently, motion and gait analysis are generally carried out relying on either of the two ways, including clinicians' visual observations and motion lab systems. For the first

approach, no extra equipments are needed. Subjects are observed in clinician's office and required to finish some locomotion, such as walking with their free-selected posture and speed, walking around an obstacle, climbing up and down stairs, and so on. During the processes, the trained specialist observes the subject's locomotion and makes the conclusion about gain analysis based on his/her expert experience. For the second one, the laboratory is equipped with highly accurate computer-based optical tracking systems, electromyography (EMG) systems, force platforms and so on, which can produce reliable and accurate analysis for whole body segments during subjects' locomotion. The clinician's observation method is inexpensive, however, the analysis results is unreliable and qualitative. While, the motion lab system can provide accurate results relying on the expensive set-up and maintenance. The shortcomings of both methods are that the monitoring and analysis of motion is constrained in a limited environment and human-related assistance is essential. Consequently, neither of them can be acceptable for the purpose of long-term monitoring and studying of motion abnormalities. The new concept of gait analysis platform that is inexpensive, can be applied in a variety of environments, and generates well qualified analysis results, needs to be brought out.

In recent years, researchers have begun to focus on the study of wearable sensor and computer interfaces. However, one domain of wearable devices named the design and implementation of sensor and computer-equipped intelligent shoes, has remained relatively unexplored. The on-going revolution in electronics, sensor, and battery miniaturization, driven largely by mobile hand-held device markets, has made it possible that an intelligent-shoe implementation is compact and lightweight such that users will notice little if any difference between their normal shoes and the proposed intelligent shoes. This proposed shoe-integrated system provides an ideal platform for our research on studying human motion abnormalities. Unlike other more intrusive motion capture technologies, based on cameras or magnetic motion trackers, the intelligent shoe system requires no specialized equipment or lab setup, allowing data to be collected not only in narrow confines of a research lab, but essentially anywhere, both indoors and outdoors.

The study and analysis of human gait has always been a challenging attempt due to

the intrinsic characteristics of gait data. Firstly, human gait need to be well represented replying on high-dimensional parameters, including kinetic, kinematic, electromyography (EMG) and so on. This high-dimensional problem is intractable via typical statistical analysis methods. Secondly, gait data is non-deterministic. Trial environments and instrumentation unavoidably result in the variabilities of gait data recordings. Besides, gait data shows variabilities between subjects, between trials, even for one subject in the same trial. Thirdly, it exhibits nonlinear relationship between the gait variables and the corresponding human motions. Recently, new developments in computational intelligence and machine learning algorithms lead to the increase applications in the fields of biomedicine and human motion analysis. The progresses overcome the limitations of the existing quantitative techniques in modeling and make possible the analysis and interpretation of complex, multi-channel gait data.

We propose methodologies for studying and modeling human motion abnormalities under the framework of the intelligent shoe-integrated system from which the information acquired can give efficient assistance in determining and alarming the users associated with abnormal motion patterns. The research work for this thesis mainly focuses on the following parts:

1. Design and implementation of the inexpensive, compact, robust shoe-integrated platform for capturing a variety of gait-related parameters wirelessly.

2. Study and classify gait patterns, including flat walking, descending stairs, and ascending stairs.

3. Detection of postural kyphosis which is one of the most common postural abnormalities.

4. Methods for studying and automatically discriminating fall-events from activities of daily living tasks based on plantar force information.

5. Classification of normal gaits and the abnormal ones including toe-in, toe-out, oversupination, and heel walking.

1.2 Related Work

In order to provide a better understanding for the need of applying shoe-integrated system for monitoring and studying motion abnormalities, we will discuss the motion measurement techniques widely used in clinical analysis. Additionally, the prior work for gait analysis based on on-shoe systems will be introduced.

1.2.1 Human Motion Measurement Techniques

In the past decade, as more and more studies on human motion have been conducted, numerous systems for human motion data acquisition and analysis are proposed. A typical motion analysis procedure generally relies on using a variety of measurement techniques for acquiring a number of biomedical variables about kinematics, kinetics, and electromyography (EMG) information. This section will mention some of the main measurement techniques used for motion analysis.

Kinematics

Kinematics analysis is related to describe how the object moves in space. There are mainly three types of kinematics analysis systems: video-based reflective marker systems, optoelectronic systems, and electromagnetic tracking systems.

For the video-based reflective maker systems, reflective markers which are also called passive markers are attached to subjects. Multiple video cameras whose lens are surrounded with infrared flash illuminators are utilized for tracking the reflections from the markers. Infrared illuminators send out infrared lights which are reflected back into the lens by the passive markers. The two major corporations for manufacturing such systems are Motion Analysis and VICON (Fig. 1.1).

The Eagle Digital RealTime System of Motion Analysis Corporation [1] is widely used in the applications of gait analysis and rehabilitation, which consists of Eagle Digital Cameras and Cortex software. The Eagle Digital Camera, with a resolution of 1.3 million pixels at 1280 $\times$ 1024 full resolution, can capture speeds of up to 500 frames per second.

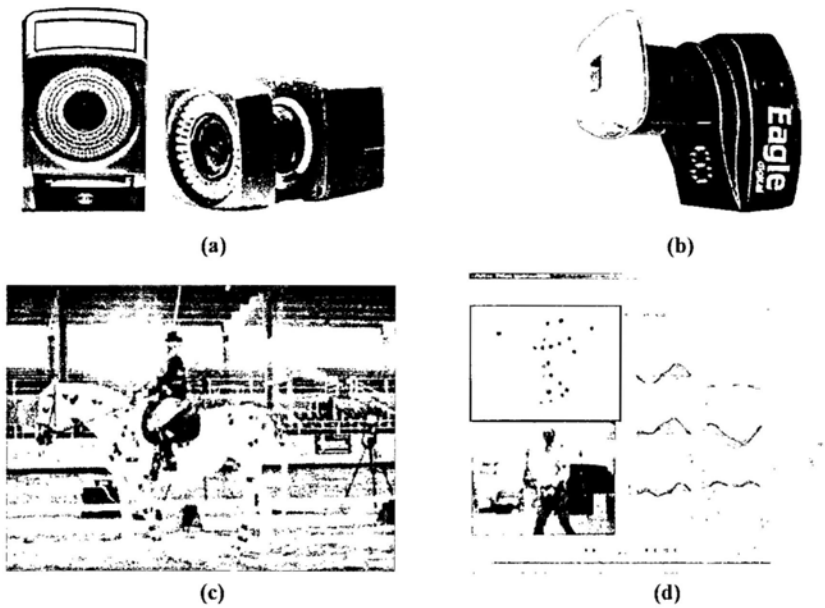

Figure 1.1: (a) VICON camera [3] (b) Eagle digital camera of Motion Analysis [1] (c) Reflective markers attached at various segments of the horse and human [4] (d) Gait analysis interface of Motion Analysis [5]

The latest innovation of Vicon, T160 [2], with a resolution of 16 megapixels, can capture 10-bit grayscale using 4704 × 3456 pixels at up to 2,000 frames per second. Such high resolution means that the details of participants can be tracked accurately even in a larger volumes with more markers.

Different the video-based reflective maker systems, from optoelectronic systems capture 3D motion information via attaching active markers, light emitting diodes (LEDs), on the segments of participants. Optotrak Certus motion capture system (Fig. 1.2(a)), with an accuracy of up to 0.1 mm and the resolution of 0.01 mm, is a commercially available optoelectronic system. The maximum number of markers is 512 per system and the maximum update rate reaches 4600 Hz [6]. The position sensor of the Optotrak Certus System which is pre-calibrated involves three cameras mounted in a rigid housing (Fig. 1.2(b)) .

Electromagnetic tracking systems involve a transmitter emitting magnetic fields and sensor coils mounted on the participant for detecting the fields. Each sensor coil tracks

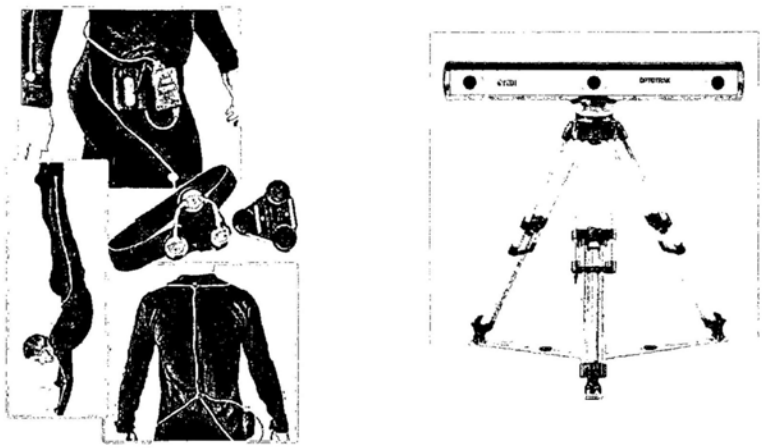

(a) (b)

Figure 1.2: (a) Optotrak Smart Markers attaching to the participant [7] (b) Optotrak Certus position sensor [8]

the object's position and orientation and delivers a six degrees-of-freedom measurement. Better than the video-based approaches, there is no cameras or tripods need to be aligned and calibrated. However, since the sensor coils must be within the range of the magnetic field emitted by the transmitter, the tracking space is limited. The operation range for the commercially used electromagnetic system, MotionSTAR Wireless LITE (manufactured by Ascension Technology Corporation) is ±3.0 m [9]. Besides, electromagnetic systems are not suitable for detailed tracking of 3D motion due to the less receiver points compared with video-based systems.

Kinetics

Kinetics concern the forces that produce movement. The ground reaction force (GRF) representing the force exerted by the supporting surface onto the body through the foot, is generally measured by force platforms. AMTI multi-axis force platforms (Advanced Mechanical Technology, Inc) are commercially available force platforms widely utilized in gait and biomechanics laboratories [10]. The force platform based on strain-gauge transducers is floor-mounted. Each platform measures three-dimensional forces (F_x, F_y, F_z) and

three-dimensional moment components (M_x, M_y, M_z). The coordinate axes of AMTI force platform are shown in Fig. 1.3(a). Motion laboratories usually utilize two or three force platforms for kinetics analysis. The limited number of platforms confines the operation range and less consecutive gait cycles can be monitored for one trial. As the alternative system for kinetics analysis, plantar pressure insoles, are suitable for investigating a variety of long-term activities, such as running, climbing stairs, or even playing basketball. The main commercially available system, Pedar insole (Novel Gmbh, Munich, Germany), involves 99 capacitance transducers for measuring pressure distribution between the foot and shoe in the dorsal, medial and lateral areas.

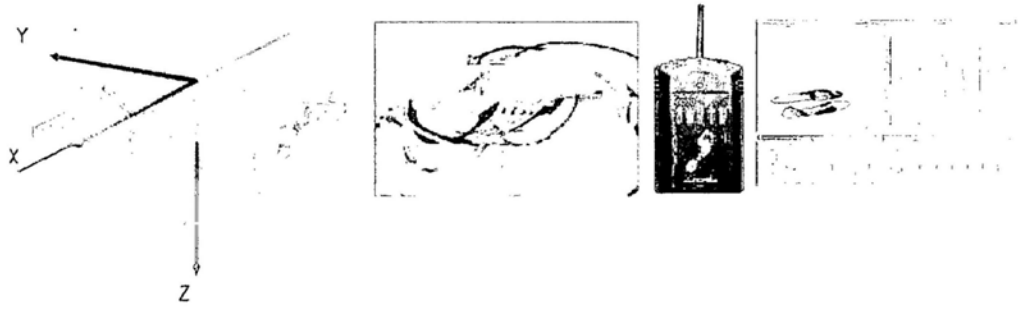

Figure 1.3: (a) AMTI force platform coordinate axes [10] (b) Pedar insole [11]

Electromyography (EMG)

Electromyography (EMG), as one part of comprehensive motion analysis, is conducted in some motion laboratories. EMG measurements have been incorporated into studies of human motion since the early 1950s [12]. EMG refers to measurements of the electrical activity of muscles. The recordings of EMG is helpful to determine muscles' function and their working sequence of the corresponding movements. The studies involving the presence and absence for the particular muscle's activities, the EMG envelope shape with respect to the muscle's on-off activity, and the relationship between EMG signal intensity and muscle effort, have drawn interests of motion laboratories. The information obtained

from specific muscles during their activities may be useful in developing effective injury prevention and rehabilitation.

The two types of EMG are surface electromyography (SEMG) and fine-wire electromyography (FWEMG). SEMG replies on taping electrodes on the skin surface over the interested muscle. The main disadvantage of SEMG is that it is more subject to cross-talk generated by muscles lying between the surface electrode and the deep muscle we interested. FWEMG overcomes this problem by injecting needle electrode directly into the deep muscles. Although both types of EMG disrupt gait in some way, SEMG is more often used due to less invasive than FWEMG.

1.2.2 Gait Analysis Based On On-Shoe Systems

Among all available systems for human motion analysis, on-shoe devices are most utilized due to the outstanding advantage of extending the usable space for human gait study.

Some initial multi-sensor based on-shoe systems have been prototyped. An in-shoe multisensory data acquisition system was developed by Morley et al. in 2001 [13]. In this system, four pressure sensors, two temperature sensors, and one humidity sensor were located under the special positions inside a shoe for recording the corresponding information, which was later downloaded to the host computer for data analysis. The hardware design and on-shoe data acquisition have been realized. The system has the potential application to provide feedback to patients with diabetes and peripheral neuropathy who are at high risk of foot skin breakdown. The reliability and validity of the developed system has been investigated in [14]. Morris et al. [15] [16] developed a wireless wearable system that was designed to provide quantitative and long-term gait analysis aiming for clinical applications. The proposed "GaitShoe" system has been proved in the application of heel-strike and toe-off timing detection.

The goal to directly measure the pressure distribution between the foot and shoe drove many early on-shoe systems. Zhu et al. [17] [18] developed a portable microprocessor-based data acquisition system for measuring discrete plantar pressures beneath foot from

ambulatory subjects. For each insole, seven pressure sensors were located under seven bony prominences, including the anterior and posterior heel, the five metatarsal heads, and the hallux of each foot. They also studied foot pressure distribution during walking and shuffling based on the proposed repeatability and portability in-shoe device [19]. Another wireless in-shoe force system was reported by Lawrence and Schmidt [20]. In this system, four thick-film force sensors were installed under the major weight-bearing points of each foot to estimate the approximate total normal force and the center of pressure (COP) on each foot. The experiment results of total force and COP component measurement were compared with the results of the AMTI force plate.

Gait phase/event analysis has become one of the most prevalent applications for on-shoe systems in recent years. Skelly and Chizeck [21] presented a two-level rule-based gait event detection algorithm. For the lower level, force sensitive resistors' signals and the progression information of the stimulator were processed for estimating the phase of gait based on a fuzzy logic classifier. The upper level acted as the supervisory function for monitoring and modifying these estimations provided by the lower level and generated the time sequences of gait events. They concluded that two force sensitive resistors (FSRs) per insole were sufficient for detecting the gait events of a single leg. Pappas et al. proposed a gait phase detection system based on a portable device including one gyroscope and three force sensitive resistors [22]. The knowledge-based and rule-based algorithm can distinguish the gait phases of stance, heel-off, swing, and heel-strike in realtime. The experimental results demonstrated the gait phase detection system was insensitive to perturbations caused by non-walking activities. Subsequently, Pappas et al. [23] presented the experimental results of combing the gait phase detection system and a programmable functional electrical stimulation (FES) system for subjects with the dysfunction of drop-foot gait pattern. The use of gait phase detection system associated with FES improved the gait-kinematics of the affected leg, which showed the potential application in rehabilitation training.

1.3 Thesis Overview

The coming chapters of this thesis are organized as follows:

- Chapter 2: Shoe-integrated Platform Design

  In this chapter, the design of the shoe-integrated platform is introduced. The implementation of the main subsystems, including the insole, the Inertial Measurement Unit, the microprocessor-based data gathering board, and the wireless communication module are described respectively. The shoe-integrated system we designed is an ideal platform for studying human motion abnormalities by modeling abnormal motions which will introduced in the following chapters.

- Chapter 3: Gait Pattern Classification

  We aim to study human gait patterns and present the design of the classifier for identifying gait patterns among flat walking, descending stairs, and ascending stairs based on continuous kinematic signals. We apply Discrete Wavelet Transform (DWT) for feature generation and Fuzzy-logic based approach for designing the multi-class classifier. Anteroposterior accelerator, vertical accelerator, and the sagittal plane gyroscope are demonstrated to provide useful information for classifying the gait patterns we focus on. The compact, wireless, and wearable system has the promising application for assisting to evaluate walking energy expenditure.

- Chapter 4: Postural Kyphosis Detection

  We present a methodology for detecting postural kyphosis under the framework of the shoe-integrated system. Eight force sensing resistors (FSRs) for gathering the pressure information under the eight bony prominences are utilized. Based on the gathered plantar pressure information, we apply Cascade Neural Networks with Node-Decoupled Extended Kalman Filtering (CNN-NDEKF) for training the model for this binary classification problem. The proposed methodology has the potential application for detecting postural kyphosis in order to assist persons in developing proper walking posture in their daily life.

- Chapter 5: Falling Detection based on Plantar Force

  A novel falling detection algorithm based on the analysis of plantar force on both feet is proposed in this chapter. Two-stage analysis algorithm is presented. For Stage-One analysis, the candidate sequences will be generated if force values of the four positions in both feet are simultaneously less than the corresponding predefined thresholds and last for a while. For Stage-Two analysis, we apply support vector machine (SVM) with genetic algorithm (GA) for generating optimal training parameters to determine whether there really exists a fall event.

- Chapter 6: Abnormal Gait Modeling

  We present the method for modeling abnormal human gait using hidden Markov model. The intelligent system focuses on modeling the following patterns: normal gait, toe in, toe out, oversupination, and heel walking abnormalities. The "similarity distance measure" criterion which reflects the similarity degree between models is introduced. Besides, the methodology of optimal SVM classifier is also applied for the problem of this chapter.

- Chapter 7: Conclusions

  In this chapter, the major contributions of this thesis are summarized and the future work are discussed.

Chapter 2

Shoe-integrated Platform Design

The foundation of this thesis is to design and implement of the shoe-integrated platform for motion analysis. This chapter introduces the design and implementation of such a platform in detail, including selection of sensors, physical implementation, and interpretation of sensor data with respect to physical parameters. Section 2.1 discusses the functional requirements of the design and introduces the overall architecture of the shoe-integrated system. Section 2.2 and Section 2.3 respectively describe the insole subsystem and Inertial Measurement Unit (IMU) subsystem. In these two sections, the detailed functions of the sensors are presented. Section 2.4 describes the microprocessor-based data gathering subsystem, and Section 2.5 introduces the wireless communication and system interface in detail.

2.1 Overview

In designing the shoe-integrated system, the fundamental requirements should be considered as follows:

First and foremost, the system should have no effect on humans' movement. Thus, the compact and lightweight sensors and electronic hardware, which subtly effect on a shoe's weight should be selected. As mentioned in previous studies, the lower-extremity loading

on the order of 1 - 2% of body weight can have subtle effects on gait [24]. Considering the studied subjects for our experiments are adolescents and adults who are weighted more than 30 kg, the weight of the prototype less than 300 g (30 kg weight $\times$ 1%) is acceptable.

Secondly, the shoe-integrated system should be convenient to wear and socially acceptable. In order to meet this requirement, the hardware is designed to be an additional part of users' normal shoe (e.g. insole) or attached on the surface of shoes aiming not to damage the shoes and interfere in humans' gait at the same time.

Thirdly, the use of the shoe-integrated system is not constrained in a relatively small environment. Wireless communication based on radio frequency (RF) is proposed to satisfy this requirement. For each shoe-integrated system, a pair of transceiver and receiver is utilized for transferring data to the remote host PC for analyzing the user's motion in real-time.

Fig. 2.1 shows the schematic diagram of the system architecture, including four major components: insole, Inertial Measurement Unit (IMU) board, microprocessor-based data gathering module, and wireless communication subsystem. The whole system is compact and lightweight (90 g) so that it can be easily integrated with a user's shoes.

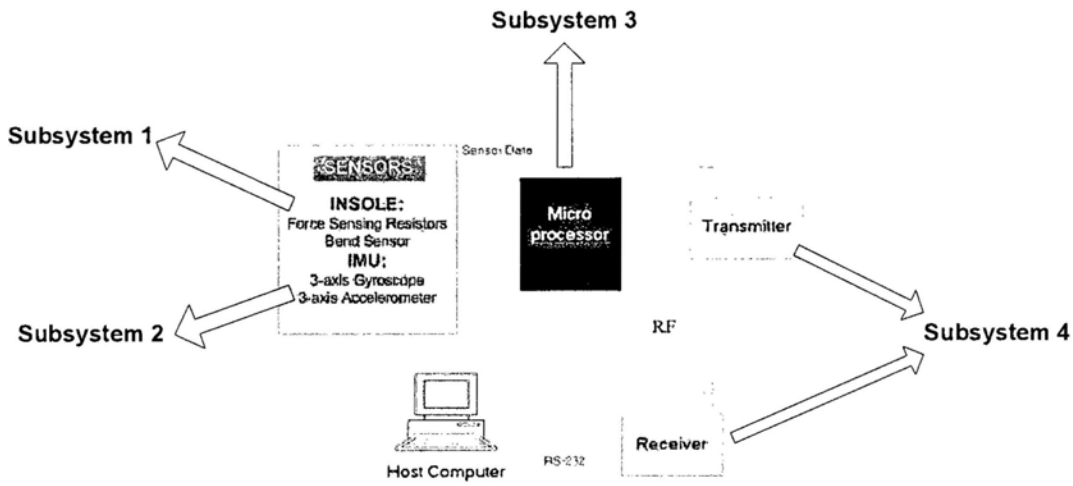

Figure 2.1: Outline of the system design

Subsystem 1 is for sensing the parameters of the insole. A suit of sensors are installed

inside the insole, including force sensing resistors and the bend sensor. For the ease of use, we limit the size of each sensor as small as possible.

Subsystem 2 is used for acquiring kinematic information from the Inertial Measurement Unit (IMU), including three single-axis gyroscopes and one three-axis accelerometer to detect the angular rates and accelerations for the x, y, and z axes while the participant moves.

Subsystem 3 is for gathering data from the insole and IMU. Furthermore, the microprocessor based module will transform the analog voltage information into scaled digital data before sending them to the host PC. The operation power of the microprocessor is limited to 5V.

Subsystem 4 is for wireless communication. This communication system is composed of a transmitter and receiver. The receiver is for collecting the data from the circuits described in subsystem 3 while the transmitter is utilized for sending the data to the host computer for further analysis.

2.2 Insole Subsystem

Insole subsystem shown in Fig. 2.2 is a flexible instrumented part for sensing the force and flexion parameters inside the shoe. Eight FSRs (Interlink Electronics, Santa Barbara, CA) and one bend sensor (Images SI, Inc.) are installed on one side of a thin insole made of foam. The bend sensor is located at the center of the insole in order to provide the flexion information of foot. Since the weight of the body is mainly supported by the metatarsal heads and toes in the front of the foot and the calcaneus in the back of the foot, the FSRs are installed underneath subcutaneous bony prominences: 1-5 metatarsal heads, hallux (big toe), and the heel (which is divided into a posterior and inside positions). Considering the different sizes of bony prominences, we select two kinds of FSRs. Two FSR-402s are installed in the first metatarsal head and hallux. Six FSR-400s are placed under the other positions.

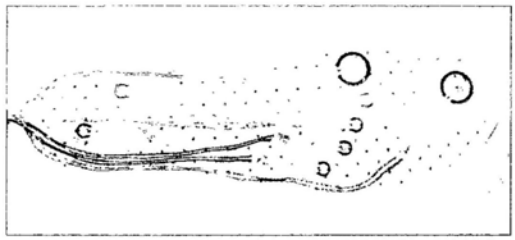

Figure 2.2: Photograph of the insole subsystem

2.2.1 Force Sensing Resistor

Force Sensing Resistors (FSRs) are polymer thick film (PTF) devices that experience a decrease in electrical resistance along with an increase in normal force applied to the active area of the sensor. Structurally, FSRs manufactured by Interlink Electronics [25] consists of three layers shown as Fig. 2.3. The bottom layer is a flexible substrate coated with printed semi-conductor material. The middle layer is a spacer adhesive providing spacer opening and vent for the active surface. The top area is a flexible substrate with printed interdigitating electrodes. The area containing the electrodes is the active area of the sensor. FSR-402 has the circular active surface of 12.7 mm diameter and 0.46 mm thickness. FSR-400 is with the circular sensing area of 5.0 mm diameter and 0.30 mm thickness. Table 2.1 lists the general characteristics of FSRs manufactured by Interlink Electronics.

Although FSR shows less actuate than a load cell or strain gauge, we select FSRs for sensing force parameters inside the shoe due to their inexpensive price and thin thickness. Besides, within the relatively small force range, FSRs show approximate linearity response. In Fig. 2.4, the inverse of resistance, conductance, is plotted versus force in the range of 0-10kg. We simply use voltage divider to measure the resistance change of FSRs. After several experimental tests, it turns out that a 1KΩ resistor is suitable to be the upper resistor which are placed between the FSR-402 and the power supply (5V) in the voltage-divider, and 2.2KΩ resistor is suitable for the FSR-400 to be used in the voltage-divider. The implementation of either FSR-402 or FSR-400 obtains nearly the full range output of

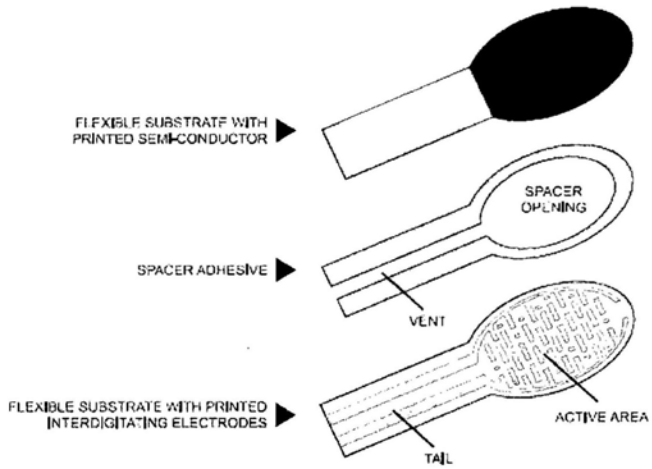

Figure 2.3: Force sensitive resistors by Interlink Electronics [25]

Table 2.1: General characteristics of Interlink FSRs [25]

Parameter	Value
Force Sensitivity Range	$<$ 100 g to $>$ 10 kg
Pressure Sensitivity Range	$<$ 0.1 kg/cm^2 to $>$ 10 kg/cm^2
Part-to-Part Force Repeatability	$\pm$15% to $\pm$25% of established nominal resistance
Single Part Force Repeatability	$\pm$2% to $\pm$5% of established nominal resistance
Force Resolution	Better than 0.5% full scale
Break Force	20 g to 100 g
Lifetime	$>$ 10 million actuations
Temperature Range	-30°C to +70°C

0-5V throughout humans' motion. The relationship between the FSR output, $Vout$, and the resistance of the FSR, R_{FSR}, is described by:

$$Vout = (\frac{R_{FSR}}{R_{FSR} + R}) \cdot V_{cc} \tag{2.1}$$

where R is the upper resistor, and V_{cc} is 5V power supply.

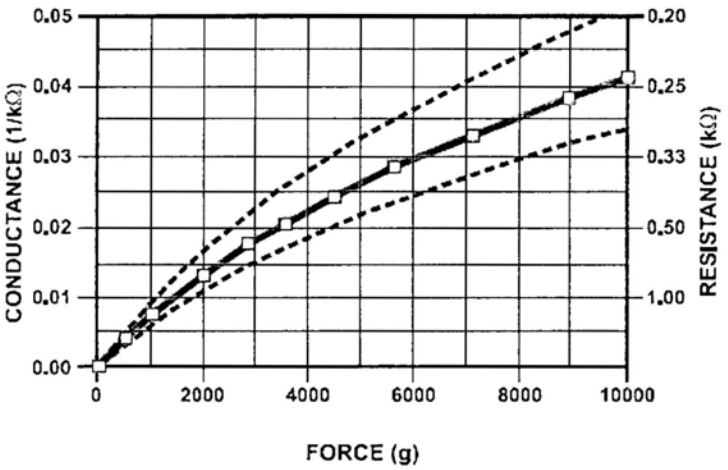

Figure 2.4: Conductance vs. force of Interlink FSR (0-10kg) [25]

2.2.2 Bend Sensor

Bend sensors, also called flexion sensors, measure the amount of deflection caused by bending the sensor. The bend sensor is characterized by an intrinsic resistance, when it is laid flat. For the uni-directional bend sensor, its resistance increases as the deflection increases in one direction, and is unchanged if bent happens in the opposite direction. We install one uni-directional bend sensor at the center of the insole for measuring the amount of flexion at the metatarsal-phalangeal joint. The output of the bend sensor contains rich information about human motion, especially the loading and uploading of feet.

The uni-directional bend sensor, FLX-01, manufactured by Images SI company [26], is 0.25" wide, 4.5" long, and 0.02" thick. An unflexed sensor has a nominal resistance of 10KΩ. As the sensor is bent in the sensitive direction, the resistance gradually increases. When the sensor is bent to 90 degrees (full deflection) in the sensitive direction, its resistance will range from 30KΩ to 40KΩ, shown as Fig. 2.5. Table 2.2 lists the general characteristics of FLX-01. The working characteristic of the bend sensor is similar to that of FSR. A voltage divider is used to measure the change in resistance of the bend sensor with the voltage-divider resistor set to 10KΩ.

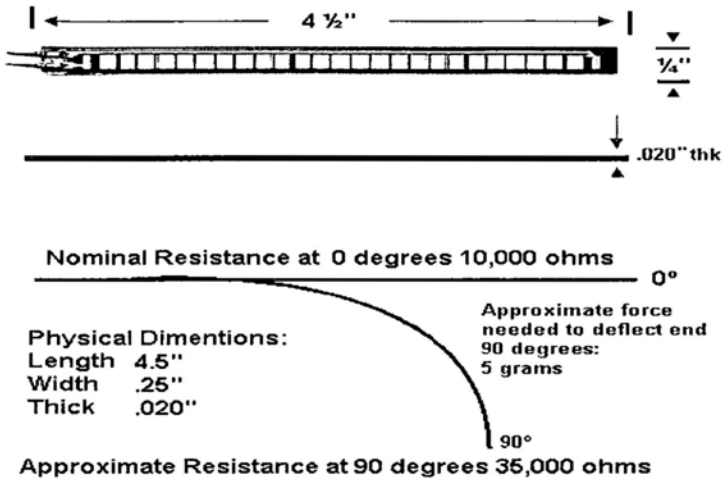

Figure 2.5: FLX-01 bend sensor (Images SI, Inc.) [26]

Table 2.2: General characteristics of FLX-01 (Images SI, Inc.)

Parameter	Value
Physical Dimensions	0.25" wide, 4.5" long, and 0.02" thick
Sensitivity Range	0 to 90 degrees
Operating Temperature	-45F to 125F

2.3 IMU Board

In biomechanics, kinematic data are important parameters for gait analysis, therefore, we design the Inertial Measurement Unit (IMU) as one of the essential parts for the whole system. Thanks to the development of MEMS technology, environmentally safe, mini-sized, and low-cost sensors are available. The IMU board (51×25×7 mm in size) mainly consists of two parts: the MEMS sensors and an analog-to-digital converter. We select three single-axis gyroscopes and one three-axis accelerometer to detect the angular rates and accelerations of foot motion for the X, Y, and Z axes. A 8-channel, 12-bit sampling analog-to-digital converter (ADC), ADS7844, manufactured by Texas Instruments, is used for transforming the analog voltage into the digital signal which is then transmitted to the

microprocessor for data packaging. Fig. 2.6 displays the photographs of the two sides of the IMU board. The left photo refers to the implementation of the 3D accelerometer, and the right one is relevant to the implementation for the 3D gyroscopes and AD conversion.

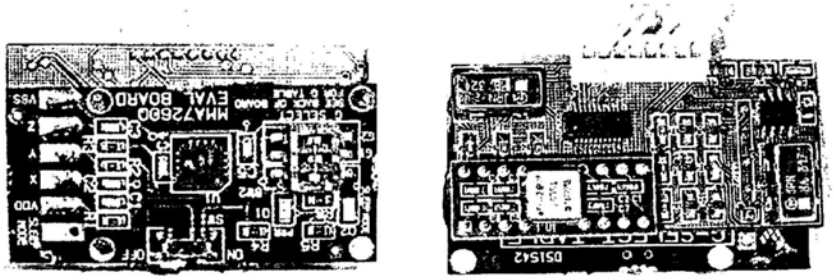

Figure 2.6: Photographs of the two sides of the IMU board

2.3.1 Accelerometer Sensor

To measure the 3D accelerations, a ±1.5-6g, three-axis accelerometer, MMA7260Q, manufactured by Freescale Semiconductor [27] is selected. The MMA7260Q is a low-cost surface-micromachined integrated-circuit accelerometer. This capacitive accelerometer has the features such as signal conditioning, a 1-pole low pass filter, temperature compensation, and g-Select which allows for selecting among 4 sensitivities. The sleep mode of this sensor makes it ideal for battery operated electronics for providing significant reduction of the operating current. Table 2.3 lists the general characteristics of MMA7260Q.

MMA7260Q is composed of two surface-micromachined capacitive sensing cells (g-cell) which can be modeled as a set of beams. The movable central beams located between fixed beams can be deflected from their neutral position when the system is subjected to acceleration. During the acceleration process, the distance from the movable center beams to one side fixed beams increases while the distance to the other side fixed beams decreases. Since the structure of beams is served as back-to-back capacitors whose capacitance will change along with the change of the distance between the beams resulted from acceleration, the difference between capacitances is then converted into voltage output which reflect the acceleration data.

Table 2.3: General characteristics of MMA7260Q [27]

Parameter	Value
Sensitivity	±1.5g/2g/4g/6g
Operation Voltage	2.2V−3.6V
Package Dimension	6 mm × 6 mm × 1.45 mm
Temperature Range	- 20 to +85°C
Low Current Consumption	500 μA
Sleep Mode	3 μA

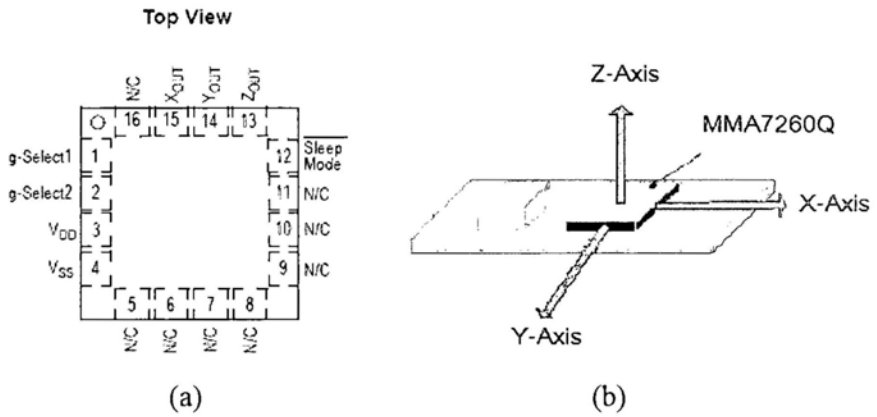

Figure 2.7: MMA7260Q 3-axis accelerometer (a) Pin connections [27] (b) Definitions of axes

MMA7260Q can measure not only dynamic acceleration, but also static acceleration resulting from gravity. Naturally, we utilize the gravitational acceleration to establish the relationship between the voltage output of the accelerometer and the acceleration unit, m/s^2. Each uniaxial signal is calibrated by measuring the outputs of +1g and -1g (g = 9.81m/s^2) under the control of rotating its sensitive axis orthogonal to the earth's surface and 180° rotation. During the rotation, the maximum and minimum values of voltage output are respectively corresponding to the values of V_{+g} and V_{-g}. The relationship between the voltage output, V_{output} (unit: V), and the Acceleration value, A (unit: m/s^2),

is described by:

$$V_{out} = V_{offset} + S \cdot A \tag{2.2}$$

In the above equation, the sensitivity, S (unit: V/m/s^2), is described as:

$$S = \frac{(V_{+g} - V_{-g})}{2g} \tag{2.3}$$

The zero offset, V_{offset} (unit: V), is defined as:

$$V_{offset} = \frac{(V_{+g} + V_{-g})}{2} \tag{2.4}$$

For each uniaxial sensor, we make six calibration tests, and for each test, eight full rotations are carried out to get eight pairs of maximum and minimum values. One full rotation means the rotation starts from the sensitive axis orthogonal to the earth's surface and ends at the sensitive axis orthogonal to the earth's surface again. The average results of the eight full rotations are regarded as the results for each calibration test.

2.3.2 Gyroscope Sensor

Two types of gyroscopes are selected to measure three-axis angular rates. They are the Analog Devices ADXRS150 [28] and the Murata ENC-03M [29]. The ADXRS150 is a yaw gyroscope which measures the rotation about the axis perpendicular to the top surface of the package. Clockwise rotation generates the positive voltage of the output. In contrast, the rotating axis of ENC-03M is parallel to the long side of the sensor. In order to measure three-axis rotation on one plane of circuit board, two ENC-03M gyroscopes (ENC-03MA and ENC-03MB) are placed perpendicularly to each other on the opposite corners of the board, with the ADXRS150 placed in the same plane. Fig. 2.8 displays the locations for the three gyroscopes on the circuit board.

Table 2.4 lists the relevant parameters of ADXRS150. The implementation of ADXRS150 is shown in Fig. 2.9. Since the electrostatic resonator is operated with 14 V to 16 V, the two capacitors C_1, C_2, and the decoupling capacitor C_3 specified as 22nF, 22nF, and 47nF,

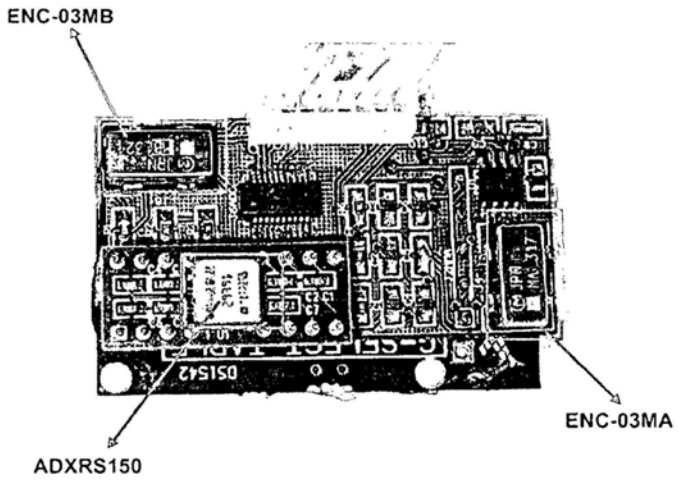

Figure 2.8: Top-side view of the PCB board for the 3D gyroscopes

respectively, are used for the charge pump to supply 16V power. Capacitors C_4 and C_5 set as 100nF are used to minimize the noise injection resulting from the charge pump. Capacitor C_6 of 100nF is utilized to limit high frequency artifacts ahead of the final amplification. The bandwidth limit capacitor, C_{out} (22 nF), is used to set for 40 Hz pass bandwidth.

Table 2.4: General characteristics of ADXRS150 [28]

Parameter	Value
Measurement Range	$\pm 150\ ^\circ/s$
Sensitivity	Min: 11.25 Type: 12.5 Max: 13.75 (mV/°/s)
Nonlinearity	0.1% of full scale
Rate Noise Density	$0.05\ ^\circ/\mathrm{s}/\sqrt{Hz}$
Initial Null	2.50 V
Frequency Response	40 Hz
Power Supply	Min: 4.75 Typ: 5.00 Max: 5.25 (V)
Package Dimension	7 mm × 7 mm × 3 mm

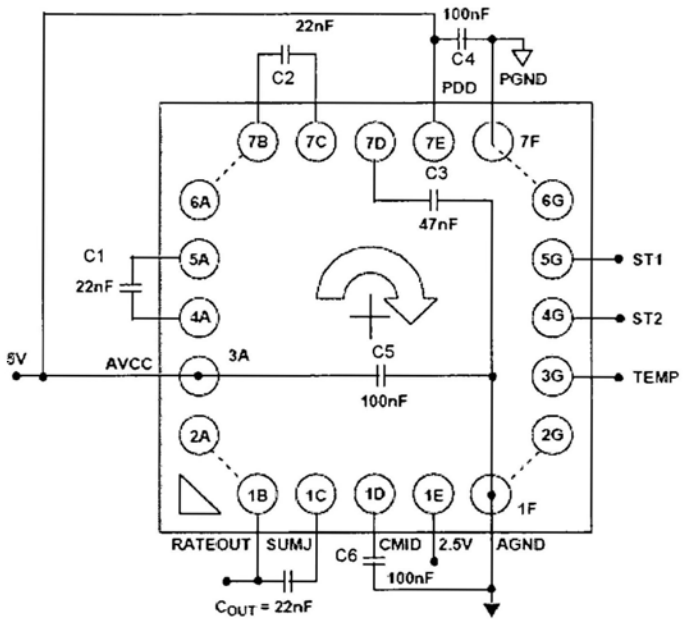

Figure 2.9: Application circuit of ADXRS150 yaw gyroscope [28]

The other type of angular velocity sensor we selected is ENC-03M which is a surface-mounted-device. ENC-03M detects angular velocity utilizing the Coriolis force and Murata's unique ceramic bimorph vibrating unit which extremely simplifies the equipment structure and circuit configuration. Two types of ENC-03M sensors are selected, ENC-03MA and ENC-03MB, which are in charge of detecting two axes angular velocities. Both of the two types have the same characteristics other than their resonant frequencies. Aiming to avoid resonant coupling happening between the two sensors, we use one ENC-03MA and one ENC-03MB instead of using two ENC-03MAs or two ENC-03MBs. The typical circuit for the implementation of ENC-03M is displayed in Fig. 2.10. In this circuit, the dashed borders represent the high-pass filter and low-pass filter respectively. In order to minimize bias drift, the high-pass filter is applied for cutting low-frequency components (<0.3 Hz), and the low-pass filter is used for suppressing high-frequency components (>1K Hz) which result in output noise. Table 2.5 lists the characteristics of ENC-03M gyroscope.

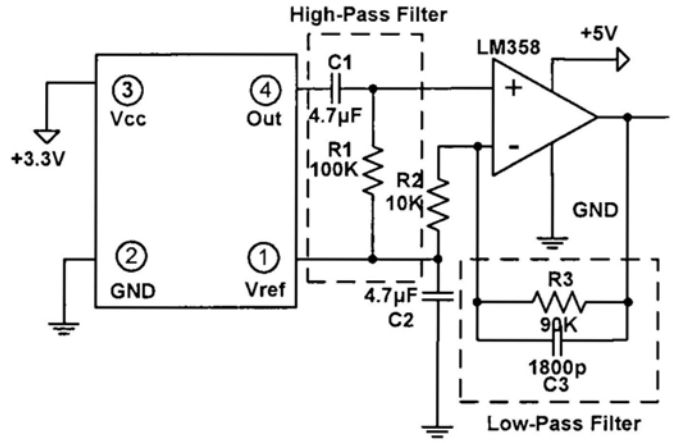

Figure 2.10: Implementation of ENC-03M gyroscope

Table 2.5: General characteristics of ENC-03M gyroscope [29]

Parameter	Value
Measurement Range	$\pm 300°/s$
Linearity	$\pm 5\%$ of full scale
Scale Factor	0.67mV/°/s
Initial Null	1.35 V
Frequency Response	50 Hz
Operating Temperature Range	-5°C to 75°C
Power Supply	2.7-5.25V
Package Dimension	12.2 mm × 7.0 mm × 2.6 mm
Weight	0.4 g

2.4 Microprocessor-Based Data Gathering Subsystem

The microprocessor-based data gathering subsystem controls the collection and transmission of the data gathered from the insole and IMU. Fig. 2.11 shows the subsystem attached to a battery. It mainly includes a microprocessor and peripheral components (resisters, capacitors, etc.). The low-power and high-performance 8-bit AVR microprocessor,

ATmega16L, manufactured by Atmel Corporation is selected. The 44-lead ATmega16L is with Thin Profile Plastic Quad Flat Package (TQFP) of 10 mm × 10 mm body size and 1.0 mm body thickness. The microprocessor runs at a clock frequency of 8 MHz with the typical operating voltage of +5 V. In our design, one 7.4 V/Li-ion cell phone battery is used as the power supply due to its long life cycles and compact size. The positive regulator, LM78L05, is applied for converting the power supply to the fixed output of +5 V. We use ADC channels with 10-bit resolution to transform the analog voltage signal generated from the FSRs and bend sensor into digital data.

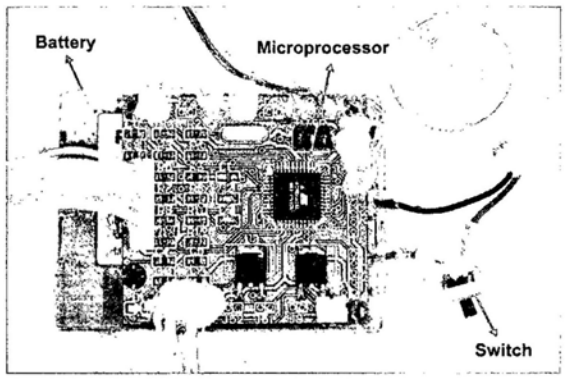

Figure 2.11: Photo of the Microprocessor-Based Data Gathering Subsystem

2.5 Wireless Communication Subsystem and System Interface

2.5.1 Wireless Communication Subsystem

The aim of this subsystem is to wirelessly transfer the digital data processed by the ATmega16L to the host computer in realtime. There were two major transfer methods of previous in-shoe data acquisition systems. One was to restore the original information in FLASH RAM and then download the data to PC after the gait trial through a parallel port for further analysis [18]. The other method was to transmit the data immediately via the RS232 serial port [13]. Both approaches introduce few transmission errors which

make the analysis result relatively stable. Despite this, there are some limitations. For the former, it is impossible to monitor human motion and provide the feedback in realtime. For the latter, the wire between the data acquisition system and the host computer makes it difficult to perform detection in a relatively large space.

In our system, the small amount of digital data makes it possible to use wireless transmission with a high sampling rate. Thus, a pair of low-power radio frequency (RF) communication modules, GW100B, manufactured by Unitel Pty Ltd. are selected. The operating frequency of GW100B is adjustable for 16-channel from 414.995MHz to 444.061MHz. The band rate can be adjusted from 1200bps to 19200bps. The GW100B is in the size of 56×27.5×12 mm, with the operating distance up to 300m in the outside space. The GW100B supports both RS232 and TTL interface. Therefore, the RF transmitter and receiver are connected with the microprocessor and the host computer directly. Additionally, the Forward Error Correction (FEC) processing of GW100B allows for a low Bit Error Ratio (BER), which enhances the whole system reliability. The photography of GW100B wireless module is displayed in Fig. 2.12.

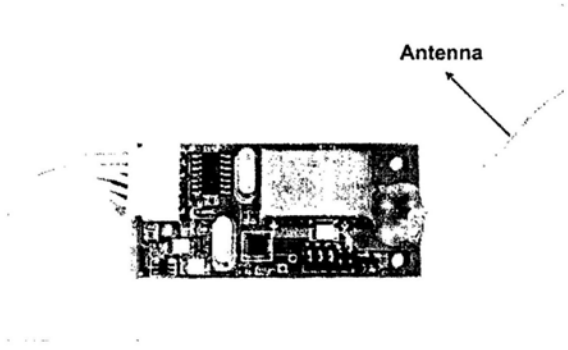

Figure 2.12: Photography of GW100B wireless communication module

2.5.2 System Interface

A friendly interface has been developed for displaying the corresponding sensor information acquired by the shoe-integrated system via wireless communication (Fig. 2.13). The received data is stored and displayed in real-time on the screen of the host computer.

This visual interface can be used for further applications.

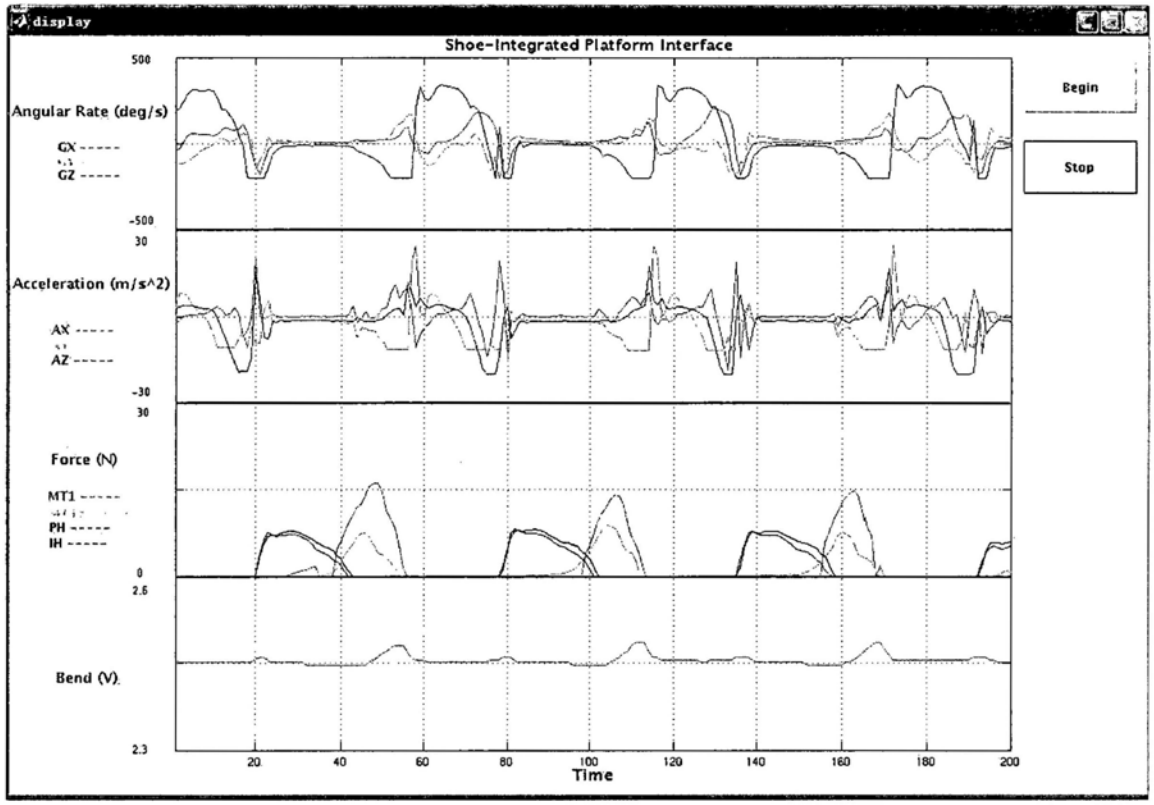

Figure 2.13: Real-time interface for displaying sensors' output

2.6 Summary

In this chapter, we present the design of the shoe-integrated platform. The implementation of the main subsystems, including the insole, the Inertial Measurement Unit (IMU), the microprocessor-based data gathering board, and the wireless communication module are described respectively. Considering the fundamental requirements of the platform design, the compact and lightweight sensors and electronics are selected as the components for each subsystem. The whole system is compact and light so that it is easily integrated with a user's shoes and he/she will notice little if any difference between his/her normal

shoes and the proposed intelligent shoes. Wireless communication based on radio frequency (RF) makes it possible to capture and analyze human gait in a relatively extensive environment. The shoe-integrated system we designed is an ideal platform for studying human motion abnormalities by modeling abnormal motions which will be discussed in the following chapters.

Chapter 3

Gait Pattern Classification

3.1 Introduction

As one of the most common daily activities, walking motion has been studied extensively. Monitoring ambulatory patterns is of significance, especially for children and elders. Some adolescents are with the problem of inappropriate walking habits, resulting in skelecton deformities. Most elders face the risk of falling which has become the potential killer for them in recent years. Assessment of different gait patterns of daily living could provides useful information in studying one individual's stability and mobility during locomotion. As the foundation of better assessment for different gait patterns, the ability to automatically identity different patterns and walking surroundings provides valuable information for further understanding the relations between gait pattern and energy consumption. Classification of gait patterns in daily activity is also helpful for evaluating the amount of daily exercise especially for elders. Besides, the ankle-foot orthotic device, which is designed for the patients of foot problems, can work better with the ability to understand the gait pattern with which the individual is walking.

In our daily activities, most of the gait patterns are related to flat walking, descending stairs, and ascending stairs. Therefore, classification of gait patterns including flat

walking, descending stairs, and ascending stairs is the primal ability for the gait pattern classification system we proposed. Several studies have been proposed for gait pattern classification. Wervey et al. studied the plantar pressure characteristics of level walking, stair climbing, and stair descent using force sensing resistors [30]. Considering kinematic signals provide useful information for estimating energy expenditure, the kinematic sensors were selected by most researchers to monitor different gait patterns. Mäntyjärvi et al. used acceleration sensors to investigate the use of principal component analysis (PCA) and independent component analysis (ICA) with wavelet transform for feature generation in the problem of human activity recognition [31]. Sekine et al. studied the walking patterns by using the wavelet-based fractal analysis method based on a triaxial accelerometer unit attached on the subject's back [32]. Nyan et al. classified gait patterns in the time-frequency domain by installing the vertical and anteroposterior accelerometers on the shoulder position of a garment [33].

In this chapter, we aim to study and classify gait patterns among flat walking, descending stairs, and ascending stairs using Inertial Measurement Unit (IMU) including triaxial accelerometers and gyroscopes. Different from the previous works, the kinematic sensors are fixed on the surface of a shoe which provides the method for studying the kinematic characteristics of foot with different gait patterns. Besides, the shoe-integrated system realizes the non-intrusive monitoring without attaching any hardware onto the body. Discrete wavelet transform (DWT) is applied for generating and extracting the useful features for our application. Based on the generated features, fuzzy logic based classifier is designed with the membership functions and rules associated with the distribution of selected features. Experimental results demonstrate the proposed methodology is efficient for classifying gait patterns during humans' daily activity.

This chapter is organized as follows. In Section 3.2 and 3.3, the architecture of the shoe-integrated system and the experimental design for gait pattern classification are introduced. We describe the proposed methodology of how to extract gait segments, apply DWT for feature generation and reduction, as well as design fuzzy logic based classifier in Section 3.4. Experimental results are discussed in Section 3.5. We draw the summary of

this chapter in the final Section.

3.2 Measurement System

Fig. 3.1 shows the system architecture, including Inertial Measurement Unit (IMU) board, microprocessor-based data gathering module, and wireless communication subsystem. The whole system is compact and lightweight so that it is easily integrated with the individual's own shoe.

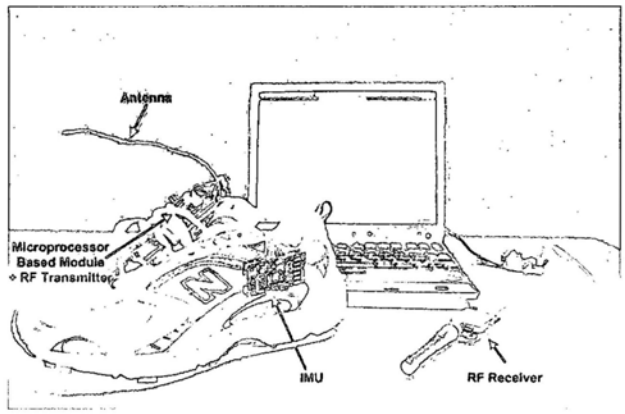

Figure 3.1: Experimental set-up

Kinematic data are important parameters for gait analysis, therefore, we design the IMU board as one of the most essential parts of the system for gait pattern classification. The 3-axis acceleration sensor MMA7260Q (Freescale Semiconductor) is selected due to its low power, high sensitivity with low noise, and small package. Each uniaxial signal is calibrated by measuring the outputs of $+1g$ and $-1g$ ($g = 9.81m/s^2$) under the control of positioning its sensitive axis orthogonal to the earth's surface and 180° rotation. Two types of angular rate sensors are utilized for our application. They are Analog Devices ADXRS150 gyroscope and the Murata ENC-03M gyroscope. The ADXRS150 is a yaw gyroscope which measures the rotation about the axis perpendicular to the plane of the sensor. In contrast, the rotating axis of ENC-03M is parallel to the long side of the sensor. In order to measure three-axis rotation on one plane of circuit board, two ENC-03M

(ENC-03MA and ENC-03MB) gyroscopes are placed perpendicularly to each other, with the ADXRS150 placed in the same plane.

The IMU is connected to the microprocessor-based data gathering module which includes a low-power and high-performance 8-bit AVR microprocessor-ATmega16L, peripheral components (resisters, capacitors, etc.), and one battery. In the IMU board, the analog-to-digital converter (ADS7844, Texas Instruments) is used for transforming analog voltage generated from IMU into digital data. Furthermore, these digital data are packaged via microprocessor-based data gathering module which effectively decreases the transmission error and increases the sampling frequency.

In our system, the small amount of digital data makes it possible to use wireless communication at a high sampling rate of 100 Hz. Thus, a low-power radio frequency (RF) communication module, GW100B, is selected for realizing wirelessly transmission in realtime. The RF transmitter and receiver are connected with the microprocessor and a laptop respectively.

3.3 Experimental Design

The experiments were performed on six subjects (four females and two males) with age between 24 and 31 years. Their heights and weights are ranged from 1.62 to 1.74 m, and 50 to 65 kg. The IMU is securely attached to the side of the (right) shoe with glue in order to ensure the fastness and consistency of the sensors' sensitive axes during the experiments. The IMU location and reference axes & planes for the acceleration sensor & gyroscopes are shown as Fig. 3.2. According to the sensor placement, the x-axis of the accelerometer records acceleration signals regarding the anteroposterior movement; the y-axis records the vertical movement; and the z-axis records the lateral movement. The ADXRS150 is applied to measure the angular rate of the foot in the sagittal plane. The sensitive axes of ENC-03MA and ENC-03MB gyroscopes are perpendicularly to the transverse and coronal planes respectively.

Gait pattern data were recorded for each subject wearing the integrated shoe in three steps. In the first step, they were asked to walk continuously under outside environment

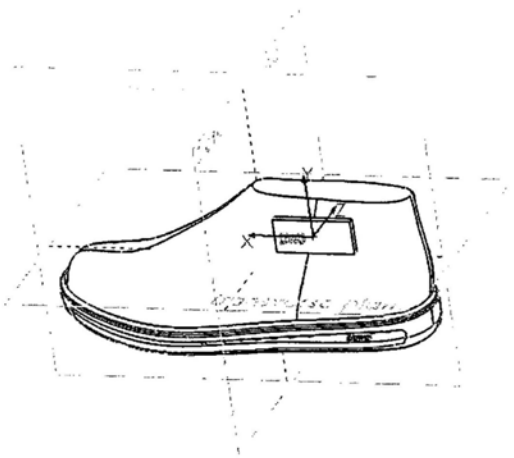

Figure 3.2: IMU location and reference axes & planes for accelerometers & gyroscopes

on the flat ground at their own selected walking speeds. In the second step, the subjects walked down the staircases at a slope of 34° continuously. In the last step, they walked up the same staircases as the second step.

3.4 Methodology

3.4.1 Gait Segments Separation

In order to detect which gait pattern the coming signal belonged to, firstly, we separate gait signals into gait segments which are further used as the units for gait pattern classification. Based on the knowledge of gait, in order to provide basic functions and minimize required energy, all locomotion of horizontal walking, stair ascending, and stair descending involves the gait event called "foot flat". During the foot-flat period, the foot is with its entire length in contact with the ground, which results in the moment of all the kinematic sensors keeping the faint change. Therefore, we define the gait signal between the consecutive two foot-flat periods as the gait segment. The problem of separating gait segments is transformed into how to well define "foot-flat period".

As mentioned in section 3.3, each subject used free speed to finish the gait patterns of flat walking, stair ascending, and stair descending. Besides, even for the same gait pattern,

they were not required keeping the regular speed. On this condition, it is unreasonable to define the uniform length of the foot-flat period based on the experience. To solve this problem, firstly, the data of x-axis acceleration are low-pass filtered, with 10-order Butterworth coefficients and 10Hz cutoff frequency. We extract the symbol points (e.g. the peaks) of each gait cycle (shown as Fig. 3.3). The distance between each two consecutive peaks is defined as the factor of length (FOL) changing along with different subjects, different patterns, or different speeds.

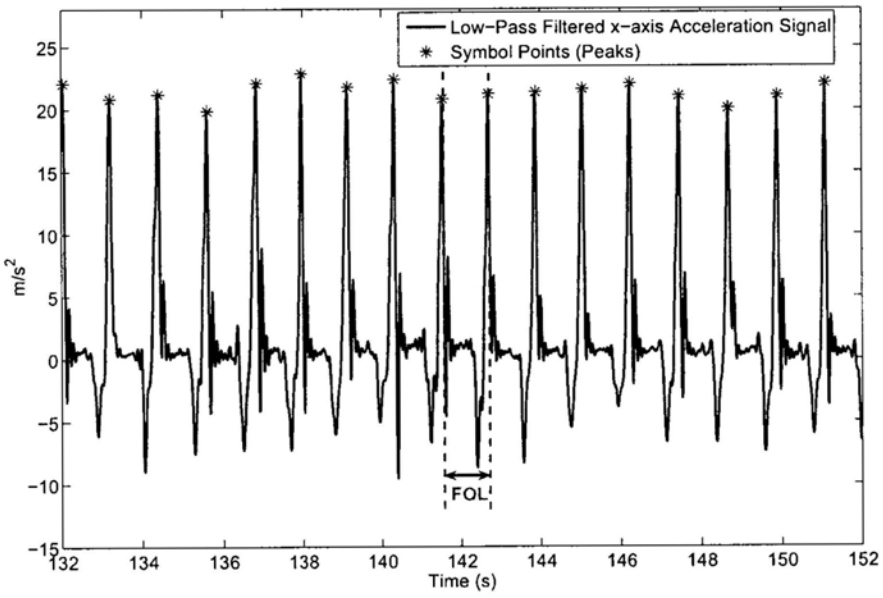

Figure 3.3: Symbol points extraction

During the period of each two consecutive symbol points, the successive gait sampling points of which the amplitudes vary in a small range and the data length is more than 1/5 of FOL are selected. The center of the above selected segment is regarded as the center of the foot-flat segment. The start point of the foot-flat segment is 1/6 length of FOL ahead of the center, and the end point is 1/6 length of FOL after the center point. The start and end points of each foot-flat segment are applied as the reference points of gait segment separation for each of the six sensor signals. Fig. 3.4 shows the results of separating gait

segments for one subject's flat walking pattern. All of the six sensor signals are low-pass filtered with 30 Hz cutoff frequency.

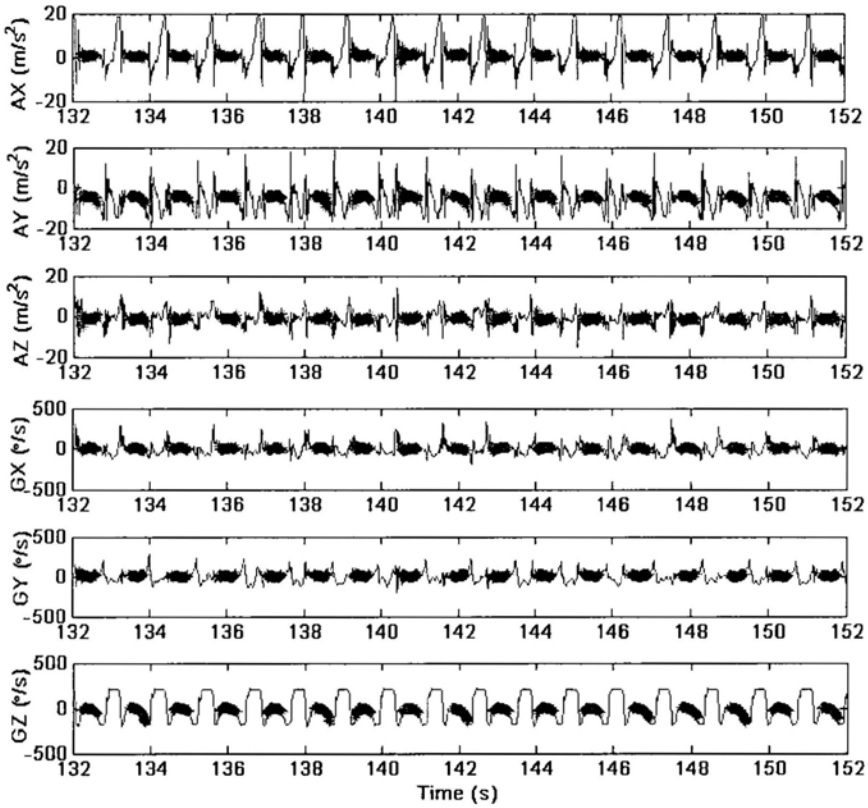

Figure 3.4: Results of separating gait segments for one subject's flat walking. Red points denote the foot-flat periods. The blue curves between each two consecutive foot-flat periods are gait segments

3.4.2 Discrete Wavelet Transform Based Feature Extraction

Discrete Wavelet Transform Theory

Wavelet decomposition in the application of signal feature reduction and extraction has been proved as an useful tool in the field of gait analysis [34] [35]. Compared with frequency-based approaches, such as Fourier transform, wavelet transform shows main advantage of illuminating both frequency and time domain information simultaneously.

Using wavelet decomposition, it is possible to describe and extract localized signal features as well as the global characteristics.

Discrete wavelet transform (DWT) decomposes the original signal $s(t)$ into the approximations $a_j(k)$ and the details $d_j(k)$ which relies on scaling function $\varphi_{j,k}(t)$ and wavelet function $\psi_{j,k}(t)$, respectively:

$$\varphi_{j,k}(t) = 2^{-j/2}\varphi(2^{-j}t - k) \tag{3.1}$$

$$\psi_{j,k}(t) = 2^{-j/2}\psi(2^{-j}t - k) \tag{3.2}$$

Here, j represents the scaling factor which controls the compression or dilation for both scaling function φ and wavelet function ψ. The shifting parameter k denotes the position shifting along the time axis.

The approximations and details of DWT are then defined as follows:

$$a_j(k) = \int s(t)\varphi_{j,k}(t)dt \tag{3.3}$$

$$d_j(k) = \int s(t)\psi^*_{j,k}(t)dt \tag{3.4}$$

where the operator $(*)$ indicates the complex conjugate.

Therefore, the original signal $s(t)$ can be reconstructed by the sum of the approximation at the depth of decomposition level J and the details from level 1 to level J:

$$s(t) = \sum_{k\in Z} a_J(k)\varphi_{J,k}(t) + \sum_{k\in Z}\sum_{j=1}^{J} d_j(k)\psi_{j,k}(t) \tag{3.5}$$

Since the wavelet function ψ and scaling function φ are determined by the high-pass and low-pass filters respectively, the DWT can be efficiently implemented by iteratively convolving the signals with a pair of high-pass and low-pass finite impulse response filters denoted as $g(n)$ and $h(n)$. The outputs of the filters are then downsampled by 2.

$$a_j(n) = \sum_{k\in Z} a_{j-1}(k)h(k - 2n) \tag{3.6}$$

$$d_j(n) = \sum_{k\in Z} a_{j-1}(k)g(k - 2n) \tag{3.7}$$

Table 3.1: Kinematic parameter definition

i	Kinematic Parameter
1	Anteroposterior Acceleration
2	Vertical Acceleration
3	Lateral Acceleration
4	Sagittal Plane Angular Rate
5	Transverse Plane Angular Rate
6	Coronal Plane Angular Rate

Feature Extraction

For each gait pattern, every extracted gait segment for each kinematic parameter at the same period is decomposed into six scales by haar mother wavelet. The average sum of squares of approximation coefficients at level 6 ($E^i_{a_6}$) and the detail coefficients from level 1 to level 6 ($E^i_{d_j}$ $j = 1, 2, 3, ..., 6$) are composed as the candidate feature vector T^i for the parameter i (listed as Table 3.1):

$$T^i = [\ E^i_{a_6},\ \ E^i_{d_6},\ \ E^i_{d_5},\ \ E^i_{d_4},\ \ E^i_{d_3},\ \ E^i_{d_2},\ \ E^i_{d_1}\ ] \tag{3.8}$$

$$E^i_{a_6} = \frac{\sum_{k=1}^{n_0} \left[a^i_6(k)\right]^2}{n_0} \tag{3.9}$$

$$E^i_{d_j} = \frac{\sum_{k=1}^{n_j} \left[d^i_j(k)\right]^2}{n_j}, j = 1, 2, 3, ..., 6 \tag{3.10}$$

where n_0 represents the number of the approximation coefficients at level 6, n_j denotes the number of the detail coefficients at level j.

By observation, from all the candidate features, the obvious features are selected as the common ones for representing the characteristics of the gait patterns that we study.

They are $E^1_{a_6}$ (the average sum of squares of approximation coefficients at level 6 for the Anteroposterior Acceleration), $E^1_{d_6}$ (the average sum of squares of detail coefficients at level 6 for the Anteroposterior Acceleration), $E^2_{d_6}$ (the average sum of squares of detail coefficients at level 6 for the Vertical Acceleration), $E^4_{a_6}$ (the average sum of squares of approximation coefficients at level 6 for the Sagittal Plane Angular Rate), $E^4_{d_5}$ (the average sum of squares of detail coefficients at level 5 for the Sagittal Plane Angular Rate), and $E^4_{d_2}$ (the average sum of squares of detail coefficients at level 2 for the Sagittal Plane Angular Rate). Fig. 3.5 to Fig. 3.10 display the normalized distribution of each selected feature for the gait patterns of flat walking, descending stairs, and ascending stairs.

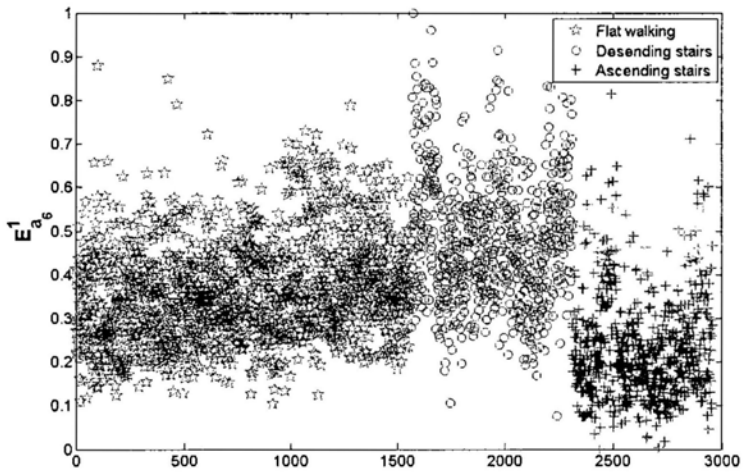

Figure 3.5: Normalized $E^1_{a_6}$ for flat walking, descending stairs, and ascending stairs from the six subjects and their relationship in classification

3.4.3 Fuzzy Logic Classifier

Based on the selected features, a simple approach for gait pattern classification is the threshold-based method. However, considering the number of selected features and the overlap of distribution region happening for some features, fuzzy logic provides a suitable method for feature fusion and generates the classifier for our propose.

For designing the fuzzy logic classifier, two major problems are considered: 1) how to determine the degree of which input features belong to each of the predefined linguistic

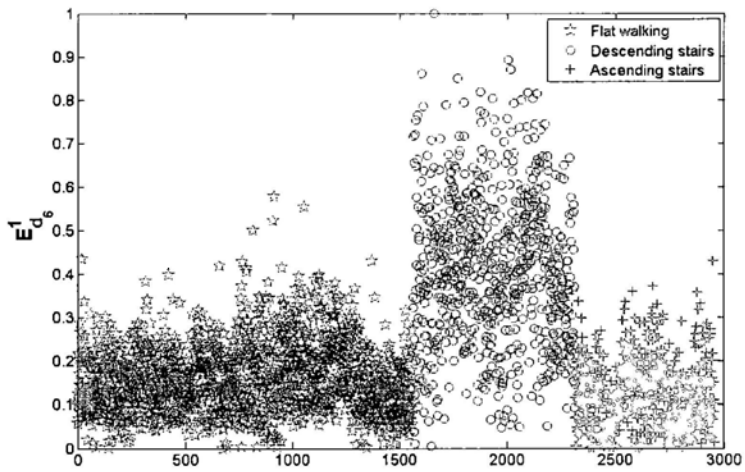

Figure 3.6: Normalized $E^1_{d_6}$ for flat walking, descending stairs, and ascending stairs from the six subjects and their relationship in classification

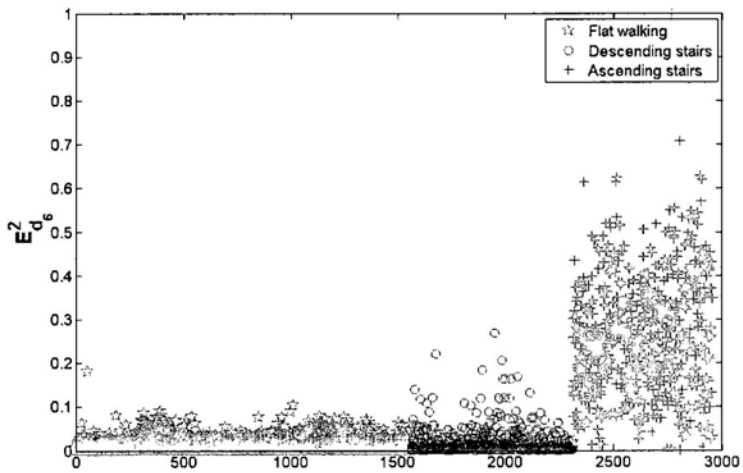

Figure 3.7: Normalized $E^2_{d_6}$ for flat walking, descending stairs, and ascending stairs from the six subjects and their relationship in classification

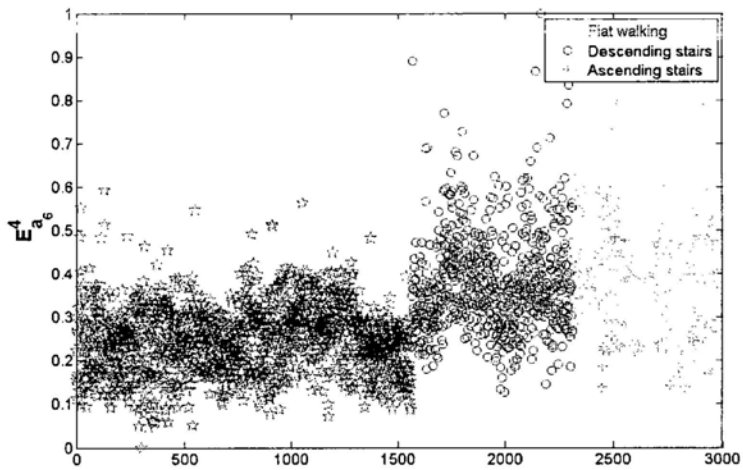

Figure 3.8: Normalized E^4_{a6} for flat walking, descending stairs, and ascending stairs from the six subjects and their relationship in classification

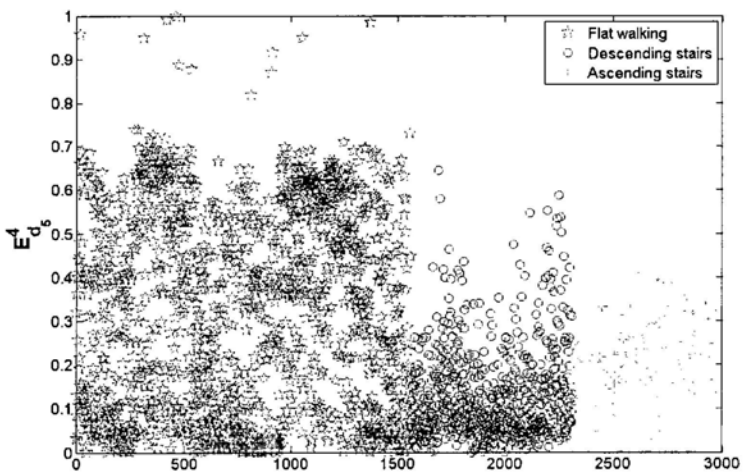

Figure 3.9: Normalized E^4_{d5} for flat walking, descending stairs, and ascending stairs from the six subjects and their relationship in classification

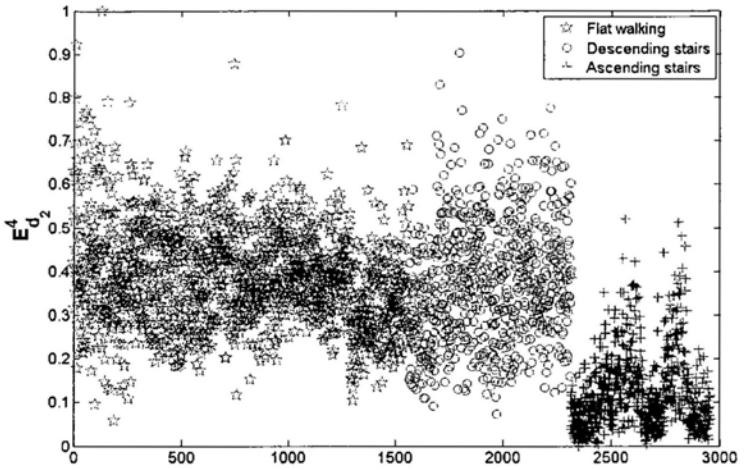

Figure 3.10: Normalized $E^4_{d_2}$ for flat walking, descending stairs, and ascending stairs from the six subjects and their relationship in classification

variables ("low" and "high") and 2) how the classification rules are defined and interpreted in programmable logic.

Membership Function

Solving the first question is equivalent to design the membership functions (MFs) for each input. For our problem, each input has two MFs displayed as Fig. 3.11. Table 3.2 lists the types of membership functions applying for each input. Based on the understanding of the feature distributions in Fig. 3.5 to Fig. 3.10, two kinds of membership functions are applied i.e. Z-shaped membership function ($z - shaped$) and two-sided Gaussian curve membership function ($Gaussian2$). Z-shaped membership function describes the asymmetrical polynomial curve expressed as (3.11):

$$f^{zmf}(x) = \begin{cases} 1, x \leq a \\ 1 - 2(\frac{x-a}{a-b})^2, a < x \leq \frac{a+b}{2} \\ 2(\frac{b-x}{a-b})^2, \frac{a+b}{2} < x \leq b \\ 0, x \geq b \end{cases} \tag{3.11}$$

Table 3.2: Membership functions for inputs

Input No.	MF 1 (low)	MF 2 (high)
1	*Gaussian2*	*Gaussian2*
2	$z-shaped$	*Gaussian2*
3	$z-shaped$	*Gaussian2*
4	*Gaussian2*	*Gaussian2*
5	$z-shaped$	$z-shaped$
6	$z-shaped$	*Gaussian2*

where the parameter a is the threshold value smaller than which the degree of membership is equal to 1 and larger than which the degree begins to decline. The parameter b locates the position from where the degree reaches the minimum zero.

Two-sided Gaussian membership function depends on two Gaussian functions which are denoted as (3.12) and (3.13):

$$f_1^{gmf}(x) = e^{\frac{-(x-c_1)^2}{2\sigma_1^2}} \tag{3.12}$$

$$f_2^{gmf}(x) = e^{\frac{-(x-c_2)^2}{2\sigma_2^2}} \tag{3.13}$$

The first function specified by the parameters c_1 and σ_1 decides the left-most shape of the two-sided Gaussian membership function. The second one specified by c_2 and σ_2 determines the right-most shape. If c_1 is smaller than c_2, the degree of the membership function is at unity (1.0) in case the interval is between c_1 and c_2. Otherwise, the membership value is the product of the two Gaussian functions.

Rule

If-then rules are established to formulate the conditional statements of fuzzy logic classifier. The "if" part of rules describes the inputs' situations. The corresponding "then"

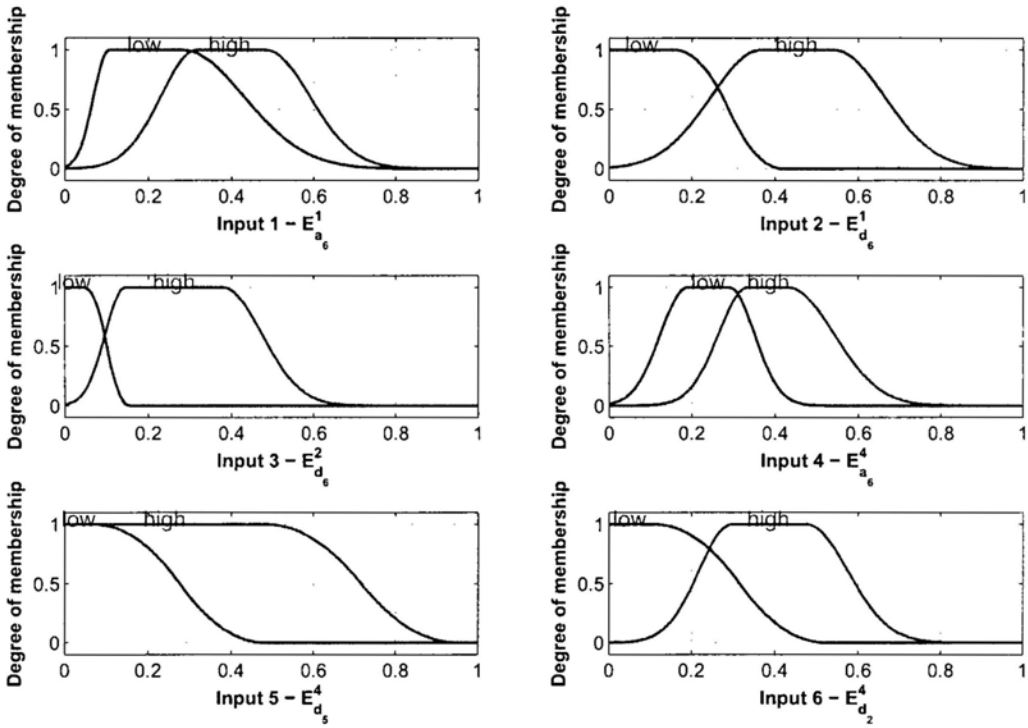

Figure 3.11: Input membership functions

Table 3.3: If-then rules

IF						THEN
$E^1_{a_6}$	$E^1_{d_6}$	$E^2_{d_6}$	$E^4_{a_6}$	$E^4_{d_5}$	$E^4_{d_2}$	Gait Pattern
high	low	low	low	high	high	Flat Walking
high	high	low	high	low	high	Descending
low	low	high	high	low	low	Ascending

part describes the fuzzy system's output in these situations. A set of rules for classifying gait patterns are listed in Table 3.3. For example, If $E^1_{a_6}$ is in the range of 'high', $E^1_{d_6}$ is 'low', $E^2_{d_6}$ is 'low', $E^4_{a_6}$ is 'low', $E^4_{d_5}$ is 'high', and $E^4_{d_2}$ is 'high'; then the human is with the locomotion of 'flat walking'.

3.5 Experimental Results

We classify gait patterns into flat walking, descending stairs, and ascending stairs based on the fuzzy logic classifier we propose. The detailed classification results for all the six subjects are listed in Table 3.4. The classifier's performance is evaluated using the common measures: sensitivity (Se) and specificity (Sp):

$$Se = \frac{TP}{TP + FN} \tag{3.14}$$

$$Sp = \frac{TN}{TN + FP} \tag{3.15}$$

In the above equations, TP, FN, TN, and FP denotes the number of true positives, false negatives, true negatives, and false positives, respectively. Take the sensitivity and specificity of "Flat Walking" for example, TP is equivalence to the number of segments for flat walking that are correctly classified as flat walking. Whereas, FN is the number of segments for flat walking which are wrongly assigned as the other two classes (descending or ascending stairs). TN is equal to the number of segments for the other two classes that are correctly identify as the corresponding class. Whereas, FP represents the number of segments for the other two classes which are incorrectly assigned as flat walking.

Table 3.4: Classification results

	Flat Walking			Descending Stairs			Ascending Stairs		
Subject No.	Segment	Se (%)	Sp (%)	Segment	Se (%)	Sp (%)	Segment	Se (%)	Sp (%)
1	271	90.04	98.03	123	96.75	93.27	135	96.30	98.91
2	275	98.18	97.64	143	96.50	97.98	71	97.18	100
3	207	92.75	97.48	126	94.44	92.42	123	91.87	99.68
4	195	88.21	94.53	111	85.59	92.07	95	100	98.16
5	345	96.52	94.06	119	91.60	94.09	115	84.35	100
6	270	97.78	90.58	127	84.25	95.99	105	90.48	100
Total	1563	-	-	749	-	-	644	-	-
Avg.	260	93.91	95.38	124	91.52	94.30	107	93.36	99.45

Sensitivity denotes the ability of the classifier that can successfully recognize the segments of a certain class without wrongly treated them as another ones. Only sensitivity is not enough to demonstrate the performance of the classifier. The measure of specificity is needed to represent how well the classifier can predict other classes.

As listed in Table 3.4, for the six subjects, the overall gait segments of flat walking, descending stairs, and ascending stairs are 1563, 749, 644, respectively. It is found that the average sensitivity is 93.91% for flat walking segments, 91.52% for descending segments, and 93.36% for ascending segments. While the values of specificity are 95.38% for flat walking segments, 94.30% for descending segments, and 99.45% for ascending segments. Except for the six subjects whose gait data were analyzed for designing the fuzzy logic classifier, another four subjects were invited to evaluate the performance of the system. Table 3.5 lists the classification results of the four test subjects.

3.6 Summary

In this chapter, we study human gait patterns and design a classifier for identifying gait patterns among flat walking, descending stairs, and ascending stairs based on continuous kinematic signals. Firstly, gait signals of the six sensors in the same period are separated into gait segments which are further used as the units for pattern feature

Table 3.5: Classification results for the test subjects

	Flat Walking			Descending Stairs			Ascending Stairs		
Subject No.	Segment	Se (%)	Sp (%)	Segment	Se (%)	Sp (%)	Segment	Se (%)	Sp (%)
1	183	91.80	96.88	115	93.91	94.22	112	97.32	99.64
2	245	90.61	92.83	140	86.43	91.12	93	92.47	99.13
3	257	94.16	97.07	144	93.75	95.88	134	97.01	98.95
4	229	91.70	98.16	123	96.75	92.40	101	93.07	99.70
Total	914	-	-	522	-	-	440	-	-
Avg.	228	92.06	96.23	130	92.71	93.40	110	94.96	99.35

analysis. We apply discrete wavelet transform (DWT) for feature generation and fuzzy logic based approach for designing the multi-class classifier. Anteroposterior acceleration, vertical acceleration, and sagittal plane angular rate are demonstrated to provide useful information for classifying the gait patterns on which we focus, and the other kinematic parameters are almost useless. Experimental results of the six training and four testing subjects demonstrate that the selected features of the average sum of squares of wavelet coefficients efficiently represent the characteristics of the gait patterns we study. Also fuzzy logic based classifier well describes the distribution of the features. The compact, wireless, and wearable system has the promising application for assisting to evaluate walking energy expenditure.

Chapter 4

Postural Kyphosis Detection

4.1 Introduction

Kyphosis generally refers to an increased curvature of the thoracic spine in the sagittal plane. Long-term kyphosis will result in thoracic deformity accompanied by pain. Since spine is of a consecutive multi-segmented structure, kyphosis can affect not only the thoracic spine, but also the cervical (upper) and lumbar (lower) spine. The exaggerated curves of cervical and lumbar spine happen in the inward direction to compensate for the increased outward curve in the thoracic spine.

To be one of the most common types of kyphosis, postural kyphosis is mainly attributed to slouching posture. Different from Scheuermann's kyphosis, postural kyphosis presents a smooth curvature while the patient bends forward. Postural kyphosis is usually diagnosed in adolescents and young adults. The traditional treatment for postural kyphosis is with education of proper posture and suitable exercises to strengthen the back and abdomen muscles so as to support proper posture. After long-term postural training, postural kyphosis will be effectively corrected and lead to no problem in the patients' future life.

Keeping proper posture in daily life is the key to amend postural kyphosis. However, few adolescents can self-consciously correct their slouching posture. In this condition, the

brace is introduced for curve correction which is custom-made for each patient. Besides, E. Lou et al. introduced a garment including two 3-axis accelerometers to monitor the kyphosis angle and provide vibration feedback to children [36]. The limitation for both brace and garment approaches is to affect the upper body appearance so as to make patients feel uncomfortable during the wearing process. Based on the study of plantar pressure for human walking, the plantar pressure distribution will shift along with the increase of curvature for the thoracic spine. That is to say, gait analysis especially based on plantar pressure provides an indirect approach for detecting postural kyphosis. We propose an intelligent shoe-integrated system from which the pressure information derived can give efficient assistance in determining and alarming the persons associated with postural kyphosis. Fig. 4.1 displays the postures of slouching and proper walking.

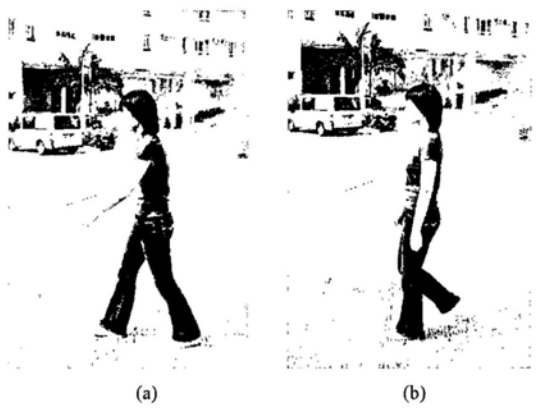

Figure 4.1: (a) Slouching walking (b) Proper walking

In this chapter, a cost-effective shoe-integrated system for detecting postural kyphosis is introduced. Eight FSRs are used for gathering the pressure information under the eight bony prominences of each foot. Based on the gathered plantar pressure information, the methodology of Cascade Neural Networks with Node-Decoupled Extended Kalman Filtering (CNN-NDEKF) is applied for training the model of detecting the gait pattern associated with postural kyphosis.

This chapter is organized as follows. In Section 4.2, the measurement system based on the architecture of the shoe-integrated system is briefly introduced and the methodology

for detecting postural kyphosis is described. Experimental results are discussed in Section 4.3. We draw the summary of this chapter in the final section.

4.2 Methodology

4.2.1 Measurement System

The measurement system includes three major components: insole, microprocessor-based data gathering module, and wireless communication subsystem.

Insole subsystem is a flexible instrumented part for sensing the force parameters inside the shoe. Eight FSRs (Interlink Electronics, Santa Barbara, CA) are installed on one side of a thin insole under subcutaneous bony prominences: 1-5 metatarsal heads, hallux (big toe) and the heel (which is divided into a posterior and inside portion). Considering the different sizes of bony prominences, we select two kinds of FSRs. Two FSR-402s are used in the first metatarsal head and hallux. Six FSR-400s are placed under the other positions. FSR is a type of polymer thick film (PTF) device exhibiting a decrease in resistance when an increase in the force is applied to the active area. In our circuit design, a voltage divider is used to measure the resistance change of the FSR in order to obtain the relationship between the applied force and the voltage.

The microprocessor-based data gathering subsystem used to gather information from the insole is mainly composed of a microprocessor-based circuit board. It includes a low-power and high-performance 8- bit AVR microprocessor-ATmega16L, peripheral components (resisters, capacitors, etc.), and one battery. The microprocessor runs at a clock frequency of 8 MHz. All circuitry operates with 5 V power which is generated by a LM78L05 regulator and powered by one 7.4 V/Li-ion battery. We use 8 ADC channels with 10-bit resolution to transform the analog voltage information generated from the FSRs into scaled digital data.

The utilize of wireless communication subsystem realizes to wirelessly transfer the digital data processed by the ATmega16L to the host computer in realtime. A low-power radio frequency (RF) communication module, GW100B, is selected. The RF transmitter

and RF receiver are connected with the microprocessor and the host computer individually.

4.2.2 FSR Sensor Calibration

In order to compensate for the nonlinearity of FSR, each sensor needs to be calibrated after it has been located on the surface of the insole. The popular digital force gauge DPS-20 (IMADA CO., LTD) is used to detect a discrete force in the range from 0 to 10 kg for the FSR-400 and 0 to 20 kg for the FSR-402. The digital outputs of the force gauge are stored in the PC via RS232. Then we can get the calibration result for each sensor according to the relationship between the applied force and the corresponding digital output of the FSR. Experimental results demonstrate that the exponential function fits well to the calibration data. One calibration curve of the FSR-402 under the big toe of the right foot is displayed in Fig. 4.2.

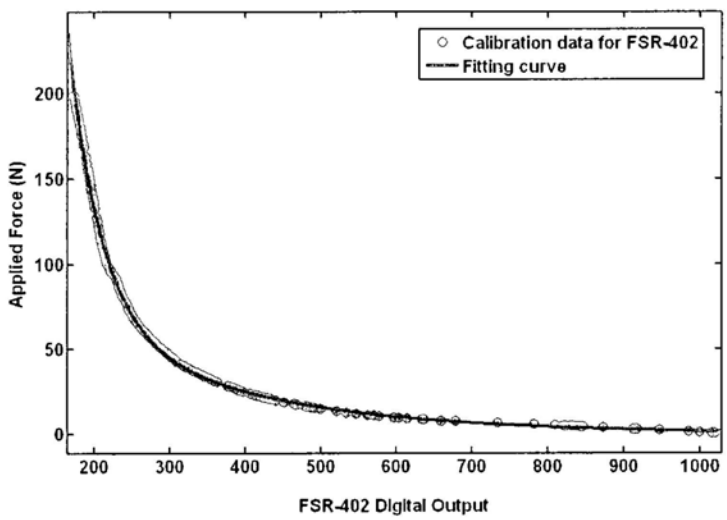

Figure 4.2: One FSR-402 calibration curve

Equation (4.1) describes the relationship f between one FSR-402 digital output x and the applied force in newton, the values of the coefficients are listed in Table 4.1.

$$f = a \cdot e^{b \cdot x} + c \cdot e^{d \cdot x} \tag{4.1}$$

Table 4.1: The values for the coefficients

Coefficient	Value
a	7324
b	-0.02291
c	136.4
d	-0.004305

4.2.3 Cascade Neural Networks with Node-Decoupled Extended Kalman Filtering for Gait Modeling

Gait analysis based on plantar pressure distribution provides an indirect way for detecting postural kyphosis. Human gait of either proper or kyphosis walking is regarded as the measurable stochastic process. The methodology that we are considering is to model human gait for realizing postural kyphosis detection. The CNN-NDEKF is applied to generate the classifier for this binary pattern recognition problem.

Nechyba and Xu proposed a new learning architecture of neural network, which combines (1) cascade neural networks (CNN), dynamically improving the architecture of the neural network to be part of the training process, and (2) node-decoupled extended Kalman filtering (NDEKF), an efficient convergent alternative to gradient-descent training algorithms. They analyzed the computational complexity of the proposed approach and demonstrated the significant improvement in learning times and/or error convergence of CNN-NDEKF compared with other machine learning approaches [37].

In our research group, CNN-NDEKF has found successful applications in modeling various human functions including learning human control strategy [38], modeling human strategy in controlling a dynamically stabilized robot [39], modeling human sensation in virtual environments [40], and learning human navigational skill for smart wheelchair [41]. In the following, we briefly summarize the CNN-NDEKF algorithm and the reason for us to adopt this algorithm for modeling human gait associated with proper and postural

kyphosis walking.

First, there is no a priori network architecture is assumed. Hidden units will be dynamically added into an initially minimal network once at a time. Fig. 4.3 illustrates the growth process for the initial two-input, one-output network with two hidden units installed one by one. Note that each new hidden unit will not only receive one input-connection from each input unit, but also from each pre-existing hidden unit. Therefore, a cascade neural network with m_i input units (including the bias unit), m_h hidden units, and m_o output units, has m_w connections where,

$$m_w = m_i m_o + m_h(m_i + m_o) + (m_h - 1)\frac{m_h}{2} \tag{4.2}$$

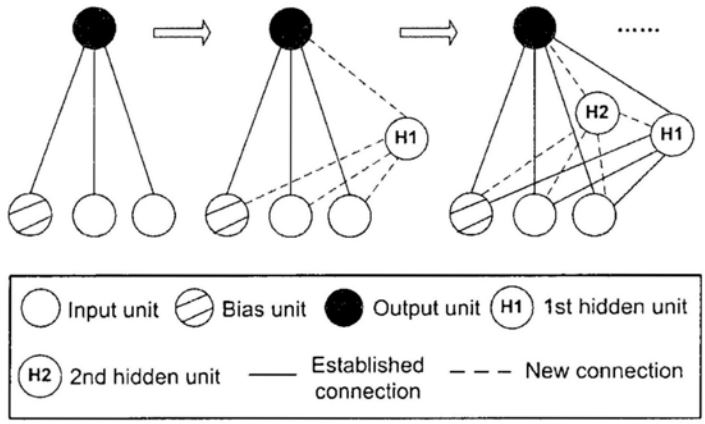

Figure 4.3: The cascade learning architecture: adding hidden units once at a time to the initial two-input, one-output network

Secondly, the activation function of each hidden unit is not constrained to be the particular type. For each new hidden unit, the activation function, which mostly reduces RMS error (e_{RMS}) for the training data will be selected. Sinusoidal, Bessel, and Gaussian functions are the typical alternatives to the standard sigmoidal activation function.

Thirdly, node-decoupled extended Kalman filtering (NDEKF) [42] fits seamlessly within the cascade learning framework, which shows better convergence properties with less computation than gradient-descent techniques (e.g. backpropagation and quickprop algo-

rithm).

Suppose P is a $w \times w$ conditional error covariance matrix storing the interdependence of every pair of w weights in the given neural network. The weight-update recursion of NDEKF is given by

$$\omega_{n+1}^i = \omega_n^i + \{(\psi_n^i)^T (A_n \xi_n)\}\phi_n^i \tag{4.3}$$

where ω_n^i is denoted as the input weight vector at iteration n, for unit $i \in \{0, 1, \ldots, m_o\}$. ξ_n is the m_o-dimensional error vector for the current training mode, ψ_n^i is the m_o-dimensional vector for the partial derivatives of the output unit signals related to the ith unit's net input, and

$$\phi_n^i = P_n^i \zeta_n^i \tag{4.4}$$

$$A_n = \left[I + \sum_{i=0}^{m_o} \{(\zeta_n^i)^T \phi_n^i\}[\psi_n^i (\psi_n^i)^T] \right]^{-1} \tag{4.5}$$

$$P_{n+1}^i = P_n^i - \{(\psi_n^i)^T (A_n \psi_n^i)\}[\phi_n^i (\phi_n^i)^T] + \eta_q I \tag{4.6}$$

where ζ_n^i is the w_i-dimensional input vector for the ith node, P_n^i is the $w_i \times w_i$ conditional error covariance matrix for the ith node, and η_q is used to alleviate singularity problem of P_n^i. In (4.3) to (4.6), []'s, {}'s, and ()'s respectively represent matrices, scalars, and vectors.

The flexible architecture of cascade neural network is ideal for modeling human gait which is characterized by dynamic, stochastic, and nonlinear properties. No a priori model structure is assumed. The model parameters are updated during the learning procedure which ensures the model to get the best classification performance. The process for CNN-NDEKF-based learning algorithm is summarized as follows. Initially, the network architecture begins with some inputs and one or more output units based on the requirement of special applications. There are no hidden units in the network architecture. Every input unit is directly connected to each output unit through a connection with pre-trained

weight. With no significant e_{RMS} reduction, the first hidden unit is picked up from the pool of candidate units. As soon as the hidden unit is installed, all input weights to the hidden unit are frozen, while the weights to the output units are trained using NDEKF. The process will repeat until the e_{RMS} reduces sufficiently or the number of hidden units achieves the predefined maximum number.

4.3 Experiments and Analysis

4.3.1 Data Acquisition and Database Formation

After A/D transformation, the digital data of all FSRs are packaged, which effectively decrease the transmission error and increase the sampling frequency to 50 Hz which is adequate for the activity of walking [43]. Then in the host computer, we obtain the corresponding information applied for each sensor based on data reconstruction and calibration. Fig. 4.4 and Fig. 4.5 individually display the force waveforms under each FSR for proper and kyphosis walking as a function of time.

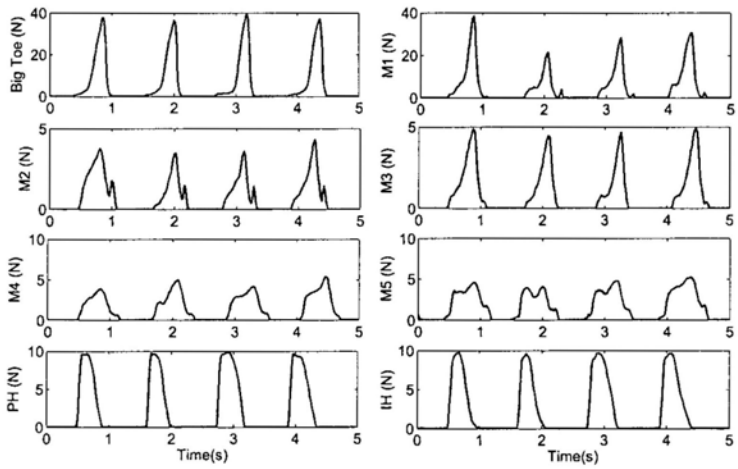

Figure 4.4: Force waveforms under eight right foot regions during proper walking posture (M1 = 1st metatarsal head, M2 = 2nd metatarsal head, M3 = 3rd metatarsal head, M4 = 4th metatarsal head, M5 = 5th metatarsal head, PH = posterior heel, and IH = inside heel)

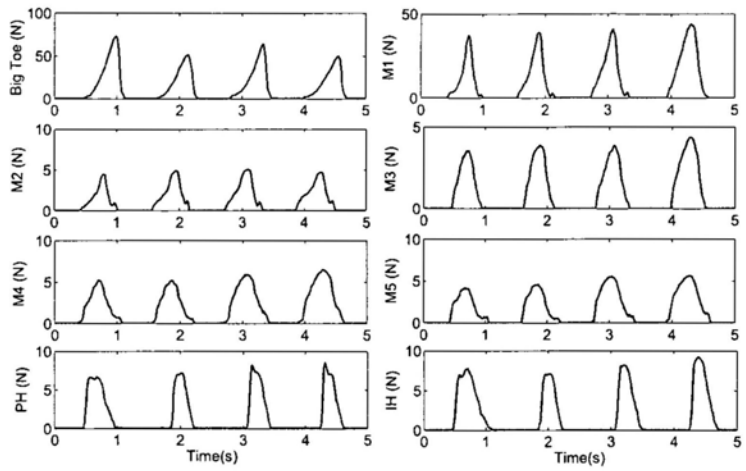

Figure 4.5: Force waveforms under eight right foot regions during kyphosis walking (M1 = 1st metatarsal head, M2 = 2nd metatarsal head, M3 = 3rd metatarsal head, M4 = 4th metatarsal head, M5 = 5th metatarsal head, PH = posterior heel, and IH = inside heel)

One young volunteer with no kyphosis was invited for this investigation. The training data with 10000 sampling points (5000 sampling points for either positive or negative sample) is gathered in outdoor environments which is then used for training the CNN-NDEKF model. Since we do data analysis by examining both the left and right feet, the dimension of the original data is 16.

4.3.2 Data Preprocessing

It is necessary and important to apply feature extraction in data preprocessing for modeling proper walking gait and the kyphosis one, since failures in feature generation can significantly diminish the efficiency of the system performance. Among the several feature extraction methods, Fast Fourier Transform (FFT), Principal Component Analysis (PCA), and Independent Component Analysis (ICA) are widely used in the application of pattern recognition.

In order to obtain the best performance of detecting postural kyphosis, different preprocessing approaches are utilized, including only using the original data, FFT, PCA, ICA, FFT+PCA, and FFT+ICA. After that, the retrieved data is applied to be the input

for training CNN-NDEKF model. Table 4.2 lists the generated data dimension after preprocessing, errors of detecting proper walking, errors of detecting postural kyphosis, and the average success rate of classification corresponding to each preprocessing method with the same training and testing samples (1500 sampling points for either positive or negative sample). We can find that the preprocessing approach of FFT is most effective for realizing the best classification performance compared with the other approaches mentioned above.

Table 4.2: Testing results using different preprocessing approaches

Preprocessing Method	Data Dimension	Errors of Proper Walking	Errors of Postural Kyphosis	Avg. Success Rate
Original Date	16	98	38	95.4%
FFT	48	18	0	99.4%
PCA	10	259	126	87.1%
ICA	10	276	95	87.6%
FFT+PCA	16	256	158	86.2%
FFT+PCA	10	320	123	85.2%
FFT+ICA	16	86	14	96.6%
FFT+ICA	10	410	156	81.1%

4.3.3 Testing Results

The classification results for the volunteer based on the trained CNN-NDEKF model with three order FFT preprocessing are listed in Table 4.3. For either proper walking or kyphosis walking, 1500, 2500, and 3500 sampling points are respectively selected as the testing data. The total success rate can reach 98% which demonstrates the shoe-integrated

system we build is efficient for the problem of detecting postural kyphosis.

Table 4.3: Testing results

Gait Pattern	Total	Correct	Failed	Success Rate
Proper Walking	1500	1482	18	98.8%
	2500	2416	84	96.6%
	3500	3342	158	95.4%
Postural Kyphosis	1500	1500	0	100%
	2500	2495	5	99.8%
	3500	3479	21	99.4%
TOTAL	15000	14714	286	98%

4.4 Summary

In this chapter, we present a methodology for detecting postural kyphosis under the framework of the shoe-integrated system. Eight force sensing resistors (FSRs) for gathering the pressure information under the 8 bony prominences are utilized. Based on the gathered plantar pressure information, we apply Cascade Neural Networks with Node-Decoupled Extended Kalman Filtering (CNN-NDEKF) to train the model for this binary classification problem. Different preprocessing approaches are utilized and experimental results demonstrate that Fast Fourier Transform (FFT) is the suitable data preprocessing approach for our problem. The proposed methodology has the potential application for detecting postural kyphosis in order to assist persons in developing proper walking posture in their daily life.

Chapter 5

Falling Detection based on Plantar Force

5.1 Introduction

Since the past two decades, falls in the aging population has always been one of the most challenging problems in public health care. Several studies show that approximately one third of the adults aged 65 or older fall every year and the number of falling tends to an upward trend year after year [44] [45] [46]. Falls have become the leading cause that results in injury-related hospitalization for elders [47]. Fall-related injuries include skin cuts and abrasions, fractures, damages to muscles and ligaments, and so on [45] [46] [48]. In many countries' health care, the medical cost associated with fall-related injuries is more than any other types and becomes the heavy financial burden [49] [50]. In this situation, a lot of fall prevention strategies have been proposed [51] [52] [53]. On the other hand, detection of fall events once they occur is more important. It is reported that more than 20% elders remain lying on the ground without any external support for 20 minutes or more after falling, which is called "long-lie" [54] [55]. "Long-lie" can result in serious consequences such as hypothermia, pressure sores and so on. Detection of falls in time

will shorten the time from a falling to the medical assistance and minimize the fall-related injuries.

A number of automatic falling detection systems have been proposed in recent years, which mainly consist of three types, vision based [56] [57], audio based [58], and wearable sensor based systems. Due to the shortcoming of vision and audio based systems that limits the effective space of falling detection, wearable sensor based approaches are widely accepted. Most of the researchers demonstrated that accelerometers and gyroscopes were applicable sensors for wearable systems of fall-event automatic detection. Bourke and Lyons [59] introduced the threshold-based fall detection algorithm which utilized a bi-axial gyroscope mounted on the trunk for measuring three thresholds of the angular acceleration, angular velocity, and change in trunk-angle. The study that investigated fall dynamics using gyroscopes was explored by Nyan et al. [60]. Gyroscopes were attached to different positions of sternum, waist, and underarm, for measuring the parameters of angular rates. A fall detector based on head worn 3-axis accelerometers was evaluated by Lindemann et al [61]. The fall-events were recognized via identifying the high velocity of motion before impact. Kangas et al. presented the study aiming to determine acceleration thresholds for placing 3-axis accelerometers at the waist, wrist, and head respectively [62]. The experimental results of two subjects showed that head and waist were optimal positions for fall detection and wrist was not.

Most of researches for falling detection based on wearable accelerometer or gyroscope systems focus on two problems. The first problem is to investigate the placements of sensors, since different location will result in different signal patterns leading to different detection algorithm. Furthermore, the second problem is how to accurately define the thresholds, which is affected by different subjects and the database of simulated falls and activities of daily living (ADL). Both of the two problems highly influence the sensitivity and specificity of falling detection. Besides, most of the accelerometer and gyroscope based detection algorithms are working on the assumption that the tilt degree of human body will change significantly when fall-events happen. However, in some situations, this assumption is not valid. For example, when people bend to pick up something from the

ground, the body position will change from upright to nearly horizontal position rapidly, however, no fall-event happens. On the other hand, not all of fall-events are accompanied with obvious change of tilt degree.

In this chapter, we propose a novel falling detection algorithm based on the analysis of plantar force on both feet, because plantar force is an important parameter directly associated with postures of human locomotion. Two force sensing resistors (FSRs) are installed on each foot's two positions (1st metatarsal head and heel position) for acquiring the force change information during subjects' locomotion. The fall-event detection algorithm consists of two stages. For Stage-One analysis, candidate sequences will be generated if force values of the four positions in both feet are simultaneously less than the corresponding predefined thresholds and last for a while. For Stage-Two analysis, we apply support vector machine (SVM) with genetic algorithm (GA) for optimal training parameters generation to determine whether there really exists a fall-event. Linear and nonlinear parameters of each candidate sequence are generated as the feature vector, which is further reduced to be more efficient features for discrimination by applying Generalized Discriminant Analysis (GDA). Considering the events of "moment of sitting" take significantly percentage in the database of non-fall events after Stage-One analysis, we separate the events of "moment of sitting" from the whole database of non-fall events to be the particular class we study. The detection results demonstrate the two-stage algorithm we proposed for fall-event detection is efficient.

This chapter is organized as follows. In Section 5.2, the materials and subjects associated with the proposed methodology are introduced. We describe the proposed two-stage falling detection algorithm in detail in Section 5.3. Experimental results are discussed in Section 5.4. We draw the summary of this chapter in the final section.

5.2 Materials and Subjects

One pair of shoe-integrated systems are designed for falling detection. Each system includes three major components: insole, microprocessor-based data gathering module, and wireless communication subsystem.

For insole subsystem, two force sensing resistors (FSRs) (Interlink Electronics, Santa Barbara, CA) are installed on one side of a thin insole under the first metatarsal head and inside heel position. The type of FSR-402 (12.7 mm diameter active surface, 0.46 mm thick) is applied for the first metatarsal head and FSR-400 (5 mm diameter, 0.3 mm thick) is placed under the heel position. FSR is a type of polymer thick film (PTF) device exhibiting a decrease in resistance when an increase in the force is applied to the active area. In our circuit design, a voltage divider is used to measure the resistance change of the FSR in order to obtain the relationship between the applied force and the voltage.

Microprocessor-based data gathering subsystem includes a low-power and high-performance 8-bit AVR microprocessor-ATmega16L, peripheral components (resisters, capacitors, etc.), and one battery. We use 2 ADC channels with 10-bit resolution to transform the analog voltage information generated from the FSRs into scaled digital data.

For each shoe-integrated system, a pair of low-power radio frequency (RF) communication modules, GW100B ($56\times27.5\times12$ mm in size), are selected for wireless communication. The RF transmitter and receiver are connected with the microprocessor and the host computer respectively. The host computer receives the force signals from the pair of shoe-integrated systems simultaneously.

The force readings beneath feet are recorded during the activities of daily living (ADL) and simulated falls via subjects wearing the shoe-integrated systems. In the first study, nine healthy subjects are invited to perform ADL tasks. In the second study, four of the nine subjects perform simulated falls in a safe controlled environment. The ages of the subjects including seven males and two females are from 23 to 32 years old (27.5 ± 3.2years old), the heights are from 1.62 to 1.82 m (1.72 ± 0.06m), and the weights are from 50 to 77 kg (65.1 ± 9.5kg).

The ADL tasks involves the activities that often happen in our daily lives and the ones that could result in false detection due to the similarity as the locomotion of falling down. Each of the nine subjects is asked to perform the ADL tasks listed as Fig. 5.1 for several times. The four subjects are monitored to perform simulated falls onto a large airbed during the process of walking. Each of the four subjects performs fall events with

free selected types and orientations for several times. Fall events and ADL tasks were also documented using a digital video camera.

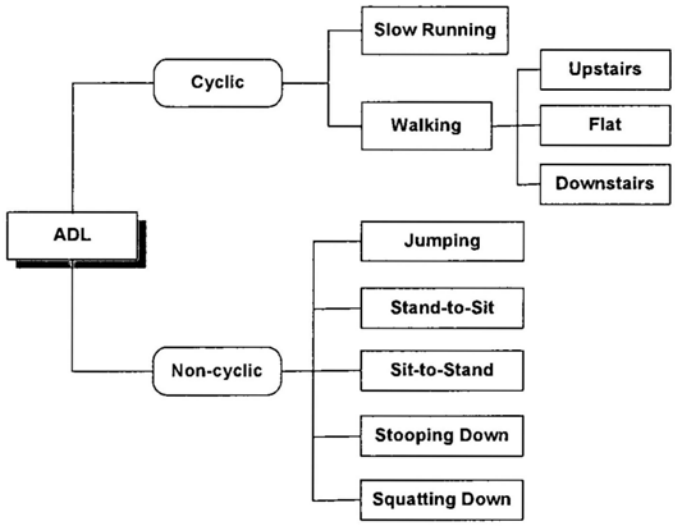

Figure 5.1: Activities of daily living (ADL) tasks

5.3 Two-Stage Fall Detection Algorithm

5.3.1 Stage-One Fall Analysis

From the study point of the force change beneath feet, the process of falling includes three phases. We call Phase One as the motion period. Since we focus on the study of the fall happening during locomotion, the forces under feet should vary for a period ahead of the moment of falling. For Phase Two, at the moment of falling, the forces under the monitored positions will be no more than the threshold values. Phase Three is defined as motionless period. In this phase, the value of each force position is still less than its predefined threshold value, which will last for a while.

The flowchart of Stage-One fall analysis is shown as Fig. 5.2. We monitor force values of the four positions in both feet simultaneously (LM: left 1st metatarsal head, LH: left heel position, RM: right 1st metatarsal head, RH: left heel position). If each force value

is no more than the corresponding predefined threshold value for a period of 1/5 seconds and the force varies during the last two seconds, we will consider the subject suffers from falling.

The threshold values for the four force positions are predefined for each subject individually. Wearing the pair of shoe-integrated systems, each subject is asked to sit with the posture of 90-degree thigh-to-calf angle, 90-degree hip angle, and 90-degree ankle angle by adjusting the chair height. The force value of each monitored plantar position is recorded as the threshold value regarding to this placement.

Letting t_0 to be the first sampling point that all force values are no more than their thresholds, we backdate and forward-date data for 2 and 4 seconds from t_0, and define the sampling points during this period $[t_{0-2}, t_{0+4}]$ as the candidate sequence. The definition of candidate sequences can be referred to Fig. 5.3. In the following, we will apply classification algorithm to determine whether there really exists a fall event.

5.3.2 Stage-Two Fall Analysis

After Stage-One analysis, we obtain the generated candidate sequences which consist of both fall and non-fall events. Furthermore, we propose the algorithm for Stage-Two analysis in order to improve the detection of fall-events. The brief introduction for Stage-Two analysis is displayed in Fig. 5.4.

Feature Generation

As mentioned in the above section, each candidate sequence $\{LM[t_{0-2}, t_{0+4}]$, $LH[t_{0-2}$, $t_{0+4}]$, $RM[t_{0-2}, t_{0+4}]$, $RH[t_{0-2}, t_{0+4}]\}$ includes 600 sampling points for each force sensor. In our work, a combination of both linear and nonlinear features of force signals is considered. For linear analysis, 600 sampling points of each sensor is further divided into seven segments, each of which includes 150 sampling points and 75 overlapping points between the successive segments. For each segment, three time domain parameters are considered. They are mean, standard deviation (SD), and root mean square (RMS). Besides, two nonlinear parameters of each candidate sequence are studied in this work, which are described

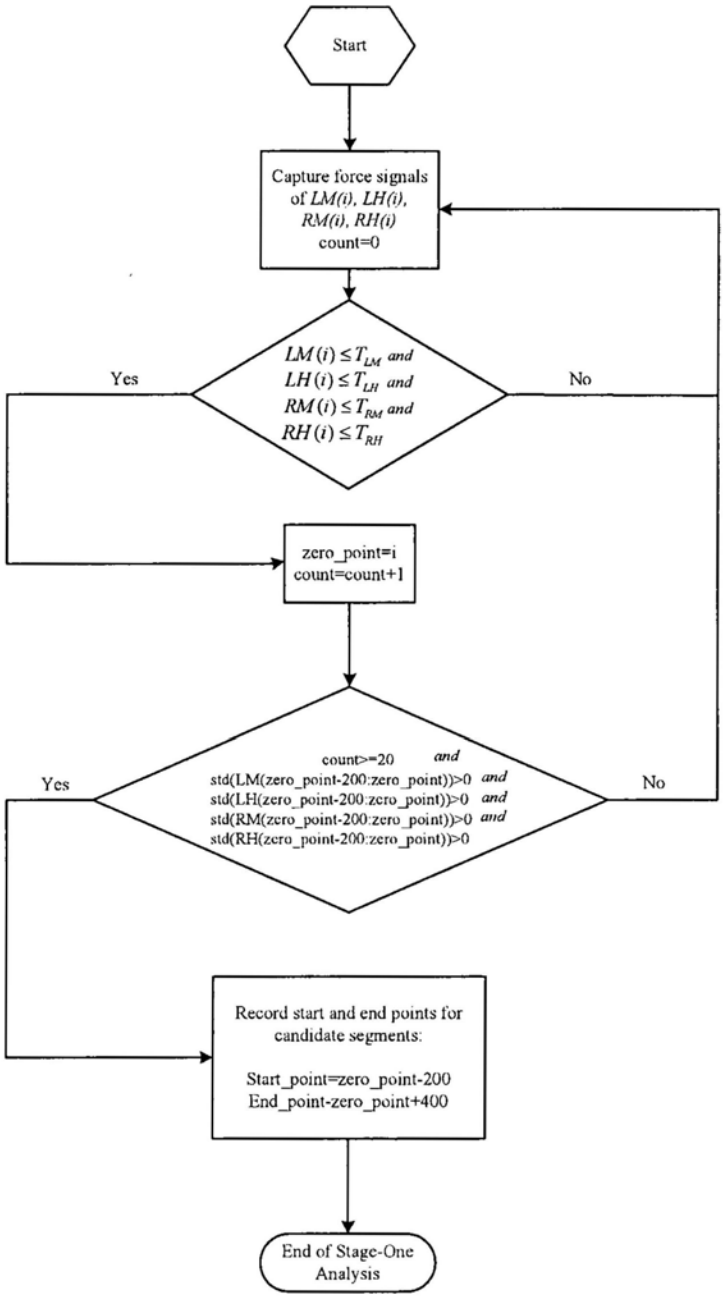

Figure 5.2: Flowchart of Stage-One fall analysis algorithm

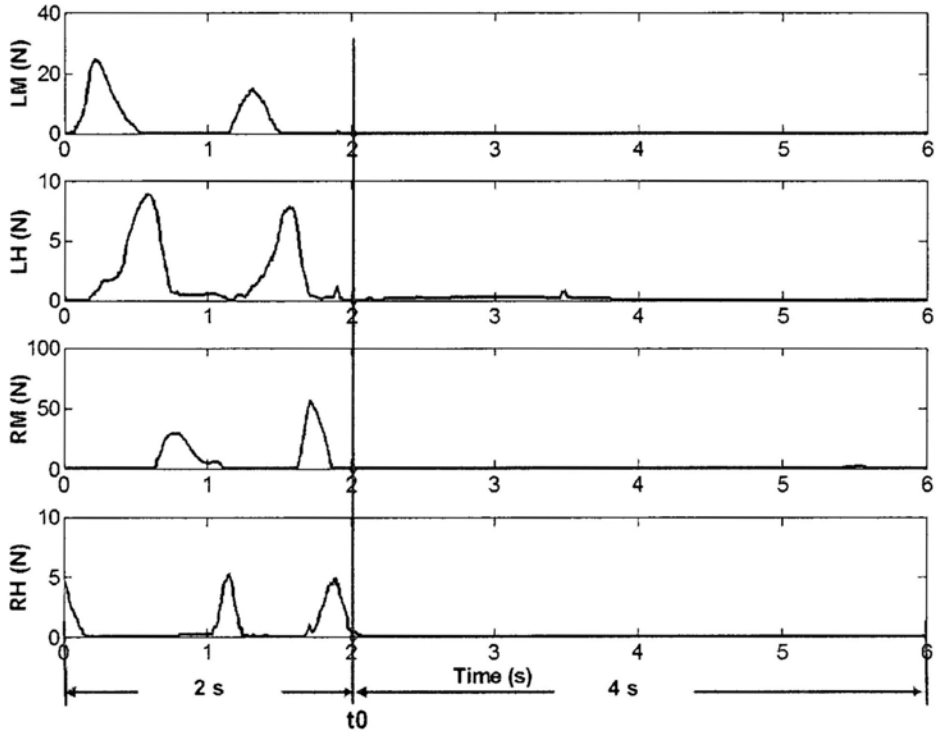

Figure 5.3: One example of candidate sequence (LM: left 1st metatarsal head, LH: left heel position, RM: right 1st metatarsal head, RH: left heel position)

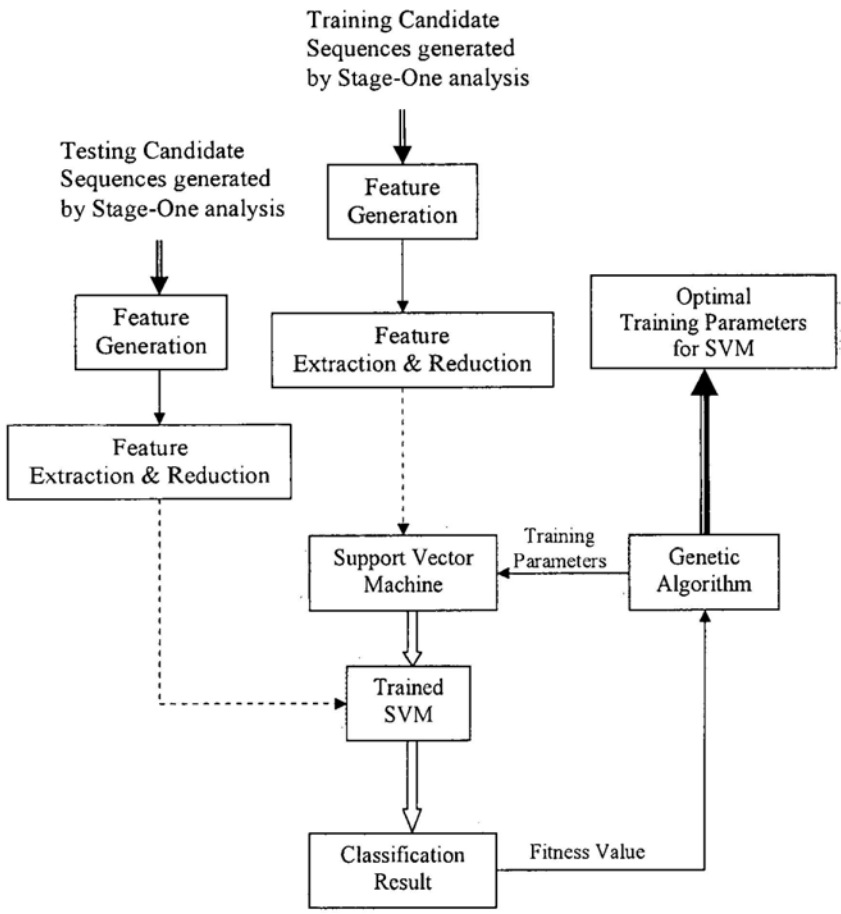

Figure 5.4: Block diagram of the software design for Stage-Two analysis

as follows.

Approximate entropy (ApEn) [63] is a nonlinear dynamics parameter to quantify the unpredictability of fluctuations in a time series. ApEn measures the creation of information in a time series and reflects the complexity of system, which is suitable for finite data sequences. A relatively small value of ApEn indicates that the time series is deterministic, while a relatively large value indicates a more irregular (random) time series.

Given a sequence S_N, consisting of N sampling points, we set the pattern length m = 2 and the criterion of similarity r = 20% of the standard deviation of the sequence. To calculate ApEn(m, r, S_N), first, S_N is divided into a series of embedding vectors with m sampling points along the observed time series, i.e., $v(n) = [S_N(n), ..., S_N(n+m-1)], n = 1, 2, ..., N-m+1$. $N_{m,r}(i)$ is counted if the difference between any pair of corresponding measurements in $v(i)$ and $v(j)$ $(j = 1, 2, ..., N-m+1)$, is less than r.

We define $C_{m,r}(i)$ as the probability to find a vector differing from $v(i)$ with the distance less than r:

$$C_{m,r}(i) = \frac{N_{m,r}(i)}{N-m+1} \tag{5.1}$$

And the average natural logarithm over all $C_{m,r}(i)$ probability is:

$$C_{m,r} = \frac{\sum_{i=1}^{N-m+1} \log(C_{m,r}(i))}{N-m+1} \tag{5.2}$$

Repeat the above procedure for pattern length=$m+1$, and obtain $C_{m+1,r}$.

ApEn is given by:

$$ApEn = C_{m,r} - C_{m+1,r} \tag{5.3}$$

Spectral Entropy (SpEn) measures the complexity of the observed time series in the frequency domain. We convert the spectrum into a probability density function (PDF), p_f, by normalizing the power spectral density (PSD) P_f at frequency f:

$$p_f = \frac{P_f}{\sum_{f=1}^{N} P_f}, f = 1, ..., N \tag{5.4}$$

Spectral Entropy is estimated as:

$$H = -\sum_{f} p_f \log(p_f) \tag{5.5}$$

Feature Extraction and Reduction via GDA

After feature generation, each candidate sequence is transferred into a 92-dimensional feature vector. On the one hand, it will increase the computational cost for directly sending the high-dimensional feature as the input for SVM classifier. On the other hand, much more discriminable features rather than the original vectors need to be extracted as the input vector for SVM classifier for obtaining better classification performance. Linear Discriminant Analysis (LDA) is a traditional dimensionality reduction technique which has been proved useful in the classification problem, especially in the filed of face recognition [64] [65]. LDA searches a set of vectors that maximize the between-class measure and minimize the within-class measure based on the class information rather than the data. However, LDA cannot perform well for nonlinear problems. Generalized Discriminant Analysis (GDA) [66], is developed for dealing with nonlinear discriminant problem by utilizing kernel operators. GDA includes two processes. Firstly, the input data is mapped into a high-dimensional space with nonlinear function, while the linear combination in the high-dimensional space is corresponding to the nonlinear combination in the input space. Secondly, in the new feature space, the classical LDA method is applied for the linearly distributed data.

Mathematically speaking, the input set X consists of M feature vectors x_j $(j = 1, 2, ..., M)$ out of N classes. By mapping the input space into a high-dimensional feature space F via a nonlinear function ϕ, the intra-class scatter matrix V and the inter-class scatter matrix B representing the within-class and between-class scatters of data can be defined as follows:

$$V = \frac{1}{M} \sum_{p=1}^{N} \sum_{q=1}^{n_p} \phi(x_{pq}) \phi^T(x_{pq}) \tag{5.6}$$

$$B = \frac{1}{M}\sum_{p=1}^{N} n_p(\frac{1}{n_p}\sum_{q=1}^{n_p}\phi(x_{pq}))(\frac{1}{n_p}\sum_{q=1}^{n_p}\phi(x_{pq}))^T \tag{5.7}$$

where x_{pq} denotes the qth feature vector of the class p. n_p is the number of feature vectors in class p.

As such for LDA, the goal of GDA is to find the projection vector v in order to maximize the between-class inertia while minimize the within-class inertia in the higher dimensional space F. Dealing with this maximization problem is equal to solving the following eigenvalue resolution:

$$\lambda V v = Bv \tag{5.8}$$

v is an eigenvector of $V^{-1}B$ associated to the eigenvalue $\lambda = \frac{v^T B v}{v^T V v}$. All of the solutions of v lie in the span of $\phi(x)$. Let us consider the expansion coefficients α, the eigenvector v can be expressed as:

$$v = \sum_{i=1}^{M} \alpha_i \phi(x_i) \tag{5.9}$$

The normalized coefficients $\alpha = \frac{\alpha}{\sqrt{\alpha^T K \alpha}}$ can be calculated by performing eigenvector decomposition for $K = (k_{ij})_{i=1,\ldots,M;j=1,\ldots,M}$.

The the projection of a feature vector x on the eigenvector v^i can be computed via:

$$z^i = v^{i^T}\phi(x) = \sum_{j=1}^{M} \alpha_j^i \phi(x_j)\phi(x) = \sum_{j=1}^{M} \alpha_j^i k(x_j, x) \tag{5.10}$$

Support Vector Machines

The feasibility of support vector machine in the application of classification problem has been proved in the fields of musical genre classification [67] [68] [69], image classification [70] [71], gender classification [72] [73] and so on.

(1) *Support Vector Classification (Binary Case)*

The basic training principle of SVMs is to map a set of training data $\{(x_1, y_1), \cdots, (x_l, y_l)\}$, ($x_i \in X \subseteq R^n$, $y_i \in \{-1, 1\}$, l is the total number of training samples) from the input space

X into a high-dimensional feature space via a nonlinear function ϕ so that the optimal separating hyperplane (OSH) can be found with the maximum margin between the two classes. A separating hyperplane in canonical form [74] [75] determines a function that can classify unseen examples accurately with the following constraints:

$$y_i[\langle \omega, x_i \rangle + b] \geq 1, \quad i = 1, \cdots, l. \tag{5.11}$$

where $\langle \cdot, \cdot \rangle$ denotes the dot product in X.

Among several separating hyperplanes, the optimal one is given by maximizing the margin which is the distance between the hyperplane and the closet point of each class. Since the distance is $\frac{2}{\|\omega\|}$ with the constraints of (5.11), finding the OSH is equivalent to minimizing the following equation:

$$\Phi(\omega) = \frac{1}{2} \|\omega\|^2 \tag{5.12}$$

Considering in most cases, the data is linearly nonseparable, we introduce positive slack variables ξ_i $(i = 1, \cdots, l)$. Equation (5.12) can be transformed into the following equation:

$$min \qquad \Phi(\omega, \xi) = \tfrac{1}{2} \|\omega\|^2 + C \sum_{i=1}^{l} \xi_i \tag{5.13}$$

$$s.t. \quad y_i[\langle \omega, x_i \rangle + b] \geq 1 - \xi_i, \quad i = 1, \cdots, l. \tag{5.14}$$

where $\frac{1}{2} \|\omega\|^2$ denotes the regularized and $\sum_{i=1}^{l} \xi_i$ represents the empirical risk.

We then construct a Lagrange function under the constraints of (5.14) in order to solve the optimization problem of (5.13):

$$L = \frac{1}{2} \|\omega\|^2 + C \sum_{i=1}^{l} \xi_i - \sum_{i=1}^{l} \beta_i \xi_i - \sum_{i=1}^{l} \alpha_i (y_i[\langle \omega, x_i \rangle + b] - 1 + \xi_i) \tag{5.15}$$

where α, β are the Lagrange multipliers. Because classical Lagrangian duality can solve the primal problem, (5.15) can be transformed to its dual problem given by,

$$\begin{aligned} max \quad & W(\alpha) = \sum_{i=1}^{l} \alpha_i - \tfrac{1}{2} \sum_{i=1}^{l} \sum_{j=1}^{l} \alpha_i \alpha_j y_i y_j x_i . x_j \\ s.t. \quad & 0 \leq \alpha_i \leq C \quad i = 1, \cdots, l, \\ & \sum_{i=1}^{l} \alpha_i y_i = 0. \end{aligned} \tag{5.16}$$

By replacing x with its mapping in the feature space $\Phi(x)$, (5.16) can be rewritten as:

$$\begin{aligned} W(\alpha) &= \sum_{i=1}^{l} \alpha_i - \frac{1}{2} \sum_{i=1}^{l} \sum_{j=1}^{l} \alpha_i \alpha_j y_i y_j \Phi(x_i).\Phi(x_j) \\ &= \sum_{i=1}^{l} \alpha_i - \frac{1}{2} \sum_{i=1}^{l} \sum_{j=1}^{l} \alpha_i \alpha_j y_i y_j K(x_i, x_j) \end{aligned} \tag{5.17}$$

As shown in (5.17), the dot product can be replaced with a function $K(x_i, x_j)$ defined as the kernel function. Radial Basis Function (RBF) kernel $K(x_i, x_j) = \exp(-\gamma \left\| x_i - x_j \right\|^2), \gamma > 0$ and polynomial kernel $K(x_i, x_j) = (x_i \cdot x_j + 1)^d$ are the commonly used kernel functions in nonlinear SVMs.

The decision function for identifying the class of the input data x is obtained by

$$y(x) = sgn(\sum_{i=1}^{l} y_i \alpha_i K(x_i, x) + b) \tag{5.18}$$

(2) *Multi-Classification with SVMs*

Two of the conventional approaches that apply SVMs to multi-classification problem are one-against-one and one-against-rest. The kernel concept of each approach is to convert the multiple problem into several binary ones. In order to reduce the training time, we select the one-against-one method in which $\frac{N(N-1)}{2}$ classifiers are created for N total classes.

The binary classification problem for training data x_k from class i and class j can be shown in the following equation:

$$\begin{aligned} min \quad & \Phi(\omega^{ij}, \xi^{ij}) = \tfrac{1}{2} \left\|\omega^{ij}\right\|^2 + C \sum_k \xi_k^{ij} \\ & (\langle \omega^{ij}, x_k \rangle + b^{ij}) \geq 1 - \xi_k^{ij}, \ x_k \in class\ i \\ s.t. \quad & (\langle \omega^{ij}, x_k \rangle + b^{ij}) \leq -1 + \xi_k^{ij}, \ x_k \in class\ j \\ & \xi_k^{ij} \geq 0. \end{aligned} \tag{5.19}$$

Each binary classification is regarded as a voting. The test observation sequence, x_t, will be designated into the class with maximum number of votes. If more than one class has the identical number of votes, we comply with the strategy of selecting the class with the smallest index.

Genetic Algorithm for SVM Model Optimization

SVM model and parameter selection are very important for obtaining the best performance in SVM training. Genetic algorithm (GA) is a heuristic searching algorithm based on the mechanics of natural approximate solutions for optimization and search problems [76]. In our work, we aim to apply GA approach to optimize the SVM classifier for the problem of fall-event detection.

(1) *Chromosome Representation*

The first work to apply GA for SVM classifier optimization is to choose the appropriate chromosome representation which defines the proposed solution to the optimization problem. Chromosome representation describes each individual of the population in the genetic algorithm.

C-SVM proposed by Vapnik and *ν-SVM* by Schölkopf et al. [77] are two kinds of commonly used SVM algorithms. We consider the optimization processes of the two kinds of SVM algorithms respectively. In *C-SVM* algorithm, we mainly pay attention to the influence of the cost parameter C which controls the balance between model complexity and the training error. The value range of C is usually from 0 to infinity, however, a large C will result in an overfitting problem. Relatively, in *ν-SVM*, ν is the regularization

parameter varying through [0, 1]. It limits the lower bound of the total support vectors and the upper bound number of the ones that lie on the wrong side of the hyperplane.

The performance of each kind of SVM algorithm is also sensitive to the selection of kernel function. In comparison with other generally used kernel functions, such as linear, polynomial, and sigmoid functions, RBF kernel is selected for our experiments because of the following reasons. Firstly, unlike the linear kernel function, RBF kernel can nonlinearly map training data into the high-dimensional feature space in order to solve the problem when the relationship between attributes and different classes is not linear. The second reason is that the RBF kernel function has less hyperparamters that influence the complexity of model selection than polynomial and sigmoid kernel functions. In the optimization process, the parameter Gamma (γ) for RBF kernel function needs to be considered for performance comparison.

Based on the analysis of SVM model and optimization variables, we define the chromosomes for the two kinds of optimization processes with the following data structures:

- *C-SVM* Model Optimization: (C, γ)
- ν-*SVM* Model Optimization: (ν, γ)

Table 5.1 lists the optimization variables and their boundary values of the two kinds of optimization processes.

Table 5.1: Optimization variables and boundary values for the two kinds of optimization processes

Model Type	Variable	Boundary Value
C-SVM	C	0-100
	γ	0-1
ν-*SVM*	ν	0-1
	γ	0-1

(2) *Fitness Function*

The fitness function is applied for evaluating the optimality of each chromosome in the population. More optimal chromosomes will be selected to breed and mix their datasets in order to produce a new generation that will be even better.

The fitness function $f(x_i)$ for the problem of SVM classifier optimization can be described by the following equation:

$$f(x_i) = min(1 - g(x_i)) \tag{5.20}$$

where $g(x_i) \subseteq (0, 1)$ is defined as the SVM classification result for each chromosome.

(3) *Computational Procedure*

According to the genetic algorithm, the computational procedures are listed as follows:

a) Initialization. Set the initial values of the following parameters for the genetic algorithm:

1) the maximum number of generations MAXGEN,

2) the population size N_p,

3) the crossover fraction $P_c \subseteq [0, 1]$ (the mutation fraction =1-P_c),

4) the number of individuals that are guaranteed to survive into the next generation ELITE COUNT.

Create a random initial population via a uniform distribution.

b) Fitness Value Scaling. Compute the fitness value $f(x_i)$ for each chromosome in the I_{th} generation. Scale each fitness value in a range based on the rank of its position in the sorted scores.

c) Selection. The motivation of the selection function is to choose parents for generating the next offspring based on the scaled fitness value. Each parent holds a certain length in a line proportional to its expectation. The algorithm moves along the line with uniform step and selects one parent for each landing.

d) Crossover. The top P_c% of parents are selected to form a new individual for the next generation in turn. The crossover algorithm randomly creates a binary vector including

elements as the same number as the chromosome's genes. Select the genes from the first parent where the vectors are "1", and select the genes from the second parent where the vectors are "0". For example,

Parent1=[a b c d e]
Parent2=[f g h i j]
Random Vector=[1 0 1 1 0]
Child=[a g c d j]

The new individuals generated by crossover function randomly inherit the characteristics of its parents.

e) Mutation. The remaining selected parents undergo mutation. The mutation function makes small random changes of the individuals in the population, which effectively avoids a local maximum and enables the GA to search in a broader space. The algorithm adds a random value with a Gaussian distribution centered on zero to each gene of an individual's chromosome in order to create a new offspring.

f) Stopping Criteria. If the present generation number I_{th} reaches the predefined maximum number of generations MAXGEN, the optimization process will stop, otherwise, the process will stop before I_{th} reaches MAXGEN if the difference of the average fitness value between generations is less than 10^{-6} for 50 consecutive generations.

5.4 Experimental Results

5.4.1 Experimental Results of Stage-One Analysis

We record threshold values of the four force sensors for each subject listed as Table 5.2. After applying the Stage-One analysis algorithm displayed as the above mentioned flow chart (Fig. 5.2), most of the ADL tasks are filtered out and candidate sequences for Stage-Two analysis are formed up. Table 5.3 lists the candidate sequences for each subject, which are composed of all fall-events and a set of non-fall events. The candidate sequences of non-fall events generated from Stage-One analysis include:

Table 5.2: Threshold values of the four force sensors for the nine subjects

Subject	*Threshold Value(N)*			
	LM	*LH*	*RM*	*RH*
#1(*Hou*)	0.7164	0.1719	0.0072	0.1483
#2(*Ye*)	0.0960	0.1640	0.0960	0.0071
#3(*Chung*)	0.6456	0.1719	0	0.2948
#4(*Yang*)	0.0659	2.8872	0.7061	0.1640
#5(*Lam*)	0.2546	0.1798	0	0.5595
#6(*Shi*)	0	0.1878	0	0.2779
#7(*Yan*)	0.0884	0.1719	0.0510	0.0724
#8(*Chen*)	0.7474	2.2434	0.0884	0.5990
#9(*Lu*)	0.8213	0.2281	0.0072	0

- Moment of jumping: refers to the moment of jumping up.
- Moment of squatting: refers to the moment of squatting down.
- Moment of walking: refers to the moment of walking or turning.
- Moment of upstair: refers to the moment of climbing stairs up.
- Moment of sit-stand: refers to the moment of posture transition from sitting to standing up.
- Moment of sitting: refers to the moment when the body touches or just before touches a chair.
- Movement after sitting: refers to the movements while sitting on a chair.
- Fall-followed movement: refers to the movements after falling down.

It is noticed that the events about "moment of sitting" take significant percentage in the database of all non-fall events, which illuminates there is much similarity between the events of moment of sitting and fall-events. Therefore, we further divide candidate sequences of non-fall events into two classes: the events of "moment of sitting" and the other non-fall events. Our purpose is also to investigate the probability to classify the events of "moment of sitting" and fall-events. Under this condition, the problem of falling detection is transferred into a multi-classification case aiming to discriminate the candidate

Table 5.3: Generated categories after Stage-One analysis (Jump: Moment of jumping, Squat: Moment of squatting, Walk: Moment of walking, SitMove: Movement after sitting, Upstair: Moment of upstair, Sit-Stand: Moment of sit-stand, Fallfollowed: Fall-followed movement, Sitting: Moment of sitting)

Subject	Non-Fall								Fall
	Jump	*Squat*	*Walk*	*SitMove*	*Upstair*	*Sit − Stand*	*Fallfollowed*	*Sitting*	
#1(*Hou*)	16		1	28				16	
#2(*Ye*)						1		2	
#3(*Chung*)			1	1	3			15	
#4(*Yang*)	6		1	3		7		11	
#5(*Lam*)			5			1		5	
#6(*Shi*)	7	2	4	13		3	16	38	52
#7(*Yan*)	1				2		5		23
#8(*Chen*)	10			6	1		9	17	27
#9(*Lu*)	8		9	17		3	4	16	22
Total	194							120	124

sequences into three classes: non-fall events (except the ones of "moment of sitting"), the events of "moment of sitting", and fall events.

5.4.2 Experimental Results of Stage-Two Analysis

After extracting both linear and nonlinear features for candidate sequences, each of them is transferred into a 92-dimensional feature vector. Applying GDA for feature reduction, each of 92-dimensional feature vector is projected into two subspaces. Fig. 5.5 and Fig. 5.6 respectively depict training and testing vectors' first two most discriminating features extracted by GDA. It is obviously shown that the features for the same class are relatively close to each other and far away from the ones related to the other classes. Therefore, the new extracted and reduced features after GDA, provide better inputs for next classification procedure of SVM.

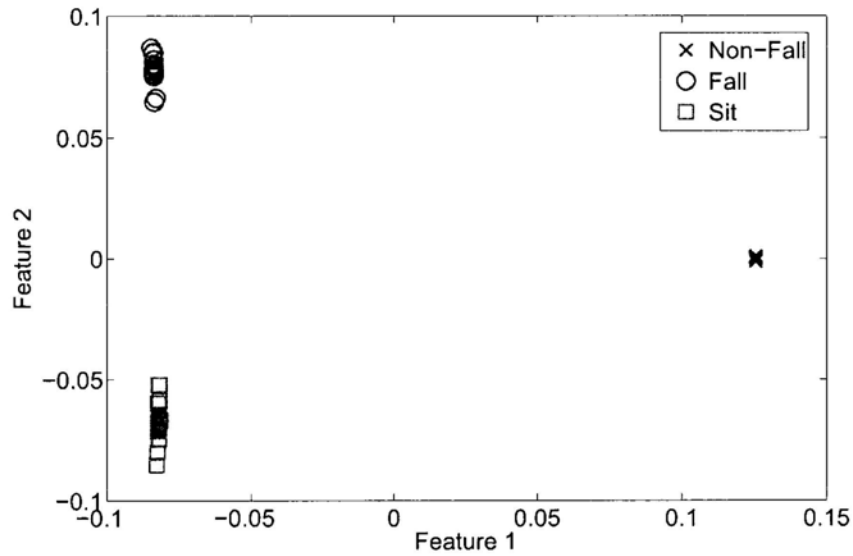

Figure 5.5: Distribution of the two new training features for three classes (Non-Fall (Non-fall events except the ones of "moment of sitting"), Fall (Fall-events), and Sitting (the events of "moment of sitting")) in GDA-based feature space

For what has been discussed in above section, SVM model and parameter selection

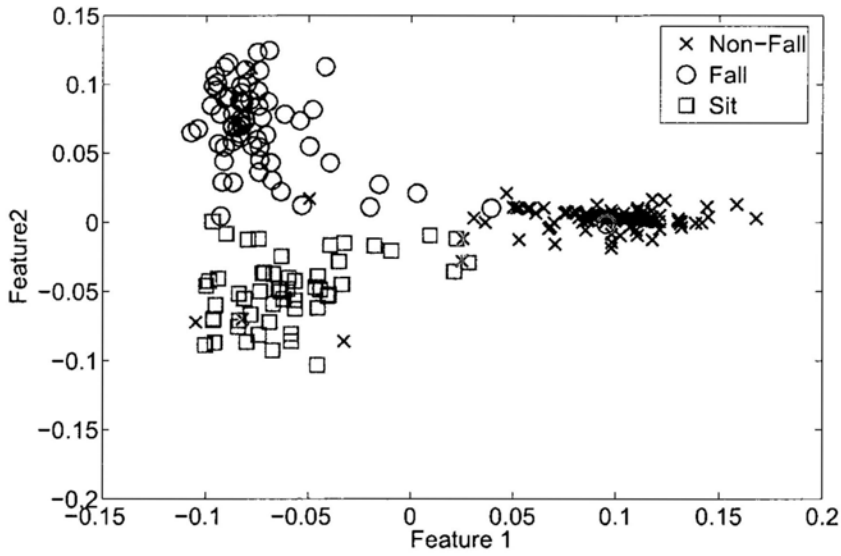

Figure 5.6: Distribution of the two new testing features for three classes (Non-Fall (Non-fall events except the ones of moment of sitting), Fall (Fall-events), and Sitting (the events of moment of sitting)) in GDA-based feature space

are very important for obtaining the best performance in SVM training. We apply genetic algorithm (GA) for generating the most suitable SVM training parameters in order to obtain the optimal SVM classifiers for the problem of fall-event discrimination. We randomly select training samples for the three classes from their databases and the left ones are regarded as the testing samples.

For generating the optimal SVM classifier, the optimization processes of *C-SVM* and ν-*SVM* with RBF kernel function are considered respectively. The optimization processes of fitness values for the two kinds of SVM algorithms are displayed in Fig. 5.7. It is noticed that after more than 50 generations, the "best fitness value" of ν-*SVM* converges to 0.038793, which is smaller than the one of *C-SVM* (0.043103). The SVM training parameters corresponding to the "best fitness value" are regarded as the optimal solution for the multi-classification problem. As a result, for the optimal SVM classifier, we apply for ν-*SVM* algorithm with the regularization parameter ν equal to 0.287 and the kernel

function of RBF with the parameter γ equal to 0.187. The sensitivity and specificity results related with the optimal SVM classifier are listed in Table 5.4, which demonstrate the optimal SVM classifier we build is efficient for the problem of fall-event detection.

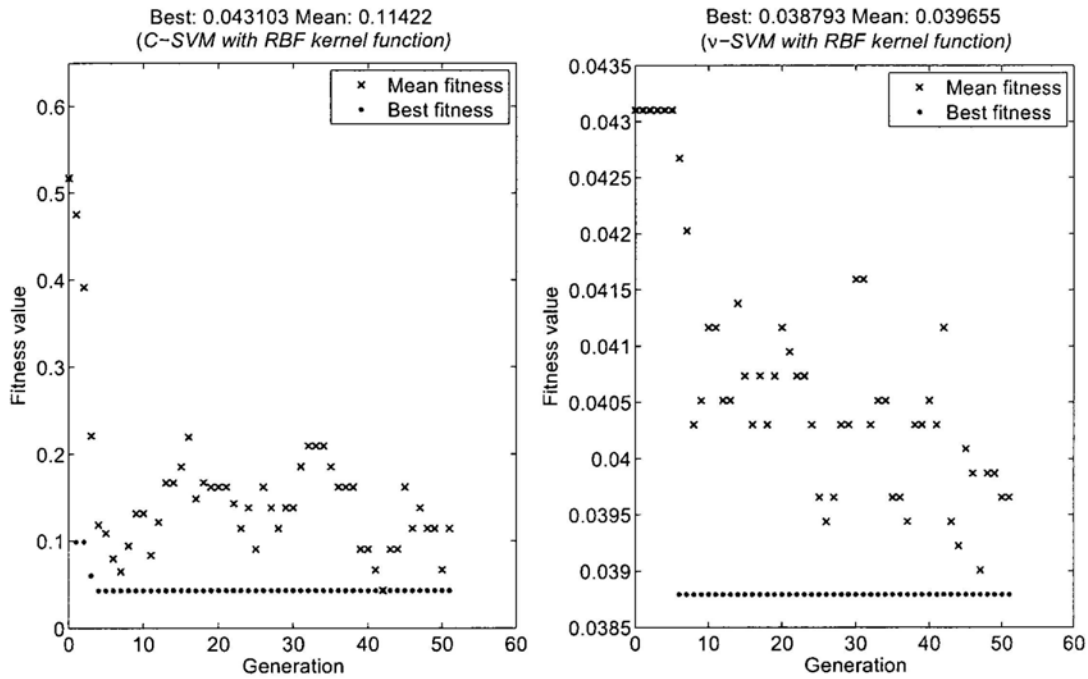

Figure 5.7: Optimization process of fitness value

Table 5.4: Sensitivity and specificity of multi-classification results

Category	*Sensitivity*(%)	*Specificity*(%)
Non-Fall	95.53 (107/112)	96.66
Fall	96.96 (64/66)	98.75
Sit	96.29 (52/54)	98.27
Avg.	96.26	97.89

5.5 Summary

Falls in the aging population has always been one of the most challenging problems in public health care. Most of the automatic fall detection systems are based on accelerometers and gyroscopes for detecting the rapid change of the body's tilt degree. Considering the assumption of accelerometer and gyroscope based algorithms are not always valid, we propose a novel falling detection algorithm based on the analysis of the plantar forces of both feet. Two force sensing resistors (FSRs) are installed on each foot's two positions (1st metatarsal head and heel position) for acquiring the force change information during subjects' locomotion. For Stage-One analysis, candidate sequences will be generated if force values of the four FSRs beneath both feet are simultaneously less than the corresponding predefined thresholds and last for a while. For Stage-Two analysis, we apply support vector machine (SVM) with genetic algorithm (GA) for generating optimal training parameters to determine whether there really exists a fall event. Linear and nonlinear parameters of each candidate sequence are generated to be the feature vector, which is further reduced to be more efficient input features for discrimination by applying GDA. Considering the events of "moment of sitting" take significantly percentage in the database of non-fall events, we separate the events of "moment of sitting" from the whole database of non-fall events to be the particular class we study. The detection results demonstrate the two-stage algorithm we propose for falling detection is efficient.

Chapter 6

Abnormal Gait Modeling

6.1 Introduction

Human gait can be generally divided into normal and abnormal ones. Keeping abnormal gait patterns will ultimately lead to pain in the feet, ankles, legs and even skeletal disease if prolonged. By monitoring the gait pattern of a human, proper motion adjustments can be advised so as to improve their walking style and long-term well being. Considering the variety of gait abnormalities, we select the typical ones including easily observed abnormalities ("toe in" and "toe out") and inconspicuous ones ("heel walking" and "oversupination" - walking on the lateral portion of the foot). For toe in/out gait, the subjects walked with an increased internal/external foot progression angle (FPA) compared with normal gait. All of them are known as the most common gait abnormalities generated either by inborn reason or ill habit. We propose an intelligent shoe-integrated system from which the information derived can give efficient assistance in determining and alarming the persons associated with abnormal gaits focusing on the above gait abnormalities. This system is of particular significance to provide feedback in the application of gait abnormality rectification.

In the past decade, as more and more studies on human gait are conducted, numerous systems for gait data acquisition and analysis are proposed, including camera-based [78] [79] [80], floor-mounted [81], and in-shoe configuration systems. However, among all

the available systems, the in-shoe device is most utilized due to the outstanding merit of extending the usable location for human gait study. An in-shoe multisensory data acquisition system has already been developed [13]. In the system, except for pressure sensors, temperature and humidity sensors were located in a shoe to monitor the corresponding information. However, they mainly focused on the hardware design and little discussion on data interpretation and analysis was introduced. Morris et al. [15] [82] developed a wireless sensor system for realtime data acquisition which had potential use in clinical gait analysis. More introductions about prototype design were presented, but the pattern recognition method was not mentioned in detail. In addition, the Pedar insole system (Novel, Munich) is a commercially available system which is widely used in clinic sites and laboratories due to its repeatability and accuracy [83]. Ray and Snyder utilized the Novel Pedar in-shoe system for gait analysis on subjects with overpronated (fallen arches) and oversupination [84]. They also investigated gait-line velocities taken on various subjects to establish dynamic patterns during normal gait using Pedar insole for data collection [85]. However, the limitations of the Pedar insole system still exist, including a heavy wireless and memory storage module, a thick insole, and an expensive price.

In this chapter, we present a methodology for human abnormal gait modeling via hidden Markov model under the framework of cost-effective shoe-integrated systems. The proposed pattern recognition approach is mainly based on Principal Component Analysis (PCA) for feature generation and hidden Markov model (HMM) for multi-pattern modeling. Besides, the methodology of optimal SVM classifier introduced in Chapter 5 is also applied for the problem of detecting abnormal gait patterns. This intelligent system has the potential application for gait abnormality rectification. Fig. 6.1 displays the outside view of the prototype.

This chapter is organized as follows. In Section 6.2, we describe the proposed approach of how to apply PCA for feature extraction and HMM for abnormal gait modeling and evaluation. Experimental results are discussed in detail in Section 6.3. We draw the summary in final Section 6.4.

Figure 6.1: Outside view of the intelligent shoe

6.2 Human Gait Modeling and Evaluation via Hidden Markov Model

We aim to model human gaits including both normal and abnormal ones into five classes: normal, toe in, toe out, oversupination, and heel walking, according to a group of gait features. The process of gait model generation and evaluation which is illustrated by a block diagram in Fig. 6.2 mainly consists of the following four procedures:
(1) Set up gait database of "normal", "toe in", "toe out", "oversupination", and "heel walking" based on the data obtained from subjects wearing the shoe-integrated systems;
(2) Use Fast Fourier Transform (FFT) to convert data from the time domain to the frequency domain;
(3) Apply Principal Component Analysis (PCA) for feature generation;
(4) Model and evaluate human gait patterns via hidden Markov model (HMM).

6.2.1 PCA for Feature Generation

It is necessary and important to apply feature generation and reduction in data preprocessing for modeling human gait patterns, since failures in feature selection can significantly diminish the efficiency of system performance. In addition, even though the present features contain enough information about the classification problem, they cannot be used

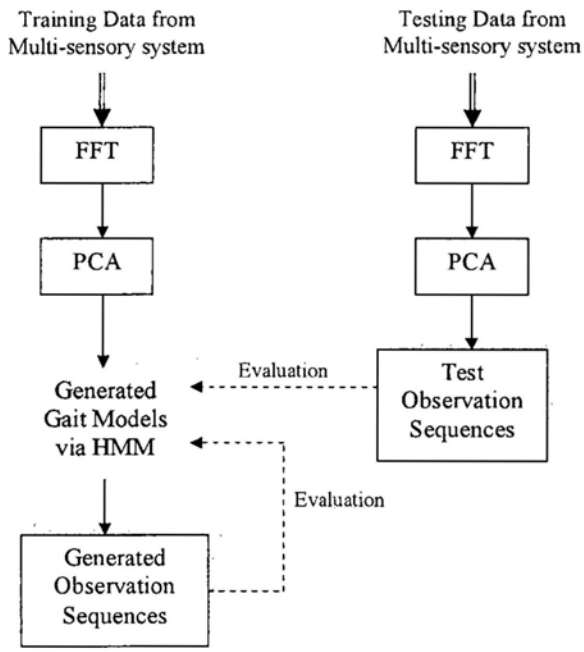

Figure 6.2: Block diagram of the software design

for predicting the output result correctly since the dimension of the feature space is so large that it requires large numbers of instances to determine the result. Among several feature extraction methods, Principal Component Analysis (PCA) is widely utilized in the field of pattern recognition and in many signal processing applications. PCA generates a new set of variables, called principal components (PCs), by projecting the original variables to mutually orthogonal axes. In the routine, singular value decomposition (SVD) is applied to efficiently computer PCs [86].

6.2.2 Training and Evaluation by HMM

Hidden Markov model (HMM) is a trainable statistical model with an underlying stochastic process which is unobservable. The internal properties of HMM can only be represented via another set of stochastic processes generating the observation sequences. The appealing feature of HMM is that no a priori assumptions are made about the statistical distribution of the data. Due to the rich mathematical structure, HMM can form

the theoretical basis using in a wide range of signal processing applications, from the wide application in speech recognition [87] to the field of action skill learning [88] and human gesture recognition [89].

The reasons to utilize HMM in the analysis of gait abnormalities are as follows:

- HMM is a doubly stochastic model. Gait data shows variabilities for one individual's same walking pattern between trials, even in the same trial. HMM has the capability to characterize the immeasurable stochastic process that represent the same gait pattern.

- HMM treats observations without explicit physical understanding. This makes it possible to model gait abnormalities regardless of less psychological and biological understanding of the stochastic process.

- HMM parameters can be optimized via efficient algorithms. The incrementally updated HMM is much flexibility in modeling gait patterns.

We develop five 6-state left-right HMMs for modeling normal gait and four kinds of abnormal ones (toe in, toe out, oversupination, and heel walking) for each subject.

A hidden Markov model is a collection of finite states $S = \{S_1, S_2, ..., S_N\}$ interconnected by transitions. Each state has a number of distinct observation symbols $V = \{v_1, v_2, ..., v_M\}$ corresponding to the physical output of the system being modeled. A HMM can be specified by the following notation:

$$\lambda = (A, B, \pi) \tag{6.1}$$

1. A - The state transition probability distribution $A = \{a_{ij}\}$, where a_{ij} denotes the probability of transition from S_i to S_j.

2. B - The observation symbol probability distribution at the given state S_i, $B = \{b_i(x)\}$.

3. π - The initial state probability distribution vector $\pi = \{\pi_i\}$.

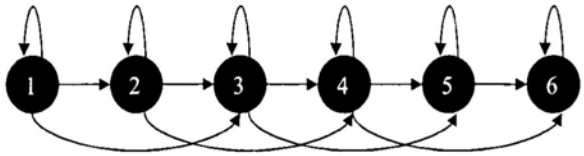

Figure 6.3: 6-state left-right HMM

From the above discussion, it can be seen that a complete description of a HMM requires the selection of model parameters: N-the number of states in the model, M-the number of distinct observation symbols per state; description of observation symbols; as well as three probability matrices A, B, and π.

The state transition coefficients of left-right HMM have the fundamental property:

$$a_{ij} = 0, i > j \tag{6.2}$$

Furthermore, the initial state probabilities satisfy:

$$\pi_i = \begin{cases} 1 & \text{if } i = 1 \\ 0 & \text{if } i \neq 1 \end{cases} \tag{6.3}$$

which means the state sequence must start in state 1 and finish in state N. In our designed left-right HMMs for human gait patterns, no more than 2 jumps are allowed for state transition coefficients in order to avoid large changes in state indices (shown in Fig. 6.3).

The state transition matrix in this case is

$$A = \begin{bmatrix} a_{11} & a_{12} & a_{13} & 0 & 0 & 0 \\ 0 & a_{22} & a_{23} & a_{24} & 0 & 0 \\ 0 & 0 & a_{33} & a_{34} & a_{35} & 0 \\ 0 & 0 & 0 & a_{44} & a_{45} & a_{46} \\ 0 & 0 & 0 & 0 & a_{55} & a_{56} \\ 0 & 0 & 0 & 0 & 0 & a_{66} \end{bmatrix} \tag{6.4}$$

Aiming to model human gaits and to preform similarity measure based on the models designed, we particularly focus on the problems of learning and evaluation (or recognition). The problem of learning is to adjust the probability matrices A, B, and π so as to maximum the likelihood $P(O|\lambda)$ based on the given observation sequences. Although there is no analytical approach known to obtain the model with the maximum probability of the given finite observation sequences, an iterative algorithm such as the Baum-Welch algorithm [90], the Expectation Maximization (EM) method [91] or gradient techniques can be used to iteratively reestimate HMM parameters so as to achieve the local maximum $P(O|\lambda)$. The definition of the evaluation problem is that given a defined hidden Markov models $\lambda = \{\lambda_1, \lambda_2, ..., \lambda_i\}$, and a sequence of observations O_k, calculate the probabilities $P(O_k|\lambda_i)$ for all the given models, then the gait pattern with the highest probability will be selected. Forward-Backward algorithm [92] [93] provides an efficient approach for solving the evaluation problem.

6.3 Experiments and Analysis

6.3.1 Data Acquisition and Database Formation

After A/D transformation, the digital data of all sensors are packaged, which effectively decreases the transmission error and the sampling frequency is increased to 50 Hz which is adequate for the activity of walking. In the host computer, we obtain the corresponding information applied for each sensor based on data reconstruction and calibration. Fig. 6.4 shows the location of the IMU board attached to the shoe-integrated system with the definition of reference axes for gyroscopes and accelerometer. Fig. 6.5 to Fig. 6.9 respectively displays the force waveforms under each FSR, the voltage change of the bend sensor, and 3D inertial parameters as a function of time for Subject#1's five gait patterns mentioned above.

Since we do data analysis by examining both the left and right feet, the training data in a 4575×22 matrix and testing data in a 11325×22 matrix for each of the five gait patterns are produced. After applying Fast Fourier Transform (FFT) processing, we transfer the

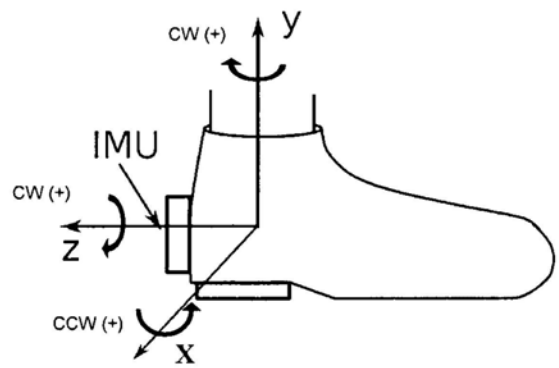

Figure 6.4: IMU location and reference axes for gyroscopes and accelerometer

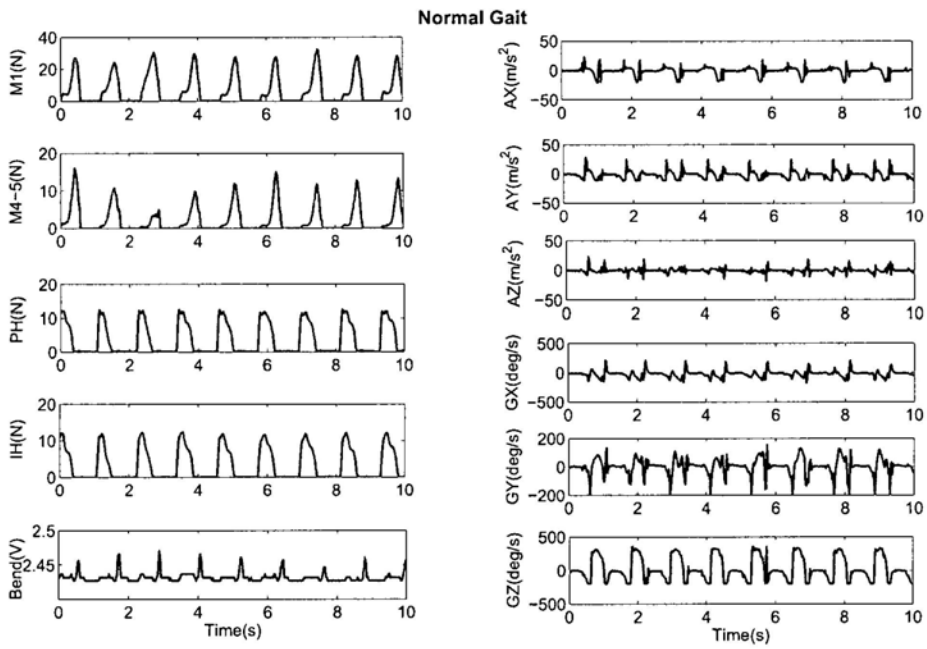

Figure 6.5: Force waveforms under 4 right foot regions, bend parameter, and 3D inertial parameters during normal walking (M1 = 1st metatarsal head, M4-5 = the position between 4th and 5th metatarsal heads, PH = posterior heel, and IH = inside heel, Bend = bend sensor, AX-AZ = 3D accelerations, GX-GZ = 3D angular rates)

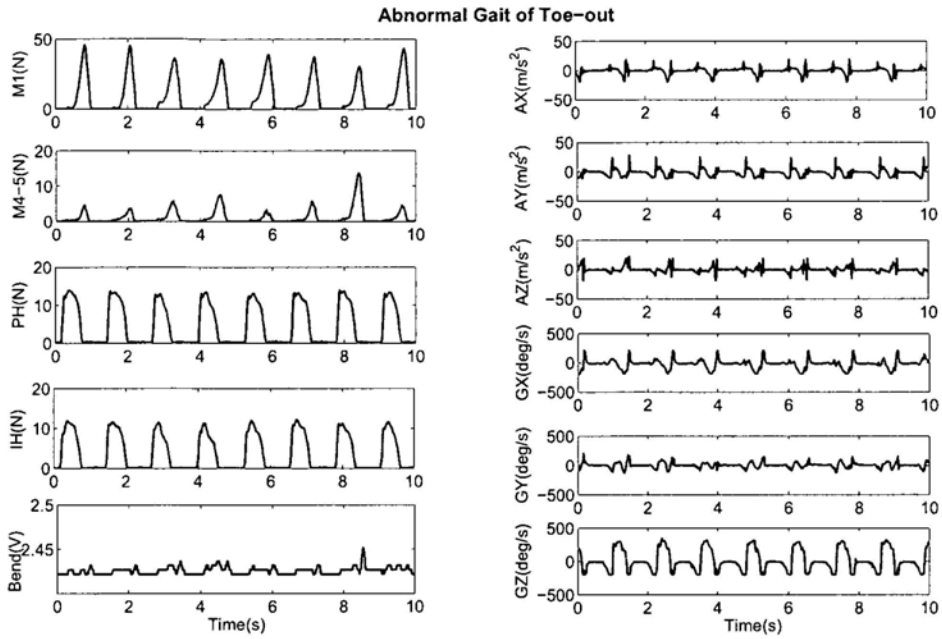

Figure 6.6: Force waveforms under 4 right foot regions, bend parameter, and 3D inertial parameters during toe-out walking (M1 = 1st metatarsal head, M4-5 = the position between 4th and 5th metatarsal heads, PH = posterior heel, and IH = inside heel, Bend = bend sensor, AX-AZ = 3D accelerations, GX-GZ = 3D angular rates)

training and testing data into a 900×66 and a 2250×66 matrix respectively with three primary coefficients selected. In order to reduce the dimension of the input data, we apply Principal Component Analysis (PCA) for feature generation. The PCA process reduces the dimension from 66 to 10. As a result, the final dimensions for the training and testing sequences are 900×10 and 2250×10. Furthermore, both the training and testing data are divided into a suit of segments, each of which contains 50 sampling points.

6.3.2 Human Gait Modeling

A discrete 6-state left-right HMM is employed to model each gait pattern denoted as $\{F1(t) - F4(t), B(t), Ax - y - z(t), Gx - y - z(t)\}$, where $F1(t) - F4(t)$ denote the force information under four plantar positions, $B(t)$ denotes the flexibility information of foot,

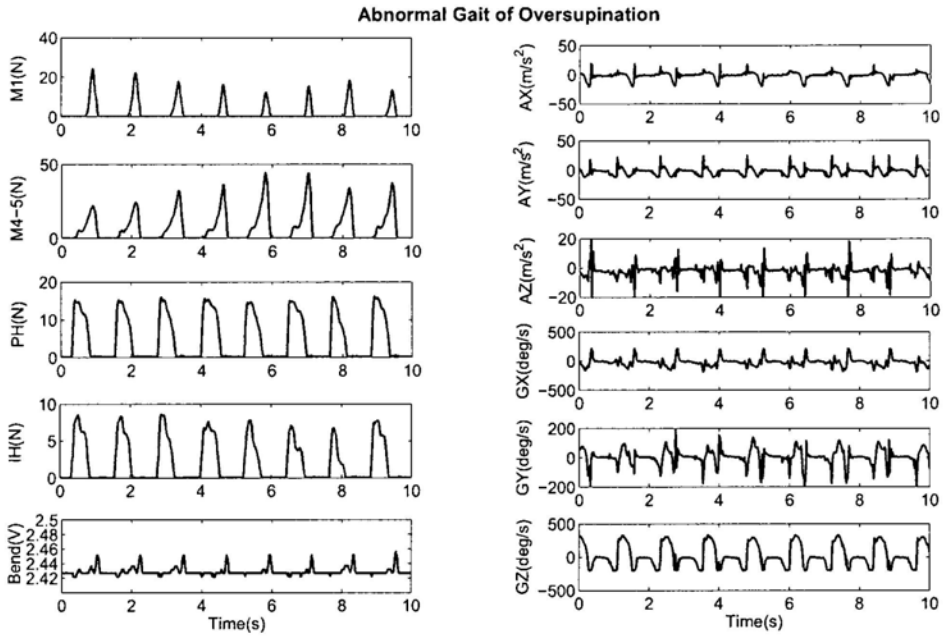

Figure 6.7: Force waveforms under 4 right foot regions, bend parameter, and 3D inertial parameters during oversupination walking (M1 = 1st metatarsal head, M4-5 = the position between 4th and 5th metatarsal heads, PH = posterior heel, and IH = inside heel, Bend = bend sensor, AX-AZ = 3D accelerations, GX-GZ = 3D angular rates)

$Ax-y-z(t)$ represents the values of three-dimensional accelerations, and $Gx-y-z(t)$ represents the values of three-dimensional angular rates.

Four healthy adult subjects, three females and one male, with normal weight and height, were invited for this investigation. We train five 6-state left-right HMMs of the five gait patterns mentioned above based on each subject's walking data. HMM parameters including the three probability matrices A, B, and π are initialized using a uniform segmentation for each training sequence. Each sequence is split into N successive sections, where N is the state number of the HMM structure. The vectors of each state are utilized to obtain the initial HMM parameters of the N-conditional distributions. The Baum-Welch algorithm is used to iteratively reestimate the parameters according to the forward and backward variables. 60 iterations are run for each training process.

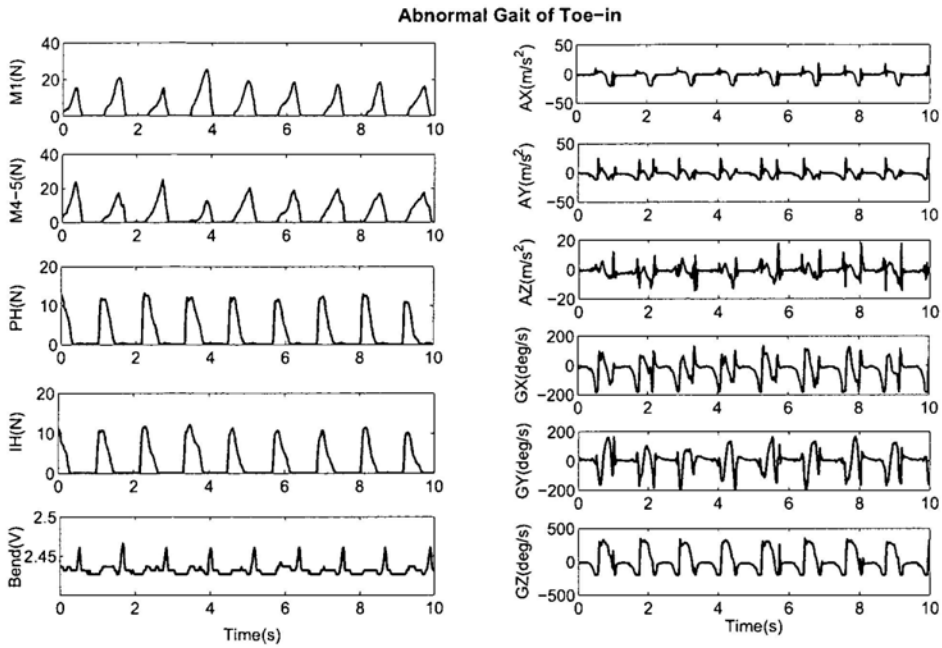

Figure 6.8: Force waveforms under 4 right foot regions, bend parameter, and 3D inertial parameters during toe-in walking (M1 = 1st metatarsal head, M4-5 = the position between 4th and 5th metatarsal heads, PH = posterior heel, and IH = inside heel, Bend = bend sensor, AX-AZ = 3D accelerations, GX-GZ = 3D angular rates)

Fig. 6.10 shows all 20 HMMs' estimation results denoted as the log-likelihood versus the learning iteration index. Eventually the log-likelihood converges to a critical point. During the training process, the increase of the log-likelihood indicates the improvement of the model parameters. After the learning iterations, 20 HMMs representing the five gait models for the four subjects are retrieved based on the training data samples.

6.3.3 Similarity Analysis: Model to Model

In order to evaluate the five trained gait models (λ_1-λ_5) for each subject, each model randomly generates two observation sequences which have the same size as the ones for the training and testing purpose.

We apply those generated observation sequences O_i as the test data to all trained

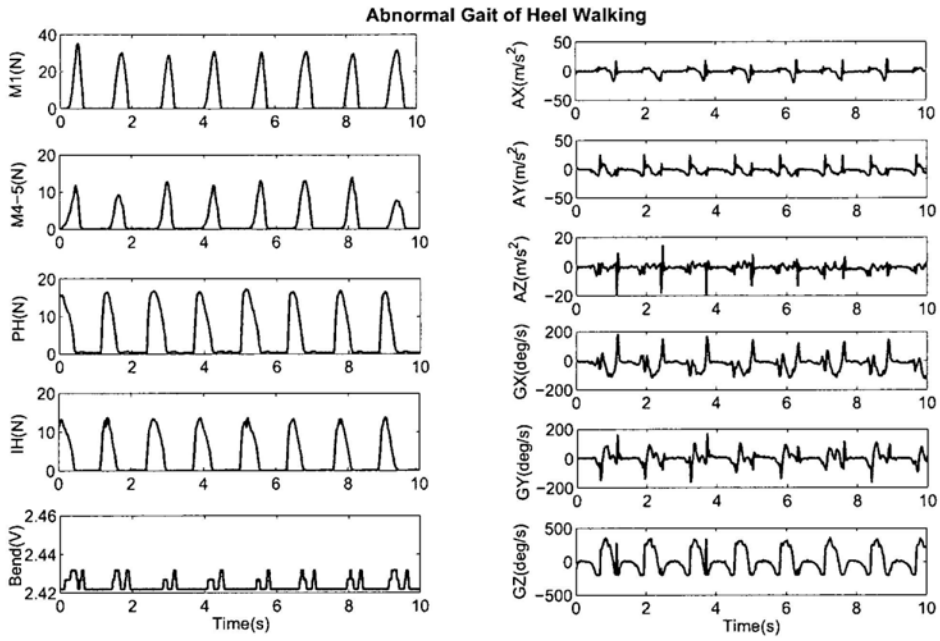

Figure 6.9: Force waveforms under 4 right foot regions, bend parameter, and 3D inertial parameters during heel walking (M1 = 1st metatarsal head, M4-5 = the position between 4th and 5th metatarsal heads, PH = posterior heel, and IH = inside heel, Bend = bend sensor, AX-AZ = 3D accelerations, GX-GZ = 3D angular rates)

models $\lambda_j (j = 1, ..., 5)$ one by one. Then we compute the probability $P(O_i|\lambda_j)$ of each generated observation sequence with respect to the model, using Forward-Backward algorithm. After calculating $P(O_i|\lambda_j)$, it is normalized by the length of the sequence T, then a *log* scale is applied in order to avoid the underflow problem of data.

As listed in Table 6.1 and Table 6.2, it is obviously shown that the log-likelihood reaches the maximum (marked with grey), when $i = j$. That is to say, each generated observation sequence is much more similar to the model generating it than all the other models. The same investigation results happen for all four subjects.

Besides, we also introduce the similarity distance measure to evaluate model to model similarity. The similarity measure $\sigma(\lambda_j, \lambda_i)$ for model λ_j to λ_i is defined as (6.5). O_i is the observation sequence generated by model λ_i. $P(O_i|\lambda_i)$ and $P(O_i|\lambda_j)$ are the log-likelihood

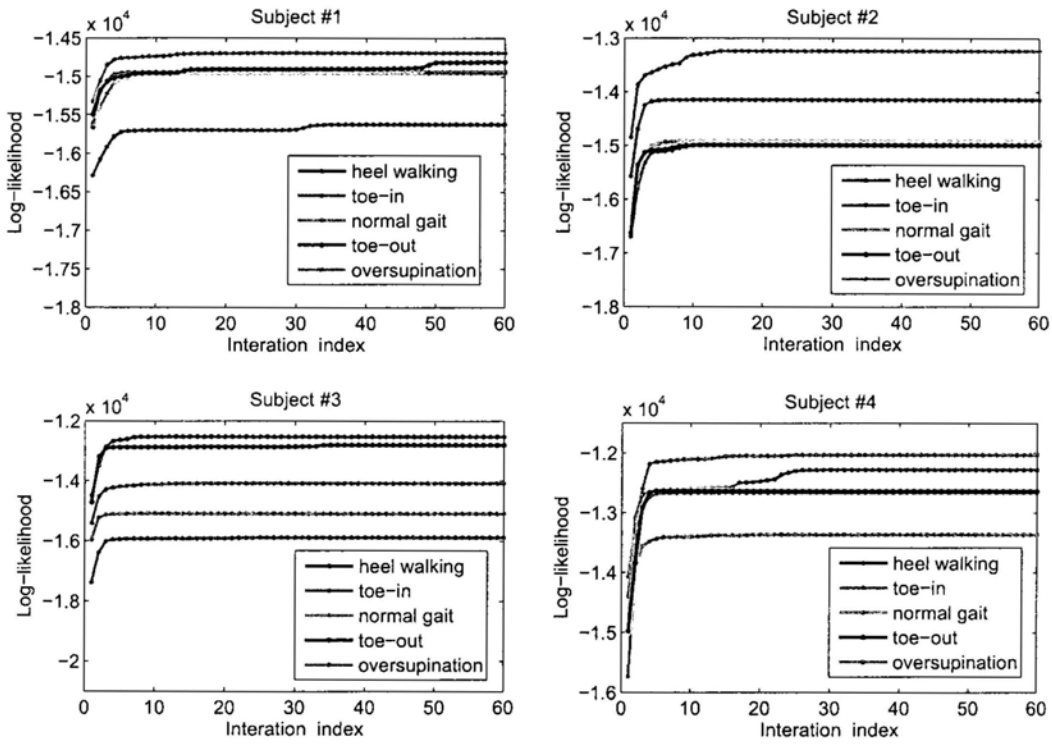

Figure 6.10: Log-likelihood versus learning iteration index in the training processes for the four subjects with N=6

Table 6.1: Log-likelihood of randomly generated sequences to the trained HMMs for subjects with N=6 ($M1$: Heel Walking, $M2$: Toe-in, $M3$: Normal Gait, $M4$: Toe-out, $M5$: Oversupination)

	Subject#1(Chen)				
Log − likelihood	$M1$	$M2$	$M3$	$M4$	$M5$
$GS\#1-1$	-819.3	-1575.4	-1150.7	-1592.6	-2063.9
$GS\#1-2$	-841.3	-1501.6	-1120.8	-1688.3	-1848.9
$GS\#2-1$	-1671.0	-887.4	-1358.6	-2759.0	-1534.6
$GS\#2-2$	-1740.8	-869.5	-1467.9	-2857.0	-1517.4
$GS\#3-1$	-1226.2	-1318.9	-831.8	-1759.4	-2094.8
$GS\#3-2$	-1271.5	-1306.1	-843.8	-1861.5	-2126.9
$GS\#4-1$	-1674.0	-1984.5	-1722.9	-838.9	-3659.5
$GS\#4-2$	-1760.3	-2037.6	-1832.4	-866.0	-3659.1
$GS\#5-1$	-1579.7	-1293.0	-1779.6	-2755.9	-823.3
$GS\#5-2$	-1637.2	-1200.7	-1604.0	-2820.8	-818.0
	Subject#2(Tong)				
Log − likelihood	$M1$	$M2$	$M3$	$M4$	$M5$
$GS\#1-1$	-820.1	-1774.5	-1284.4	-1171.9	-2013.9
$GS\#1-2$	-825.0	-2193.3	-1548.5	-1506.1	-2310.6
$GS\#2-1$	-1737.0	-769.0	-981.3	-1695.6	-1421.2
$GS\#2-2$	-1715.3	-804.1	-1014.6	-1804.3	-1332.9
$GS\#3-1$	-1451.5	-1278.2	-939.0	-1381.8	-1822.7
$GS\#3-2$	-1428.8	-911.1	-786.1	-1342.8	-1858.8
$GS\#4-1$	-1237.4	-1886.5	-1252.1	-868.0	-1933.7
$GS\#4-2$	-1246.7	-1838.3	-1254.6	-869.3	-2023.8
$GS\#5-1$	-2192.4	-1501.3	-1714.0	-2307.9	-745.0
$GS\#5-2$	-2219.8	-1418.1	-1747.4	-2373.3	-704.3

Table 6.2: Log-likelihood of randomly generated sequences to the trained HMMs for subjects with N=6 ($M1$: Heel Walking, $M2$: Toe-in, $M3$: Normal Gait, $M4$: Toe-out, $M5$: Oversupination)

	Subject#3(Liu)				
Log − likelihood	$M1$	$M2$	$M3$	$M4$	$M5$
$GS\#1-1$	-735.1	-2548.0	-1481.7	-1569.6	-1653.9
$GS\#1-2$	-754.4	-2195.0	-1543.6	-1756.2	-1520.0
$GS\#2-1$	-2738.5	-899.8	-1575.4	-3078.5	-1719.9
$GS\#2-2$	-2565.1	-901.9	-1582.8	-3052.7	-1631.0
$GS\#3-1$	-2033.3	-1530.0	-821.2	-2365.8	-1495.7
$GS\#3-2$	-2452.0	-1382.4	-867.1	-2819.6	-1501.7
$GS\#4-1$	-1396.3	-2693.0	-1718.3	-746.9	-1683.3
$GS\#4-2$	-1584.8	-2873.6	-1858.6	-691.7	-1702.5
$GS\#5-1$	-1812.9	-1366.4	-1238.4	-2579.3	-751.0
$GS\#5-2$	-1569.5	-1479.0	-1205.8	-2238.5	-733.2
	Subject#4(Qian)				
Log − likelihood	$M1$	$M2$	$M3$	$M4$	$M5$
$GS\#1-1$	-656.1	-2938.5	-1535.6	-1584.5	-5836.5
$GS\#1-2$	-702.5	-2822.4	-1610.1	-1483.1	-5800.4
$GS\#2-1$	-3961.0	-703.9	-2283.8	-2235.7	-2703.2
$GS\#2-2$	-3451.2	-670.1	-1925.2	-2038.6	-2725.4
$GS\#3-1$	-1653.5	-1653.2	-762.7	-1136.4	-4029.8
$GS\#3-2$	-1528.2	-1742.4	-764.7	-1552.4	-4288.0
$GS\#4-1$	-1724.0	-2664.7	-1097.3	-728.7	-5311.7
$GS\#4-2$	-1814.2	-2214.0	-1215.3	-785.1	-5047.0
$GS\#5-1$	-3806.1	-3026.4	-4508.3	-3104.9	-682.8
$GS\#5-2$	-3963.4	-2972.6	-4702.7	-3066.0	-653.9

for O_i to λ_i and λ_j. The results of the similarity distance measure are shown in Table 6.3 and Table 6.4.

$$\sigma(\lambda_j, \lambda_i) = 10^{[P(O_i|\lambda_i) - P(O_i|\lambda_j)]/P(O_i|\lambda_i)} \tag{6.5}$$

6.3.4 Similarity Analysis: Human to Model

Besides using randomly generated observation sequences to evaluate trained HMMs, we also apply test observation sequences for human to model similarity evaluation. As introduced above, the test data in a 2250×10 matrix for each gait pattern is divided into 45 data segments, each of which including 50 sampling points. Totally 225 test segments for five gait patterns are used to evaluate the five gait models we build for each subject.

In the model to model similarity evaluation, the trained models are all based on the HMM structure of 6-state. For the human to model similarity evaluation, we also consider the selection of HMM parameter N, since different state numbers may influence obtaining the best identification performance. Fig. 6.11 displays the identification results based on different state numbers ranging from 5 to 14 for each subjects's five gait patterns. A conclusion can be made that the identification result will drift within a small range with the state number N ranging from 5 to 14. Considering that a larger state number will increase the model complexity, we select the smaller one if it can equal the best performance as the HMM structure with higher state number. Based on the above rule, the state numbers for Subject#1, Subject#2, Subject#3, and Subject#4 are 5, 6, 5, and 8.

The identification rates for the four subjects based on the optimal state numbers are shown in Table 6.5. Taking the identification rate of Subject#2 's toe-in gait as an example, we utilize 45 test segments of toe-in gait ($M2-TS$) to calculate the log-likelihood values for all of the five gait models we built for Subject#2. The vote is designated to the model with the maximum log-likelihood. As a result, 43 of 45 test segments are successfully recognized as toe-in gait abnormality, and the other two segments are falsely considered to be normal gait ($M3$). The average success rate for all the four subjects' five gait patterns reaches 99.33%.

Table 6.3: Model to model similarity distance measure via randomly generated sequences for subjects with N=6 ($M1$: Heel Walking, $M2$: Toe-in, $M3$: Normal Gait, $M4$: Toe-out, $M5$: Oversupination)

	Subject#1(Chen)				
σ	$M1$	$M2$	$M3$	$M4$	$M5$
$GS\#1-1$	1.0000	0.1194	0.3939	0.1138	0.0303
$GS\#1-2$	1.0000	0.1641	0.4653	0.0984	0.0634
$GS\#2-1$	0.1309	1.0000	0.2944	0.0078	0.1865
$GS\#2-2$	0.0995	1.0000	0.2050	0.0052	0.1798
$GS\#3-1$	0.3357	0.2597	1.0000	0.0767	0.0303
$GS\#3-2$	0.3113	0.2833	1.0000	0.0622	0.0302
$GS\#4-1$	0.1010	0.0431	0.0883	1.0000	0.0004
$GS\#4-2$	0.0927	0.0444	0.0765	1.0000	0.0006
$GS\#5-1$	0.1206	0.2689	0.0689	0.0045	1.0000
$GS\#5-2$	0.0996	0.3405	0.1094	0.0036	1.0000
	Subject#2(Tong)				
σ	$M1$	$M2$	$M3$	$M4$	$M5$
$GS\#1-1$	1.0000	0.0686	0.2716	0.3724	0.0350
$GS\#1-2$	1.0000	0.0220	0.1328	0.1494	0.0158
$GS\#2-1$	0.0551	1.0000	0.5296	0.0624	0.1418
$GS\#2-2$	0.0736	1.0000	0.5473	0.0570	0.2200
$GS\#3-1$	0.2845	0.4352	1.0000	0.3375	0.1145
$GS\#3-2$	0.1522	0.6935	1.0000	0.1958	0.0432
$GS\#4-1$	0.3753	0.0671	0.3610	1.0000	0.0592
$GS\#4-2$	0.3680	0.0768	0.3604	1.0000	0.0470
$GS\#5-1$	0.0114	0.0965	0.0500	0.0080	1.0000
$GS\#5-2$	0.0070	0.0969	0.0330	0.0043	1.0000

Table 6.4: Model to model similarity distance measure via randomly generated sequences for subjects with N=6 ($M1$: Heel Walking, $M2$: Toe-in, $M3$: Normal Gait, $M4$: Toe-out, $M5$: Oversupination)

	Subject#3(Liu)				
σ	$M1$	$M2$	$M3$	$M4$	$M5$
$GS\#1-1$	1.0000	0.0034	0.0965	0.0732	0.0563
$GS\#1-2$	1.0000	0.0123	0.0900	0.0470	0.0967
$GS\#2-1$	0.0090	1.0000	0.1775	0.0038	0.1226
$GS\#2-2$	0.0143	1.0000	0.1758	0.0041	0.1554
$GS\#3-1$	0.0334	0.1370	1.0000	0.0132	0.1508
$GS\#3-2$	0.0149	0.2546	1.0000	0.0056	0.1854
$GS\#4-1$	0.1351	0.0025	0.0501	1.0000	0.0558
$GS\#4-2$	0.0512	0.0007	0.0206	1.0000	0.0346
$GS\#5-1$	0.0385	0.1516	0.2244	0.0037	1.0000
$GS\#5-2$	0.0723	0.0961	0.2267	0.0088	1.0000
	Subject#4(Qian)				
σ	$M1$	$M2$	$M3$	$M4$	$M5$
$GS\#1-1$	1.0000	0.0003	0.0457	0.0385	0.0000
$GS\#1-2$	1.0000	0.0010	0.0511	0.0774	0.0000
$GS\#2-1$	0.0000	1.0000	0.0057	0.0067	0.0014
$GS\#2-2$	0.0001	1.0000	0.0134	0.0091	0.0009
$GS\#3-1$	0.0679	0.0680	1.0000	0.3236	0.0001
$GS\#3-2$	0.1004	0.0527	1.0000	0.0933	0.0000
$GS\#4-1$	0.0431	0.0022	0.3119	1.0000	0.0000
$GS\#4-2$	0.0489	0.0151	0.2831	1.0000	0.0000
$GS\#5-1$	0.0000	0.0004	0.0000	0.0003	1.0000
$GS\#5-2$	0.0000	0.0003	0.0000	0.0002	1.0000

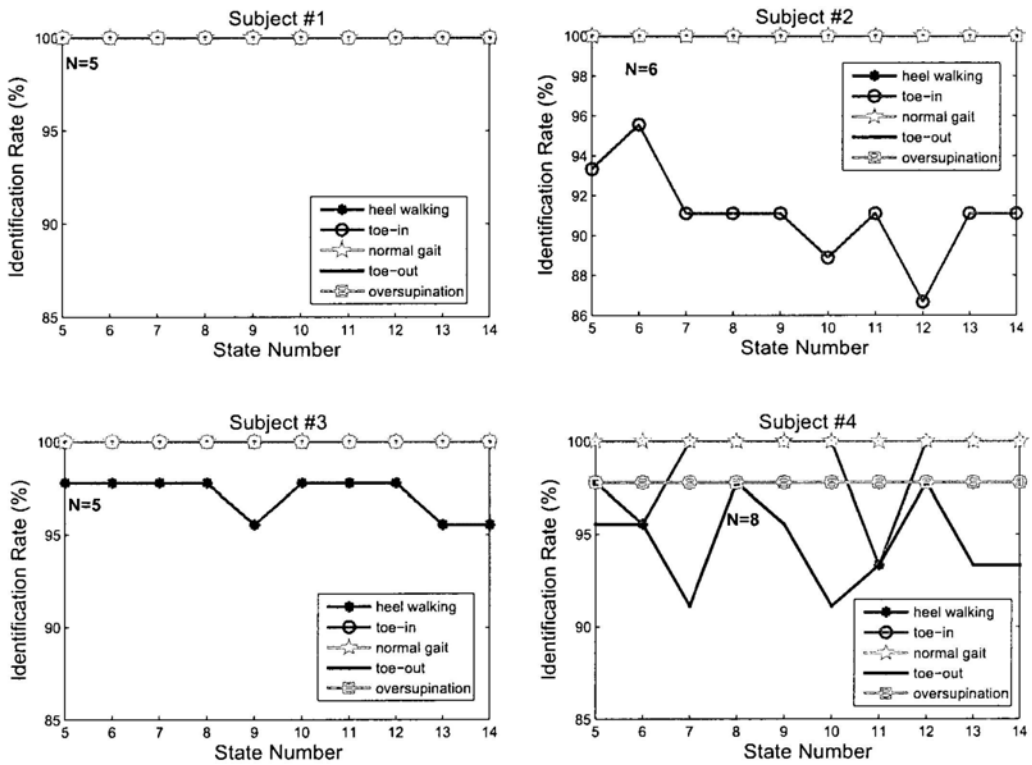

Figure 6.11: The identification rate vs different state number for the four subjects

Table 6.5: The success rate of identification for the four subjects with optimal state number ($M1$: Heel Walking, $M2$: Toe-in, $M3$: Normal Gait, $M4$: Toe-out, $M5$: Oversupination)

	Subject#1(Chen)					
Count	$M1$	$M2$	$M3$	$M4$	$M5$	*Identification Rate*
$M1-TS$	45	0	0	0	0	100%
$M2-TS$	0	45	0	0	0	100%
$M3-TS$	0	0	45	0	0	100%
$M4-TS$	0	0	0	45	0	100%
$M5-TS$	0	0	0	0	45	100%
	Subject#2(Tong)					
Count	$M1$	$M2$	$M3$	$M4$	$M5$	*Identification Rate*
$M1-TS$	45	0	0	0	0	100%
$M2-TS$	0	43	2	0	0	95.55%
$M3-TS$	0	0	45	0	0	100%
$M4-TS$	0	0	0	45	0	100%
$M5-TS$	0	0	0	0	45	100%
	Subject#3(Liu)					
Count	$M1$	$M2$	$M3$	$M4$	$M5$	*Identification Rate*
$M1-TS$	44	0	1	0	0	97.77%
$M2-TS$	0	45	0	0	0	100%
$M3-TS$	0	0	45	0	0	100%
$M4-TS$	0	0	0	45	0	100%
$M5-TS$	0	0	0	0	45	100%
	Subject#4(Qian)					
Count	$M1$	$M2$	$M3$	$M4$	$M5$	*Identification Rate*
$M1-TS$	45	0	0	0	0	100%
$M2-TS$	0	44	1	0	0	97.77%
$M3-TS$	0	0	45	0	0	100%
$M4-TS$	1	0	0	44	0	97.77%
$M5-TS$	0	0	1	0	44	97.77%

6.3.5 Support Vector Machine Approach

In addition to modeling and evaluating human abnormal gaits via hidden Markov models, the intelligent learning algorithm mentioned in Chapter 5, i.e. support vector machines (SVM) associated with genetic algorithm (GA) for optimizing SVM classifiers is also introduced to build multi-pattern model for the problem of abnormal gait detection.

For the training data segment, a 4575×22 matrix for each of the five gait patterns is produced. After applying Fast Fourier Transform (FFT) processing, we transfer each data segment into a 900×66 dimension matrix with three primary coefficients selected. After that, the PCA process reduces the data segments from 66-D to 10-D. The original testing data for each the five gait patterns is with 11325×22 matrix. After data preprocessing which is the same as the approach we apply for the training data, the total test segment for estimating the generated multi-classification model is with 11250×10 (2250×10 for each gait pattern).

For what has been discussed in Chapter 5, SVM model and parameter selection are very important for obtaining the best performance in SVM training. For the problem of abnormal gait detection, we also apply genetic algorithm (GA) for generating the most suitable SVM training parameters so as to obtain the optimal SVM classifier for each subject. The optimization processes of *C-SVM* and ν-*SVM* with RBF kernel function are considered respectively.

The optimization processes of fitness values for the two kinds of SVM algorithms are displayed from Fig. 6.12 to Fig. 6.15 for the four subjects. The SVM algorithm with smaller "best fitness value" will be selected as the optimal model type. The SVM training parameters corresponding to the best fitness value listed in Table 6.6 for the four subjects are regarded as the optimal solutions. The multi-classification results for the four subjects based on the optimal SVM classifiers are shown in Fig. 6.16. The average success rates listed in Table 6.7 demonstrate the SVM classifiers we build are robust and efficient for the problem of detecting abnormal gaits.

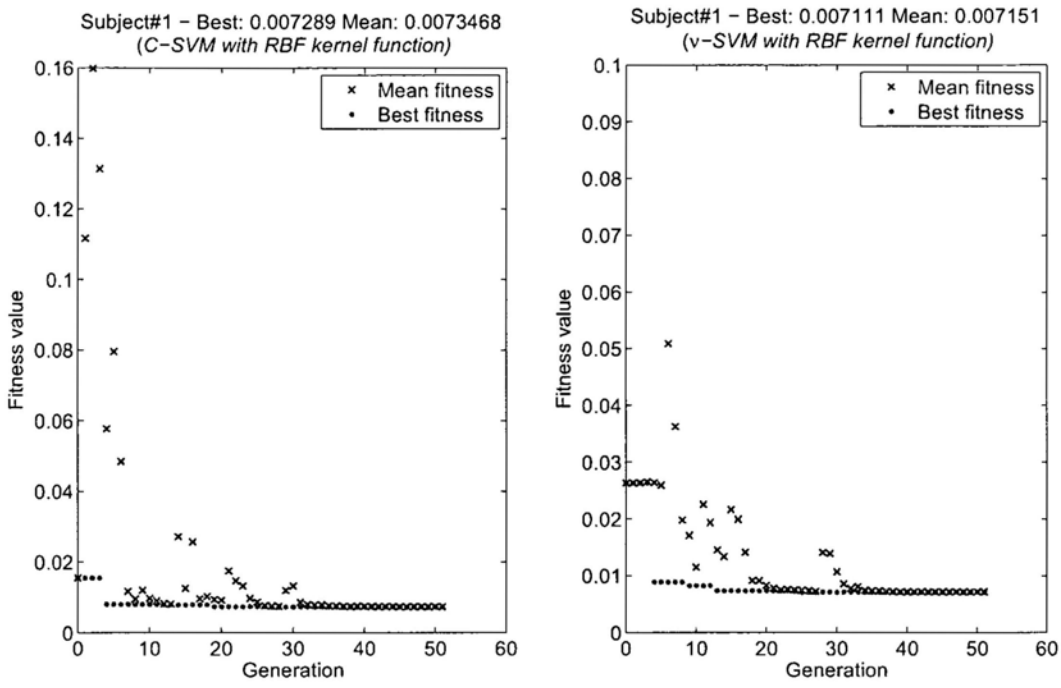

Figure 6.12: Optimization process of fitness value for Subject#1

Table 6.6: Optimal training parameters for the four subjects

Subject ID	*Optimal Parameters*		
	Model Type	*Variable Value*	
#1	*ν-SVM*	ν	0.174
		γ	0.0157
#2	*ν-SVM*	ν	0.128
		γ	0.035
#3	*C-SVM*	C	0.162
		γ	0.0081
#4	*ν-SVM*	ν	0.033
		γ	0.001

6.4 Summary

This chapter presents the methodology for modeling abnormal human gaits using hidden Markov model under the framework of shoe-integrated systems. The intelligent sys-

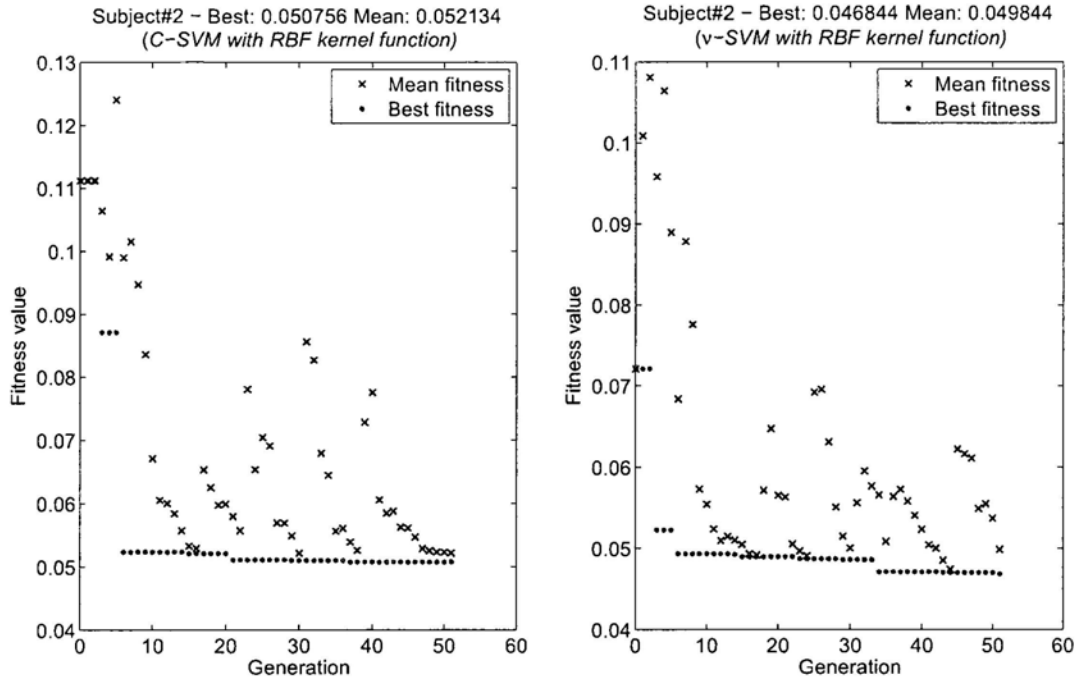

Figure 6.13: Optimization process of fitness value for Subject#2

Table 6.7: Average success rates for the four subjects

Subject ID	#1	#2	#3	#4
Average Success Rate (%)	99.28	95.31	97.50	95.59

tem focuses on modeling the following patterns: normal gait, toe in, toe out, heel walking, and oversupination abnormalities. In the developed prototype, an Inertial Measurement Unit (IMU) consisting of three-dimensional gyroscopes and accelerometers is employed to measure the angular velocities and accelerations of the foot. Four force sensing resistors (FSRs) and one bend sensor are arranged on the insole of each foot for force and flexion information acquisition. The proposed method is mainly based on Principal Component Analysis (PCA) for feature generation and hidden Markov model (HMM) for multi-pattern modeling. The "similarity distance measure" criterion which reflects the

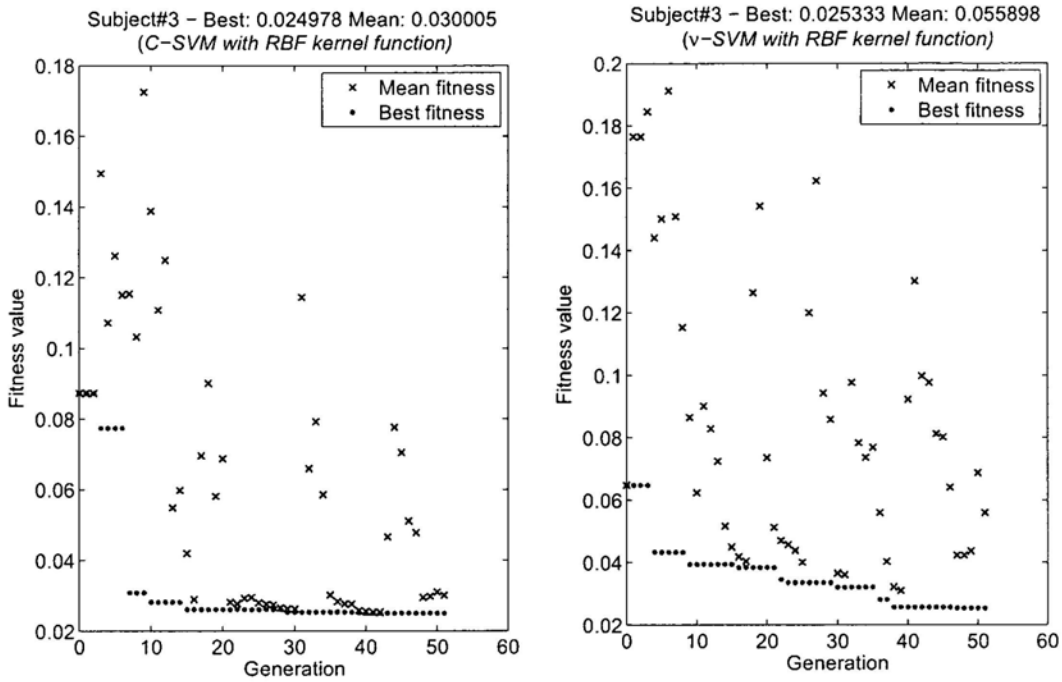

Figure 6.14: Optimization process of fitness value for Subject#3

similarity degree between models is introduced. Besides, the methodology of optimal SVM classifier introduced in Chapter 5 is also applied for the problem of detecting abnormal gait patterns. Experimental results of both HMM and SVM methodologies demonstrate the shoe-integrated system is robust and efficient in detecting abnormal gait patterns. Our goal is to provide a cost-effective system for detecting gait abnormalities in order to assist persons with abnormal gaits in developing a normal walking pattern in their daily life.

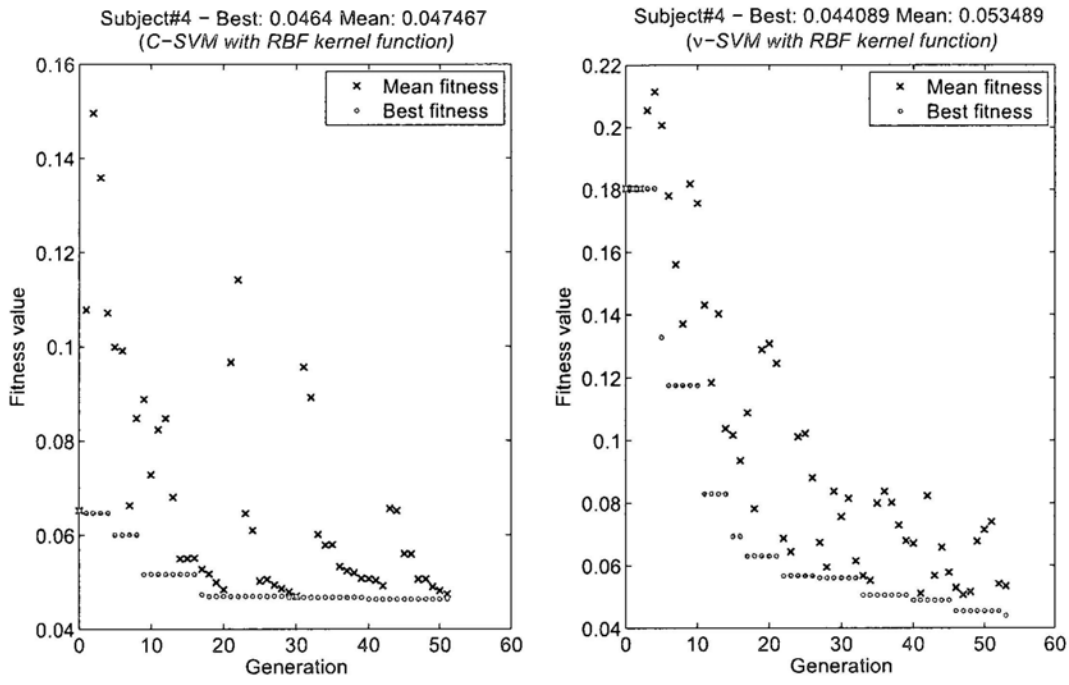

Figure 6.15: Optimization process of fitness value for Subject#4

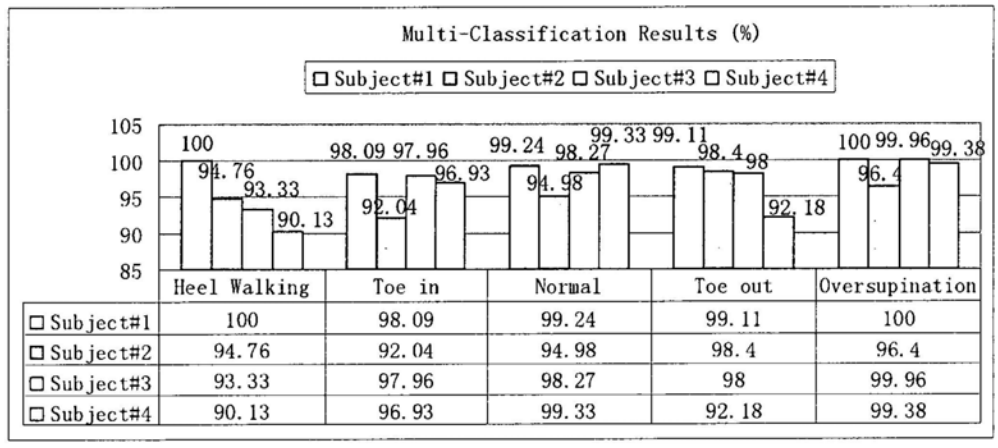

	Heel Walking	Toe in	Normal	Toe out	Oversupination
Subject#1	100	98.09	99.24	99.11	100
Subject#2	94.76	92.04	94.98	98.4	96.4
Subject#3	93.33	97.96	98.27	98	99.96
Subject#4	90.13	96.93	99.33	92.18	99.38

Figure 6.16: Classification results for the four subjects with optimal training parameters

Chapter 7

Conclusions

This thesis has investigated some significant problems related to the study of human motion abnormality under the framework of the intelligent shoe-integrated platform. In the final chapter, we summarize the research and briefly describe some areas of future research.

7.1 Conclusions

The design of the shoe-integrated platform has realized a wireless wearable system including a suite of sensors for capturing human gait parameters. The system architecture consists of four major subsystems: the insole, the Inertial Measurement Unit, the microprocessor-based data gathering subsystem, and the wireless communication module. Considering the fundamental requirements of the platform design, the compact and lightweight sensors and electronics are selected as the components for each subsystem. The whole system is compact and light so that it can be easily integrated with a user's shoes and he/she will notice little if any difference between his/her normal shoes and the proposed intelligent shoes. Wireless communication based on radio frequency (RF) makes it possible to capture and analyze human gait in a relatively extensive environment. The designed shoe-integrated system is an ideal platform for studying human motion abnormalities.

We studied human gait patterns and presented the design of the classifier for identifying gait patterns among flat walking, descending stairs, and ascending stairs based on continuous kinematic signals. Kinematic parameters in the same period were separated into gait segments which were further used as the units for pattern feature analysis. We applied discrete wavelet transform (DWT) for feature generation and fuzzy logic based approach for designing the multi-class classifier. Anteroposterior acceleration, vertical acceleration, and sagittal plane angular rate were demonstrated to provide useful information for classifying the gait patterns we focused, and the other kinematic parameters were almost useless. Experimental results of the six training and four testing subjects demonstrated that the selected features of the average sum of squares of wavelet coefficients efficiently represented the characteristics of the gait patterns we studied. Also fuzzy logic based classifier well described the distribution of the features.

The methodology for detecting postural kyphosis under the framework of the shoe-integrated system has been presented. Eight force sensing resistors (FSRs) for gathering the pressure information under the eight bony prominences were utilized. Based on the gathered plantar pressure information, we applied Cascade Neural Networks with Node-Decoupled Extended Kalman Filtering (CNN-NDEKF) for training the model for this binary classification problem. Different preprocessing approaches were utilized and experimental results demonstrated that Fast Fourier Transform (FFT) was the suitable data preprocessing approach for our problem.

In addition, we developed a novel falling detection algorithm based on the analysis of plantar force on both feet. Two FSRs were installed on each foot's two positions (1st metatarsal head and heel position) for acquiring the force change during subjects' locomotion. For Stage-One analysis, the candidate sequences were generated if force values of the four positions in both feet were simultaneously less than the corresponding predefined thresholds and lasted for a while. For Stage-Two analysis, we applied support vector machine (SVM) with genetic algorithm (GA) for generating optimal training parameters to determine whether there really existed a fall event. Linear and nonlinear parameters of each candidate were generated to be the feature vector, which was further reduced to

be more efficient input features for discrimination by applying Generalized Discriminant Analysis (GDA). The detection results demonstrated the two-stage algorithm we proposed for fall-event detection was efficient.

For gait abnormality study, we proposed the methodology for modeling abnormal human gaits using hidden Markov model. The intelligent system focused on modeling the following patterns: normal gait, toe in, toe out, heel walking, and oversupination abnormalities. In the developed prototype, an Inertial Measurement Unit (IMU) consisting of three-dimensional gyroscopes and accelerometers was employed to measure the angular velocities and accelerations of the foot. Four force FSRs and one bend sensor were arranged on the insole of each foot for force and flexion information acquisition. The proposed method was mainly based on Principal Component Analysis (PCA) for feature generation and hidden Markov model (HMM) for multi-pattern modeling. The "similarity distance measure" criterion which reflected the similarity degree between models was introduced. Besides, the methodology of optimal SVM classifier was also applied for this problem. Experimental results of both methodologies of HMM and SVM demonstrated the proposed shoe-integrated system was robust and efficient in detecting gait abnormalities and had the potential application for assisting persons with abnormal gaits in developing a normal walking pattern in their daily life.

7.2 Contributions

The contributions of this thesis are concluded as follows:

- The inexpensive, compact, and lightweight shoe-integrated platform has been designed and implemented for capturing a variety of gait-related parameters. Compared with the traditionally utilized human motion measurement systems, the shoe-integrated platform shows well performances in non-invasive and wireless motion data acquisition in a relatively extensive space, which is demonstrated as the ideal platform for the study of human motion abnormalities.

- A new gait pattern classification system has been built, based on the study of foot

movement during flat walking, descending stairs, and ascending stairs. We study the characteristics of kinematic parameters and demonstrate the parameters of antero-posterior acceleration, vertical acceleration, and sagittal plane angular rate provided useful information for gait pattern discrimination. The designed fuzzy-logic based classifier well describes the distribution of the common features generated by Discrete Wavelet Transform (DWT) of different gait patterns. The proposed system will make it possible for assisting to evaluate walking energy expenditure.

- The methodology of automatically detecting postural kyphosis has been investigated. The basic idea is to monitor and study the pressure distribution of feet during locomotion. We demonstrate gait analysis relying on plantar pressure provided an indirect but efficient approach for detecting postural abnormality of the upper body. The proposed system from which the pressure information derived could give efficient assistance in determining and alarming the persons associated with postural kyphosis.

- An automatic method for discriminating fall events from activities of daily living tasks based on plantar force information has been developed. By using the two-stage analysis algorithm we proposed, fall events could be detected efficiently in various situations.

- The methodology for modeling and classifying gait abnormalities has been presented, via machine learning algorithms, hidden Markov model (HMM) and support vector machine (SVM) based on a suite of gait parameters. The trained models after learning could realize gait abnormality identification.

The intelligent shoe-integrated system is a novel research tool different from the traditional measurement systems, which realizes realtime investigation in outdoor environments. It provides a good human-computer interface to understand human motion behavior. The proposed data processing methodologies fit to solve complex human motion data with the shoe-integrated system. Through use of pattern recognition, the proposed

system can provide efficient assistants in the applications of kinetic analysis of gait, rehabilitation assessment and so on. The conclusions of abnormality detection are valuable to biomedical and rehabilitation study. The shoe-integrated system has a great potential to be commercialized especially for adolescents and elders.

7.3 Future Work

Human motion analysis is a challenging mission. This thesis mainly addresses the fundamental problems of how to design an intelligent shoe-integrated platform and how to study and model human motion abnormalities under this measurement system. However, there are still some improving works and research ideas:

For the current falling detection trials, young volunteers were invited for gathering samples of activities of daily living (ADL) tasks and simulated falls. Considering the motion patterns of elderly people are different from younger ones' due to their reduced muscle strength with old age, in the future work, we will also invite elderly subjects to perform ADL tasks, which will enrich the database and increase the robustness of the detection methodology. Besides, the optimal number and position of force sensing resistors (FSRs) installed beneath foot for falling detection will be discussed. For the further study of postural kyphosis and gait abnormalities, we will investigate the effect on the classification result cased by different ground situations.

The proposed robust and scalable platform, also allows the intelligent shoe to act as a programmable control interface. Based on our current research that we can identify gait patterns among flat walking, descending stairs, and ascending stairs, we can utilize these movements to be the specific control signals. And other simple motions such as tapping the foot can also be modeled, recognized and, finally, defined to control specific external devices.

We will develop algorithms for estimating the Cartesian path of an individual wearing the intelligent shoe. Compared with other portable devices, shoe-integrated system seems more suitable for tracking the motions of elderly and children, since they may not feel uncomfortable for using it and have less chance of missing it. We propose to embed

the localization system into ordinary shoes such that the location of the wearer can be determined and their motion path can be identified. Under the shoe-integrated system, we will combine the proposed methodology of falling detection with the ability of user localization.

We believe, based on our research, with the endeavor of our colleagues and other researchers and engineers, with the further development of MEMS technologies, embedded system technologies, data processing algorithms and so on, the day when the shoe-integrated system is widely used will come soon.

Appendix A

Schematics and Layouts of Circuit Boards

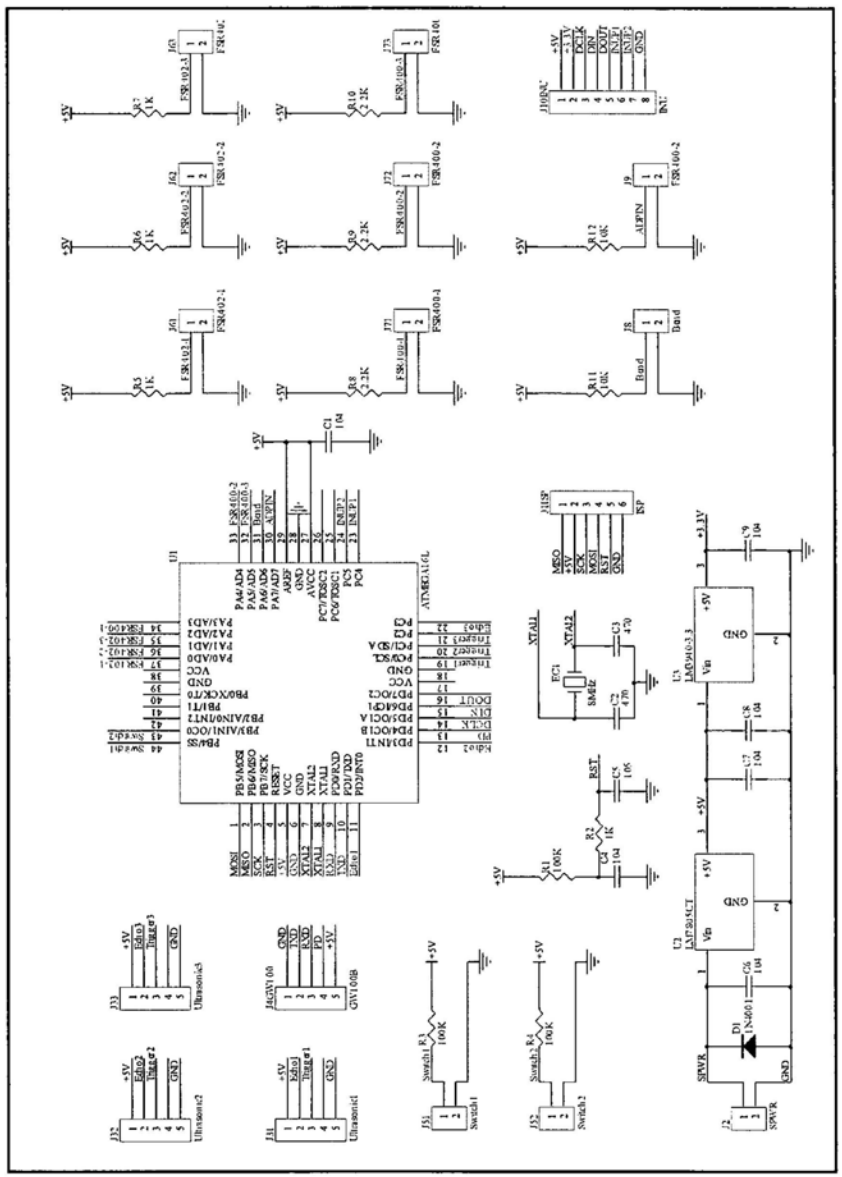

Figure A.1: Schematic of the main board including microprocessor-based subsystem, the power, FSR & bend sensors implementation

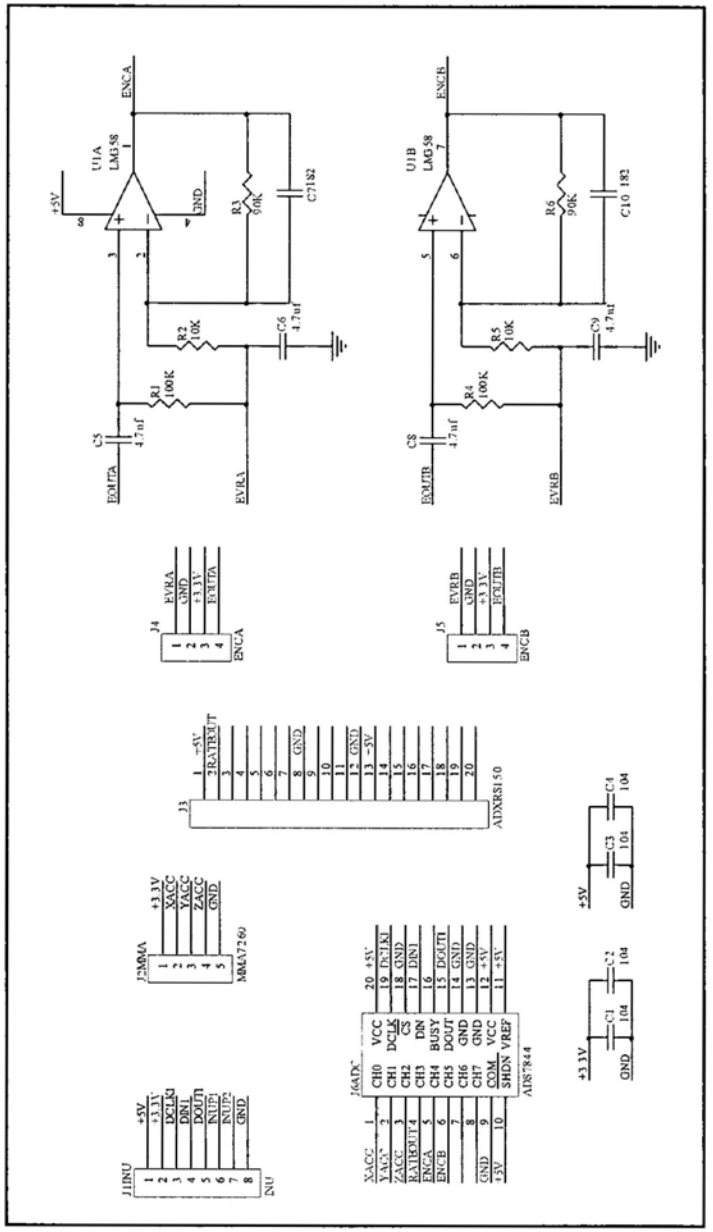

Figure A.2: Schematic of the IMU board

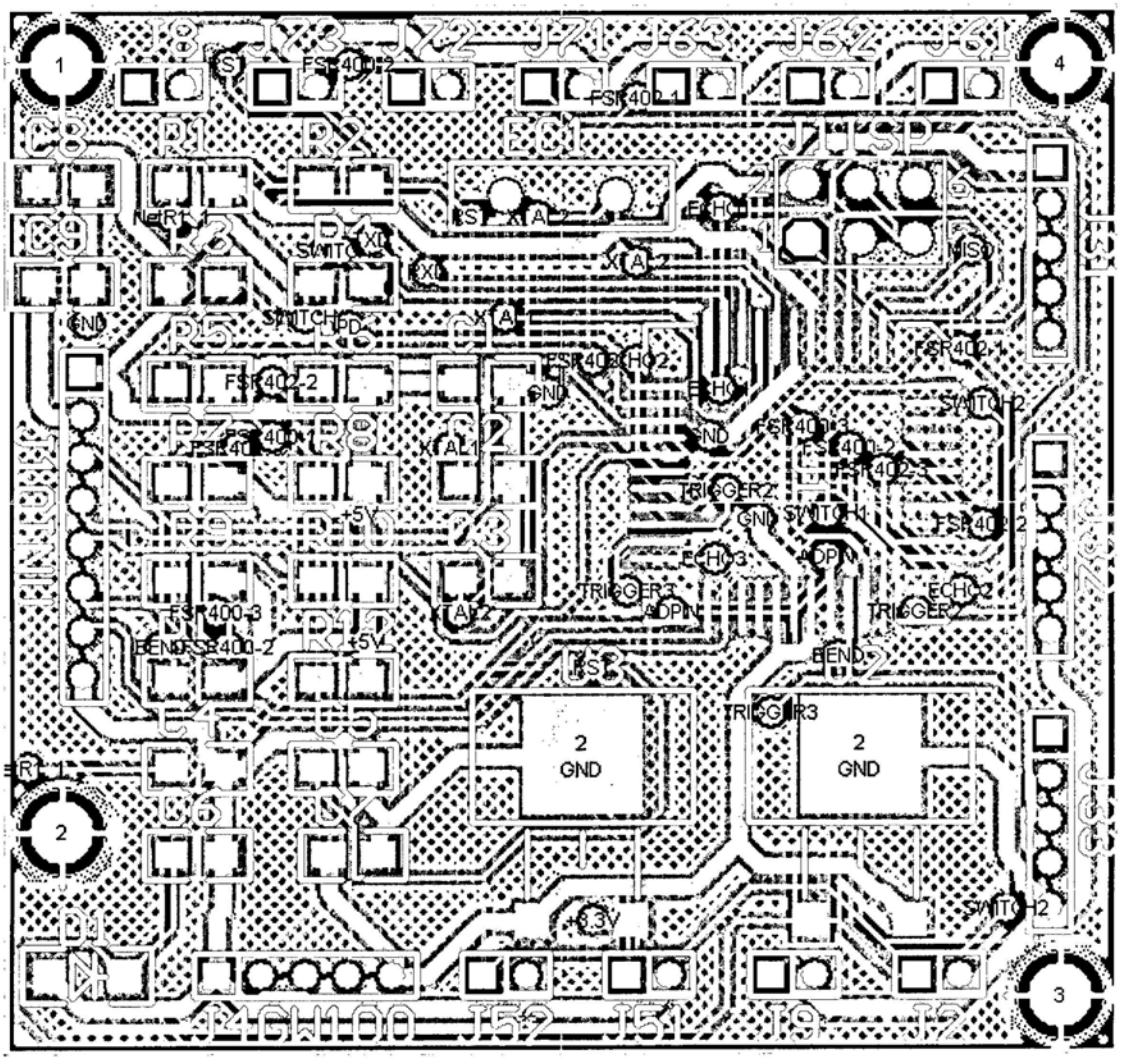

Figure A.3: Layout of the main board

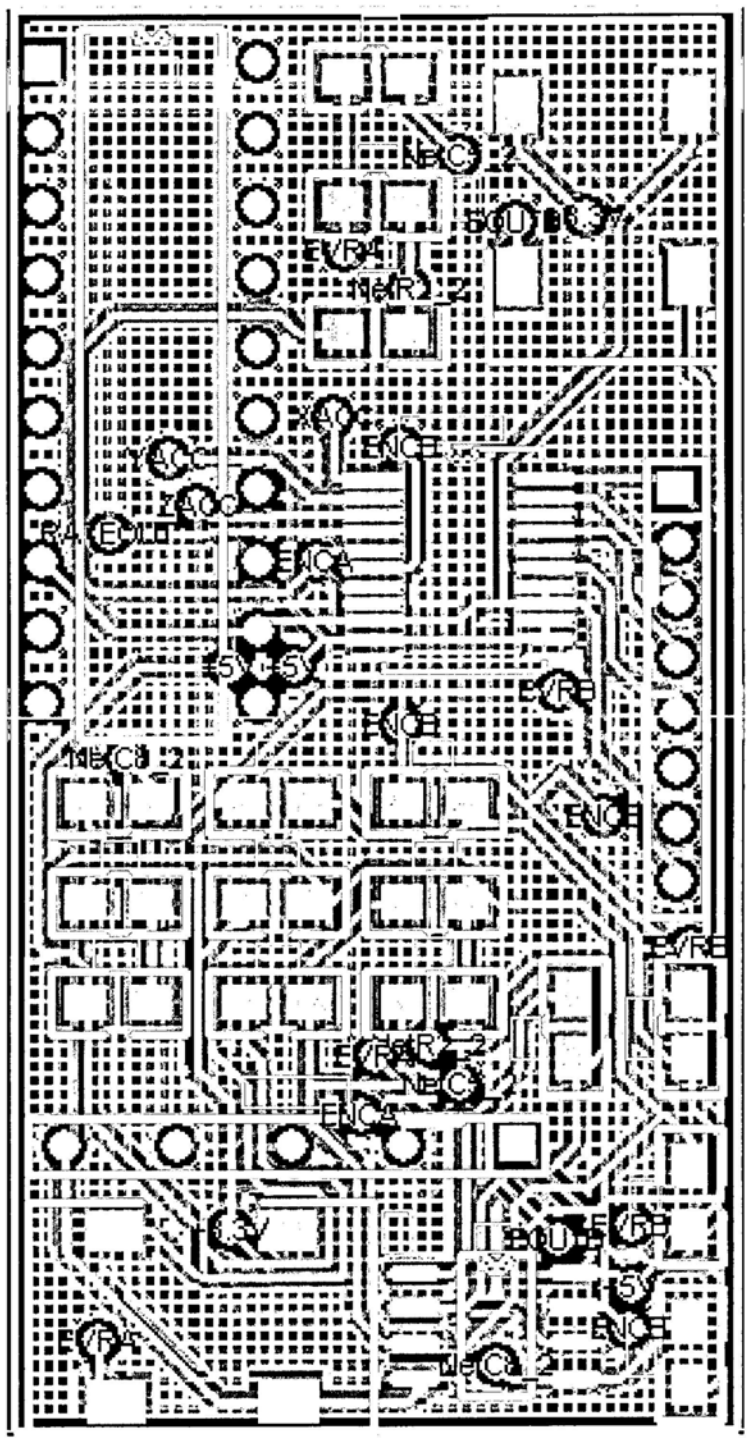

Figure A.4: Layout of the IMU board

Appendix B

Author's Publications

[1] Meng Chen, Jingyu Yan, and Yangsheng Xu,"Gait Pattern Classification with Integrated Shoes," *The 2009 IEEE/RSJ International Conference on Intelligent Robots and Systems*, pp. 833-839, St. Louis, USA, October 11-15, 2009.

[2] Meng Chen, Bufu Huang, and Yangsheng Xu, "Intelligent Shoes for Abnormal Gait Detection," *2008 IEEE International Conference on Robotics and Automation*, pp. 2019-2024, Pasadena, CA, USA, May 19-23, 2008.

[3] Meng Chen, Bufu Huang, and Yangsheng Xu, "Postural Kyphosis Detection Using Intelligent Shoes," *2008 IEEE International Conference on Robotics and Automation*, pp. 2954-2958, Pasadena, CA, USA, May 19-23, 2008.

[4] Meng Chen, Bufu Huang, and Yangsheng Xu, "Abnormal Gait Detection Using Intelligent Shoes," *International Journal of Information Acquisition*, Vol. 4, No. 3, pp. 215-226, 2007.

[5] Meng Chen, Bufu Huang, and Yangsheng Xu, "Human Abnormal Gait Modeling via Hidden Markov Model," *Proceedings of the 2007 International Conference on Information Acquisition*, pp. 517-522, Jeju City, Korea, July 9-11, 2007.

[6] Meng Chen, Bufu Huang, Ka Keung Lee, and Yangsheng Xu, "An Intelligent Shoe-Integrated System for Plantar Pressure Measurement," *Proceedings of the 2006 IEEE*

International Conference on Robotics and Biomimetics, pp. 416-421, Kunming, China, December 17-20, 2006.

[7] Bufu Huang, Meng Chen, and Weizhong Ye, "Intelligent Shoes for Human-Computer Interface" *Chapter 5 in Intelligent Wearable Interfaces* by Yangsheng Xu, Wen Jung Li, and Ka Keung Lee, Wiley-Interscience, 2008.

[8] Bufu Huang, Meng Chen, Ka Keung Lee, and Yangsheng Xu, "Human Identification Based on Gait Modeling," *International Journal of Information Acquisition*, Vol. 4, No. 1, pp. 27-38, 2007.

[9] Bufu Huang, Xiaoning Meng, Meng Chen, and Yangsheng Xu, "Human Gait Modeling and Similarity Evaluation based on Hidden Markov Models," *The 13th International Conference on Advanced Robotics*, pp. 868-873, Jeju, Korea, August 21-24, 2007.

[10] Bufu Huang, Meng Chen, Xi Shi, and Yangsheng Xu, "Gait Event Detection with Intelligent Shoes," *Proceedings of the 2007 International Conference on Information Acquisition*, pp. 579-584, Jeju City, Korea, July 9-11, 2007.

[11] Bufu Huang, Meng Chen, Panfeng Huang, and Yangsheng Xu, "Gait Modeling for Human Identification," *2007 IEEE International Conference on Robotics and Automation*, pp. 4833-4838, Roma, Italy, April 10-14, 2007.

[12] Bufu Huang, Meng Chen, Weizhong Ye, and Yangsheng Xu, "Intelligent Shoes for Human Identification," *Proceedings of the 2006 IEEE International Conference on Robotics and Biomimetics*, pp. 601-606, Kunming, China, December 17-20, 2006.

Bibliography

[1] http://www.motionanalysis.com/html/movement/eagle.html

[2] http://www.vicon.com/products/t160.html

[3] http://www.vicon.com/products/cameras.html

[4] http://www.motionanalysis.com/

[5] http://www.motionanalysis.com/html/movement/gait.html

[6] http://www.ndigital.com/lifesciences/certus-motioncapturesystem.php

[7] http://www.ndigital.com/lifesciences/smartmarkers.php

[8] http://www.ndigital.com/lifesciences/certus-accessories-vinten.php

[9] http://www.ascension-tech.com/realtime/MotionSTARWirelessLITE.php

[10] http://amti.biz/

[11] http://www.novelusa.com/index.php?fuseaction=systems.pedar

[12] J. J. Rechtien, J. B. Gelblum, A. J. Haig, and A. J. Gitter, "Technology Assessment: Dynamic Electromyography in Gait and Motion Analysis," *Muscle & Nerve*, vol. 19, issue 3, pp. 396-402, 1996.

[13] R. E. Morley, Jr., E. J. Richter, J. W. Klaesner, K. S. Maluf, and M. J. Mueller, "In-Shoe Multisensory Data Acquisition System," *IEEE Transactions on Biomedical Engineering*, vol. 48, no. 7, pp. 815-820, July 2001.

[14] K. S. Maluf, R. E. Morley Jr., E. J. Richter, J. W. Klaesner, and M. J. Mueller, "Monitoring In-Shoe Plantar Pressures, Temperature, and Humidity: Reliability and Validity of Measures from a Portable Device," *Arch. Phys. Med. Rehabil.*, vol. 82, no. 8, pp. 1119 - 1127, Aug. 2001.

[15] S. J. Morris and J. A. Paradiso, "Shoe-Integrated Sensor System for Wireless Gait Analysis and Real-time Feedback," *Proceedings of the Second Joint EMBS/BMES Conference*, pp. 2468 - 2469, Houston, TX, USA, October 23-26, 2002.

[16] S. J. M. Bamberg, A. Y. Benbasat, D. M. Scarborough, D. E. Krebs, and J. A. Paradiso, "Gait Analysis Using a Shoe-Integrated Wireless Sensor System," *IEEE Transactions on Information Technology in Biomedicine*, vol. 12, no. 4, pp. 413 - 423, July 2008.

[17] H. S. Zhu, N. Maalej, J. G. Webster, W. J. Tompkins, P. Bach-y-Rita, and J. J. Wertsch, "An Umbilical Data-Acquisition System for Measuring Pressures Between the Foot and Shoe," *IEEE Transactions on Biomedical Engneering*, vol. 37, no. 9, pp. 908 - 911, Sep. 1990.

[18] H. S. Zhu, G. F. Harris, J. J. Wertsch, W. J. Tompkins, and J. G. Webster, "A Microprocessor-Based Data-Acquisition System for Measuring Plantar Pressures from Ambulatory Subjects," *IEEE Transactions on Biomedical Engineering*, vol. 38, no. 7, pp. 710-714, July 1991.

[19] H. S. Zhu, J. J. Wertsch, G. F. Harris, J. D. Loftsgaarden, and M. B. Price, "Foot Pressure Distribution during Walking and Shuffling," *Arch. Phys. Med. Rehabil.*, vol. 72, no. 6, pp. 390 - 397, May 1991.

[20] T. L. Lawrence and R. N. Schmidt, "Wireless In-shoe Force System," *Proceedings of the 19th International Conference of the IEEE/EMBS*, pp. 2238 - 2241, Chicago, IL. USA, Oct. 30-Nov. 2, 1997.

[21] M. M. Skelly and H. J. Chizeck, "Real-Time Gait Event Detection for Paraplegic FES Walking," *IEEE Transactions on Neural Systems and Rehabilitation Engineering*, vol. 9, no. 1, pp. 59 - 68, March 2001.

[22] I. P. I. Pappas, M. R. Popovic, T. Keller, V. Dietz, and M. Morari, "A Reliable Gait Phase Detection System," *IEEE Transactions on Neural Systems and Rehabilitation Engineering*, vol. 9, no. 2, pp. 113 - 125, June 2001.

[23] I. P. I. Pappas, T. Keller, S. Mangold, M. R. Popovic, V. Dietz, and M. Morari, "A Reliable Gyroscope-Based Gait-Phase Detection Sensor Embedded in a Shoe Insole," *IEEE Sensors Journal*, vol. 4, no. 2, pp. 268-274, April 2004.

[24] J. M. Hausdorff, L. Zemany, C. K. Peng, and A. L. Goldberger, "Maturation of Gait Dynamics: Stride-to-Stride Variability and its Temporal Organization in Children," *J. Appl. Physiol.*, vol. 86, issue 3, pp. 1040-1047, 1999.

[25] Force sensing resistor integration guide and evaluation parts catalog, Interlink Electronics, originally available from http://www.interlinkelectronics.com/

[26] FLX-01 bend sensor Specifications, Images SI, Inc., available from http://www.imagesco.com/sensors/flex-sensor.html (accessed October 2005)

[27] MMA7260Q Data Sheet, Freescale Semiconductor, available from http://www.freescale.com/files/sensors/doc/data_sheet/MMA7260Q.pdf

[28] ADXRS150 Data Sheet, Analog Devices, available from http://www.analog.com/static/imported-files/data_sheets/ADXRS150.pdf

[29] ENC-03M Specifications, Murata, available from http://search.murata.co.jp/Ceramy/CatalogAction.do?sHinnm=? &sNHinnm=ENC-03M&sNhin_key=ENC-03M&sLang=en&sParam=ENC

[30] R. A. Wervey, G. F. Harris, and J. J. Wertsch, "Plantar Pressure Characteristics During Stair Climbing and Descent," *Proceedings of the 19th International Conference of the IEEE/ EMBS*, pp. 1746-1748, 1997.

[31] J. Mäntyjärvi, J. Himberg, and T. Seppänen, "Recognizing Human Motion with Multiple Acceleration Sensors," *IEEE International Conference on Systems, Man, and Cybernetics*, vol. 2, pp. 747-752, 2001.

[32] M. Sekine, T. Tamura, M. Akay, T. Fujimoto, T. Togawa, and Y. Fukui, "Discrimination of Walking Patterns Using Wavelet-Based Fractal Analysis," *IEEE Transactions on Neural Systems and Rehabilitation Engineering*, vol. 10, no. 3, pp. 188-196, 2002.

[33] M. N. Nyan, F. E. H. Tay, K. H. W. Seah, and Y. Y. Sitoh "Classification of Gait Patterns in the Time-Frequency Domain," *Journal of Biomechanics*, vol. 39, no. 14, pp. 2647-2656, 2006.

[34] F. Verdini, T. Leo, S. Fioretti, M. G. Benedetti, F. Catani, and S. Giannini,"Analysis of Ground Reaction Forces by means of Wavelet Transform," *Clinical Biomechanics*, vol. 15, no. 8, pp. 607-610, 2000.

[35] A. D. Stefano, R. Allen, J. H. Burridge, and V. T. Yule, "Application of Complex Wavelets for EMG Analysis during Gait of Asymptomatic and Pathological Subjects," *International Journal of Wavelets, Multiresolution and Information Processing*, vol. 1, no. 4, pp. 425-448, 2003.

[36] E. Lou, M. J. Moreau, D. L. Hill, V. J. Raso, and J. K. Mahood, "Smart Garment to Help Children Improve Posture," *Proceedings of the 28th IEEE EMBS Annual International Conference*, pp. 5374-5377, New York City, USA, Aug. 30-Sep. 3, 2006.

[37] M. C. Nechyba and Y. S. Xu, "Cascade Neural Networks with Node-Decoupled Extended Kalman Filtering," *Proceedings of IEEE Int. Symp. on Computational Intelligence in Robotics and Automation*, vol. 1, pp. 214-219, 1997.

[38] M. C. Nechyba and Y. S. Xu, "Human Control Strategy: Abstraction, Verification, and Replication," *IEEE Control Systems Magazine*, vol. 17, no. 5, pp. 48-61, 1997.

[39] Y. S. Xu, W. K. Yu, and K. W. Au, "Modeling Human Strategy in Controlling a Dynamically Stabilized Robot," *Proceedings of the 1999 IEEE/RSJ International Conference on Intelligent Robots ond Systems*, vol. 1, pp. 507-512, 1999.

[40] K. K. Lee and Y. S. Xu, "Human Sensation Modeling in Virtual Environments," *Proceedings of the 2000 IEEE/RSJ International Conference on Intelligent Robots and Systems*, vol. 1, pp. 151-156, 2000.

[41] H. N. Chow, Y. S. Xu, and S. K. Tso, "Learning Human Navigational Skill for Smart Wheelchair," *Proceedings of the 2002 IEEE/RSJ International Conference on Intelligent Robots ond Systems*, vol. 1, pp. 996-1001, 2002.

[42] G. V. Puskorius and L. A. Feldkamp, "Decoupled Extended Kalman Filter Training of Feedforward Layered Networks," *International Joint Conference on Neural Networks*, vol. 1, pp. 771-777, 1991.

[43] T. W. F. Mittlemeier and M. Morlock, "Pressure Distribution Measurements in Gait Analysis: Dependency on Measurement Frequency," *39th Annual Meeting of the Orthopaedic Research Society*, San Francisco, Calif, 1993.

[44] M. E. Tinetti, M. Speechley, and S. F. Ginter, "Risk Factors for Falls among Elderly Persons Living in the Community", *N Engl J Med*, vol. 319, no. 26, pp. 1701-1707, 1988.

[45] A. Salva, I. Bolibar, G. Pera, and C. Arias, "Incidence and Consequences of Falls among Elderly People Living in the Community," *Med Clin (Barc)*, vol. 122, no. 5, pp. 172-176, 2004.

[46] S. R. Lord, C. Sherrington, and H. B. Menz, "Falls in Older People: Risk Factors and Strategies for Prevention," *Cambridge University Press*, 2001.

[47] P. Kannus, H. Sievanen, M. Palvanen, T. Jarvinen, and J. Parkkari, "Prevention of Falls and Consequent Injuries in Elderly People," *Lancet*, vol. 366, no. 9500, pp. 1885-1893, 2005.

[48] M. E. Tinetti and C. S. Williams, "Falls, Injuries due to Falls, and the Risk of Admission to a Nursing Home," *N Engl J Med*, vol. 337, no. 18, pp. 1279-1284, 1997.

[49] P. E. Cotter, S. Timmons, M. O'Connor, C. Twomey, and D. O'Mahony, "The Financial Implications of Falls in Older People for an Acute Hospital," *Ir J Med Sci*, vol. 175, no. 2, pp. 11-13, 2006.

[50] B. Roudsari, B. Ebel, P. Corso, N. Molinari, and T. Koepsell, "The Acute Medical Care Costs of Fall-Related Injuries Among the U.S," *Older Adults Injury*, vol. 36, no. 11, pp. 1316-1322.

[51] W. Walker, "Promoting a Safe Environment for Confused Older People at Risk from Falling in Hospital," *J Orthop Nurs*, vol. 8, no. 2, pp. 72-76, 2004.

[52] M. Weatherall, "Multifactorial Risk Assessment and Management Programmes Effectively Prevent Falls in the Elderly," *Evid Based Healthc Public Health*, vol. 8, no. 5, pp. 270-272, 2004.

[53] M. Melinda, M. Gardner, C. Robertson, R. McGee, and A. J. Campbell, "Application of a Falls Prevention Program for Older People to Primary Health Care Practice," *Prev Med*, vol. 34, no. 5, pp. 546-53, 2002.

[54] B. Vellas, F. Cayla, H. Bocquet, F. De Pemille, and J. L. Albarede, "Prospective Study of Restriction of Activity in Old People after Falls," *Age Ageing*, vol. 16, no. 3, pp. 189-193, 1987.

[55] M. B. King and M. E. Tinetti, "Falls in Community Dwelling Older Persons," *J. Am. Geriatr. Soc.*, vol. 43, pp. 1146-1154, 1995.

[56] L. Hazelhoff, J. G. Han, and P. H. With, "Video-Based Fall Detection in the Home Using Principal Component Analysis," *Advanced Concepts for Intelligent Vision Systems*, vol. 5259, pp. 298-309, 2008.

[57] Z. M. Fu, T. Delbruck, P. Lichtsteiner, and E. Culurciello, "An Address-Event Fall Detector for Assisted Living Applications," *IEEE Transactions on Biomedical Circuits and Systems*, vol. 2, no. 2, pp. 88-96, June 2008.

[58] X. D. Zhuang, J. Huang, G. Potamianos, and M. Hasegawa-Johnson, "Acoustic Fall Detection Using Gaussian Mixture Models and GMM Supervectors," *Proceedings of the IEEE International Conference on Acoustics, Speech and Signal Processing*, pp. 69-72, 2009.

[59] A. K. Bourke and G. M. Lyons, "A Threshold-Based Fall-Detection Algorithm Using a Bi-Axial Gyroscope Sensor," *Medical Engineering & Physics*, vol. 30, pp. 84-90, 2008.

[60] M. N. Nyan, F. E. H. Tay, A. W. Y. Tan, and K. H. W. Seah, "Distinguishing Fall Activities from Normal Activities by Angular Rate Characteristics and High-Speed Camera Characterization," *Medical Engineering & Physics*, vol. 28, pp. 842-849, 2006.

[61] U. Lindemann, A. Hock, M. Stuber, W. Keck, and C. Becker, " Evaluation of a Fall Detector Based on Accelerometers : A Pilot Study," *Medical & Biological Engineering & Computing*, vol. 43, no. 5, pp. 548-551, 2005.

[62] M. Kangas, A. Konttila, I. Winblad, and T. Jämsä, "Determination of Simple Thresholds for Accelerometry-Based Parameters for Fall Detection," *Proceedings of the 29th Annual International Conference of the IEEE EMBS*, pp. 1367-1370, Cité Internationale, Lyon, France, August 23-26, 2007.

[63] S. M. Pincus, "Approximate Entropy as a Measure of System Complexity," *Proc. Natl. Acad. Sci. USA*, vol. 88, pp. 2297-2301, March 1991.

[64] P. N. Belhumeur, J. P. Hespanha, and D. J. Kriegman, "Eigenfaces vs. Fisherfaces: Recognition Using Class Specific Linear Projection," *IEEE Transactions on Pattern Analysis and Machine Intelligence*, vol. 19, no. 7, pp. 711-720, July, 1997.

[65] W. Zhao, R. Chellappa, and A. Krishnaswamy, "Discriminant Analysis of Principal Components for Face Recognition," *Proceedings of the 3rd IEEE International Conference on Automatic Face and Gesture Recognition*, pp. 336-341, Nara, Japan, 14-16 April, 1998.

[66] G. Baudat and F. Anouar, "Generalized Discriminant Analysis using a Kernel Approach," *Neural Computation*, vol. 12, no. 10, pp. 2385-2404, 2000.

[67] C. S. Xu, N. C. Maddage, X. Shao, F. Cao, and Q. Tian, "Musical Genre Classification using Support Vector Machines," *Proceedings of the IEEE International Conference on Acoustics, Speech, and Signal Processing*, vol. 5, pp. 429-432, 2003.

[68] N. Scaringella and G. Zoia, "On the Modeling of Time Information for Automatic Genre Recognition Systems in Audio Signals," *Proceedings of the 6th Int. Symposium on Music Information Retrieval*, London, UK, 2005.

[69] T. Lidy and A. Rauber, "Evaluation of Feature Extractors and Psycho-Acoustic Transformationsfor Music Genre Classification," *Proceedings of the 6th Int. Symposium on Music Information Retrieval*, London, UK, 2005.

[70] O. Chapelle, P. Haffner, and V. N. Vapnik, "Support Vector Machines for Histogram-based Image Classification," *IEEE Transactions on Neural Networks*, vol. 10, no. 5, pp. 1055-1064, Sep. 1999.

[71] D. Amit and L. Boaz, "Support Vector Machine-based Image Classification for Genetic Syndrome Diagnosis," *Pattern Recognition Letters*, vol. 26, 2005, pp. 1029 - 1038.

[72] B. Moghaddam and M. H. Yang, "Gender Classification with Support Vector Machines," *Proceedings of the 4th IEEE International Conference on Automatic Face and Gesture Recognition*, vol. 10, no. 5, pp. 306-311, March 2000.

[73] L. Lu and P. F. Shi, "A Novel Fusion-Based Method for Expression-Invariant Gender Classification," *IEEE International Conference on Acoustics, Speech and Signal Processing (ICASSP2009)*, pp. 1065-1068, 19-24 April, 2009.

[74] C. Cortes and V. Vapnik, "Support-Vector Networks," *Machine Learning*, vol. 20, no. 3, pp. 273-297, 1995.

[75] V. Vapnik, "Statistical Learning Theory," *Wiley-Interscience* , 1998.

[76] D. E. Goldberg, "Genetic Algorithms in Search, Optimization and Machine Learning," *Addison-Wesley Professional*, Boston, MA, USA, 1989.

[77] B. Schölkopf, A. J. Smola, R. C. Williamson, and P. L. Bartlett, "New Support Vector Algorithms," *Neural Computation*, vol. 12, issue 5, pp. 1207-1245, 2000.

[78] S. Sarkar, P. J. Phillips, Z. Y. Liu, I. R. Vega, P. Grother, and K. W. Bowyer, "The HumanID Gait Challenge Problem: Data Sets, Performance, and Analysis," *IEEE Transactions on Pattern Analysis and Machine Intelligence*, vol. 27, no. 2, Feb. 2005, pp. 162-177.

[79] C. W. Cho, W. H. Chao, S. H. Lin, and Y. Y. Chen, "A Vision-based Analysis System for Gait Recognition in Patients with Parkinson's Disease," *Expert Systems with Applications: An International Journal*, vol. 36, issue 3, Apr. 2009, pp. 7033-7039.

[80] C. Bauckhage, J. K. Tsotsos, and F. E. Bunn, "Detecting Abnormal Gait," *Proceedings of the Second Canadian Conference on Computer and Robot Vision (CRV' 05)*, May 9-11 2005, pp. 282-288.

[81] B. Westhoff, A. Petermann, M. A. Hirsch, R. Willers, and R. Krauspe, "Computerized Gait Analysis in Legg Calvé Perthes Disease—Analysis of the Frontal Plane," *Gait & Posture*, vol. 24, issue 2, Oct. 2006, pp. 196 - 202.

[82] A. Y. Benbasat, S. J. Morris, and J. A. Paradiso, "A Wireless Modular Sensor Architecture and its Application in On-Shoe Gait Analysis," *Proceedings of IEEE Sensors*, 2003, pp. 1086 - 1091.

[83] H. L. Hurkmans, J. B. Bussmann, E. Benda, J. A. Verhaar, and H. J. Stam, "Accuracy and Repeatability of the Pedar Mobile System in Long-term Vertical Force Measurements," *Gait and Posture*, vol. 23, issue 1, Jan. 2006, pp. 118-125.

[84] J. Ray and D. Snyder, "Pedobarographic Gait Analysis on Male Subjects," *Proceedings of the Fifteenth Southern Biomedical Engineering Conference*, pp. 25-27, March 1996.

[85] J. Ray, D. Needhamr, and D. Snyder, "Utilizing Gaitline Velocity in Dynamic Gait Analysis," *Proceedings of the 1997 Sixteenth Southern Biomedical Engineering Conference*, pp. 161-164, Apr. 4-6 1997.

[86] I. T. Jolliffe, "Principal Component Analysis," *Springer-Verlag*, 1986.

[87] X. D. Huang, Y. Ariki, and M. A. Jack, "Hidden Markov Models for Speech Recognition," *Edinburgh University Press*, Edinburgh, 1990.

[88] J. Yang, Y. S. Xu, and C. S. Chen, "Hidden Markov Model Approach to Skill Learning and its Application to Telerobotics," *IEEE Trans. on Robotics and Automation*, vol. 10, no. 5, pp. 621-631, 1994.

[89] J. Yang, Y. S. Xu, and C. S. Chen, "Human Action Learning via Hidden Markov Model," *IEEE Transactions on Systems, Man and Cybernetics-Part A: Systems and Humans*, vol. 27, no. 1, pp. 34-44, Jan. 1997.

[90] L. E. Baum, T. Petrie, G. Soules, and N. Weiss, "A Maximization Technique Occurring in the Statistical Analysis of Probabilistic Functions of Markov Chains," *Ann. Math. Stat.*, vol. 41, no. 1, pp. 164-171, 1970.

[91] A. P. Dempster, N. M. Laird, and D. B. Rubin, "Maximum Likelihood from Incomplete Data via the EM Algorithm," *J. Roy. Stat. Soc.*, vol. 39, no. 1, pp. 1-38, 1977.

[92] L. R. Rabiner, "A Tutorial on Hidden Markov Models and Selected Applications in Speech Recognition," *Proceedings of the IEEE*, vol. 77, no. 2, pp. 257-286, 1989.

[93] L. R. Rabiner and B. H. Juang, "An Introduction to Hidden Markov Models," *IEEE ASSP Magazine*, pp. 4 - 15, Jan. 1986.